Characterization of the Curli Nucleator CsgB

by

Neal D. Hammer

A dissertation submitted in partial fulfillment
of the requirements for the degree of
Doctor of Philosophy
(Microbiology and Immunology)
in The University of Michigan
2009

Doctoral Committee:

Assistant Professor Matthew R. Chapman, Chair
Professor James Bardwell
Professor Victor J. DiRita
Assistant Professor Jason E. Gestwicki
Assistant Professor Mary X.D. O'Riordan
Assistant Professor Maria B. Sandkvist

in memory of my grandmother Julia Hammer
and to Ann Arbor Silver Club Coffehouse

Acknowledgements

The work presented here would not have been possible without the support of many people. I was fortunate to be surrounded by a very talented group of people during my tenure in the Chapman lab. Dr. Michelle Barnhart, Dr. Xuan Wang, and Dr. Elisabeth Ashman Epstein immediately helped me get acquainted to the common protocols the lab used. Michelle helped me to a fantastic start by providing much needed advice while I troubleshot several protocols. Working in the same locale as Xuan was fantastic. He always provided a unique point of view for the problem, concern, or question of the day. Most of all, I am thankful for his encouragement. Daniel Smith and Ryan Frisch began their graduate work the same year I did, and I am lucky to call these guys my peers. They are both very intelligent and were fun to talk to about science or any other topic. Dr. Robert Bender was always around to address any inquiry I had, no matter how bizarre, and I am also grateful that I was a GSI for his AIDS and Other Pandemics course. Yizhou Zhou has been a more than suitable replacement after the departure of Dr. Wang. She has a very promising career ahead of her. I have only interacted with Maggie Evans, Will ‘the thrill’ Depas, and Matt Badtke for a short time, but the future of the Chapman lab is bright with the addition of these new members. I look forward to following their work. I also had the privilege of teaching two very talented undergraduates, Bryan McGuffie

and Katie Parzych. Both are currently at Harvard University where I am sure they will do spectacular things. Bryan, in particular, has a unique understanding of science that will serve him well. I also had the pleasure of meeting and working with Ashley Nenninger and Jerry Pinkner while fishing up some collaborative work with the Hultgren group. Both are hard working, bright, and friendly people whose correspondence proved to be invaluable.

I am honored to call Dr. Matt Chapman my mentor. He provided unparallel advice. For example, he reminded that things often don't go as we plan and that we need to adapt in order it achieve our goals. Matt is one of the most humble people I know, and I appreciated that he frequently invited all of us over to his house for time to unwind. He was very hospitable and it showed that he appreciated my work. When presenting my work at meetings it was clear that he was proud of the contribution I made to his lab. There is not enough space and words cannot describe how important Matt has been to my development as a scientist. Frankly, I have achieved much more than I thought I could and Matt is the reason why.

Much of the work presented here has been published or will be published in the near future. Chapter I was published as a review in the Journal of Alzheimer's Disease. Xuan Wang wrote the Alzheimer's section of this chapter and Bryan McGuffie contributed by creating illustrations used in the figures.

Chapter II was published in the Proceedings of the National Academy of Sciences. Jens Schmidt was a talented German exchange student we hosted for a short time, and he provided CsgA for the seeding experiments and performed the IAPP-CsgA seeding specificity experiment. We are also grateful for the technical assistance provided by the Ursula Jakob laboratory while completing the circular dichroism experiments. We thank the German Academic Exchange Service for supplying funding for Jens Schmidt.

Chapter III will be submitted for peer review in the near future. Several key people recorded data in Chapter III including Bryan McGuffie and Ashley Reinke. Bryan performed all the *in vivo* analysis for the repeating unit deletion constructs and Ashley recorded most of the EM data. I would also like to thank Yizhou Zhou and Matt Badtke for supplying purified CsgA needed for the seeding experiments. I appreciate the insight and discussion all the Chapman lab members (including Ryan) have provided for my writings, and I thank the Hultgren laboratory for supplying us with many, many strains and plasmids.

I would like to thank my committee members Dr. James Bardwell, Dr. Jason Gestwicki, Dr. Mary O'Riordan, Dr. Vic DiRita, and Dr. Maria Sandkvist. They are an all-star cast of protein fold experts and microbial geneticists. They challenged me and presented alternative perspectives of my results thus broading my point of view. They all helped me become a better scientist.

The memories I have of my roommates and friends at Michigan, who are too numerous to list, are priceless. I have learned a great deal from them and they provided a fantastic environment for success. I cherish these memories and look forward to seeing and or working with the people I met here in the future.

My trips back to Illinois always provided a much-needed reprieve and for that I thank my parents, siblings, and old friends. It was always so much fun to return home. I am grateful these relationships have grown in spite of the distance. They have all provided more support than they realize, and I am blessed that they are part of my life.

Table of Contents

List of Figures

List of Tables

Chapter I

Introduction

[This chapter is a modified version of Hammer, N.D., Wang, X., McGuffie, B.A., and Chapman M.R. accepted for publication to the Journal of Alzheimer's Disease May, 2008]

Amyloids: Friend or Foe?

Amyloidogenesis is recognized as being the underlying cause of neurodegenerative diseases such as Alzheimer's, Huntington's and Parkinson's disease. Amyloid fibrils have biochemical and biophysical properties that distinguish them from other biological polymers. Amyloid fibers are incredibly stable, detergent insoluble, β–sheet rich structures that many proteins can form [1]. Amyloid fibers associated with neurodegenerative diseases are considered the product of a protein-misfolding event. The pathology of neurodegenerative diseases defined amyloid polymerization as an aberrant process where misfolded proteins aggregate and cause disease. However, there are a number of examples where organisms can utilize either the amyloid fiber itself or intermediates formed during the amyloid polymerization process to fulfill specific biological functions [2-9]. Unlike disease-associated amyloidogenic proteins, functional amyloid assembly is a regulated process that minimizes the cellular

toxicity associated with disease-associated amyloids. There are, though, examples where organisms utilize the toxicity of the amyloid fold to carry out a function. Understanding mechanisms that promote functional amyloidogenesis will provide an unprecedented glimpse into amyloidogenic systems in general and will lead to new ideas for preventing disease-associated amyloidogenesis. Guided by this perspective we compare and contrast amyloid-β (Aβ) amyloidogenesis as it relates to Alzheimer's disease to several systems where functional amyloidogenesis occurs presenting ideas about how these functional amyloid systems prevent the build up of amyloid associated toxicity.

Alzheimer's Disease

Alzheimer's disease (AD) is the most common neurodegenerative disease. More than 4 million people are afflicted with this neurodegenerative disease in the United States alone (http://www.ahaf.org). The clinical and neuropathological characteristics were first reported in 1906 by Alois Alzheimer. The abnormal deposits, described as both plaques and tangles, were found in the postmortem diseased brain and were later called amyloid plaques [10]. The plaques were found to be composed of long, unbranched 4-10 nanometer wide fibers when viewed with an electron microscope (Fig.1.1A) [11, 12]. These structures were discovered to be proteinaceous in nature and contained a uniquely stable cross-beta sheet quaternary structure. Fibers with similar structural characteristics have now been described in other neurodegenerative disorders including Parkinson's disease and Huntington's disease [13, 14].

The Aβ polypeptide was purified from AD associated plaques and was determined to be the major protein component of amyloid plaques [15, 16]. Aβ is formed when the amyloid precursor protein (APP) is sequentially cleaved by β- and γ-secretases [17]. It is proposed that APP plays important physiological roles in cell adhesion, neurite outgrowth, synaptogenesis and synapse remodeling [18], however, the function of the Aβ polypeptide is currently unknown. There are two major cleavage products, Aβ40 and Aβ42 [19]. The primary sequences of Aβ40 and Aβ42 only differ in that Aβ42 has 2 additional C-terminal residues, Ile^{41} and Ala^{42}. Mutations in presenilins, a central component of γ-secretase, account for most cases of familial AD. These mutations increase the production of Aβ42 in both transfected cells and transgenic mice [20]. In sporadic AD cases the apolipoprotein E (APOE) ε4 allele is the genetic risk factor most often linked to disease onset [21]. In cultured neuronal cells APOE4 enhances Aβ production by modulating APP processing [22]. In addition, it was reported that APOE4 also modulates the degradation and clearance of deposited Aβ [23-26].

Several lines of evidence link APP and misfolded Aβ to AD (for review see [27-29]). However, the molecular mechanism behind Aβ misfolding and how this leads to AD remains unclear. Hardy and Selkoe proposed the “amyloid cascade hypothesis” in which the central event in AD development is an imbalance between Aβ production and clearance [30]. The biochemical species of Aβ that induces pathogenesis is still a hotly debated topic. Experimental evidence suggest two models: (1) the final amyloid fiber product causes neuronal damage

or (2) neuronal cells are exposed to a toxic intermediates formed as Aβ polymerizes into the amyloid fiber.

In vitro self assembly of Aβ polypeptides is characterized by nucleation-dependent polymerization kinetics (Fig. 1.1B blue line) [31, 32]. Before mature fiber aggregates are detectable, there is a time period where the Aβ polypetide polymerization appears to be stagnant. However, during this lag phase trace amounts of dimer, trimer, and eventually, nucleus (oligomer) are formed (Fig. 1.1C) [33-35]. Nucleus formation is the rate-limiting step of fibril assembly. Once a nucleus has formed, monomer addition to the growing fiber becomes thermodynamically favorable and occurs quickly (Fig. 1.1B and C) [32]. As with any dynamic polymerization process where different folding intermediates are present at any one time, Aβ monomer, oligomer, protofibrils (short fibrillar aggregates) and fibrils have been observed using different techniques including atomic force microscopy [35, 36]. Amyloid formation inhibitors such as Congo red and curcumin potentially reduce neurotoxicity by stabilizing the monomeric state of Aβ, thus reducing the amount of oligomer intermediates formed [33, 34, 37, 38]. Therefore neurotoxicity seems to be linked to aggregation of monomers to higher ordered structures [39-41].

Amyloid laden plaques are often found in post-mortem AD brains, which led to the suggestion that mature insoluble fiber aggregates are the causative agent for AD. However, statistical analyses have found only a weak correlation between the number of amyloid aggregates and the severity of AD [42, 43]. In addition, high molecular weight Aβ42 aggregates do not correlate with toxicity in

the *Caenorhabiditis elegans* AD model [44]. The formation of high molecular weight protein aggregates may be a mechanism to protect cells from cytoxicity by sequestering the toxic intermediates present formed during Aβ misregulation [45, 46]. A wide range of nonfibrillar Aβ forms including dimer, trimer, oligomer, spherical aggregates and protofibrils have been reported to be cytotoxic and support this idea [36, 47-54]. Different Aβ forms, including the small diffusible Aβ oligomer, high molecular weight oligomer, and fibers affect cortical neurons differently [55]. Collectively, this data suggest nonfibrillar intermediates trigger neuropathologies. Therefore, the development of nuerodegeneration could be induced by a complicated combination of several toxic Aβ conformers including the fibers themselves.

Despite evidence that prefibrillar aggregates may be the causative agents AD toxicity, many researchers have reported that mature Aβ fibers are toxic to cultured neuronal cells [48, 55-58]. How can this apparently conflicting data be reconciled? Recent study has demonstrated that the amyloid fiber is not a static structure. For instance, amyloid fibers formed from an SH3 domain showed very dynamic properties, in which molecules can be recycled by a dissociation and re-association mechanism within the fibril population [59]. Therefore amyloid fibrils could provide a reservoir for toxic soluble oligomers, which could trigger the pathology [29]. Under different experimental conditions amyloid fibrils may have different potentials to liberate soluble oligomers, which may be cytotoxic to the cultured neurons. Nevertheless, the ability to effectively develop therapeutics that will deter AD development is difficult due to the lack of experimental evidence

defining a toxic species. Moreover, the molecular mechanism behind the initial misfolding events that convert soluble Aβ into an amyloid fiber *in vivo* has not been forthcoming. Perhaps exploring systems where amyloid formation occurs as a natural functional process will provide answers to these questions.

Amyloid as a functional fold

Functional Bacterial Amyloids

Curli

The first example of a functional amyloid fiber was demonstrated in the common laboratory bacterium *Escherichia coli*. *E. coli* and other Gram-negative enteric bacteria produce a functional amyloid fiber called curli (Fig. 1.2A). These fibers mediate many important physiological functions for the cell. Curli fibers are the major proteinacious component of the extracellular matrix produced by bacteria during growth in biofilms. Curli also induce a potent host inflammatory response, initiate binding to host cells, and increase the ability of the bacteria to persist within the environment and the host [60-66]. The genetic and biochemical tools afforded by *E. coli* have provided an in depth look at how bacteria control the assembly of amyloid fibers [2].

Biosynthesis of curli fibers is dependent on two divergently transcribed operons, *csgDEFG* and *csgBA*, both of which are under the control of a complex regulatory network [67-70]. The *csgBA* operon encodes the minor and major curli subunit proteins, CsgB and CsgA, respectively. The stability and secretion of

both CsgA and CsgB is dependent on the outer-membrane localized CsgG protein [2, 71-73]. The functions of CsgF and CsgE have not been elucidated, but it is clear that CsgE plays an important role in the stability of both CsgB and CsgA, while CsgF is required for efficient curli biogenesis [2].

CsgA and CsgB are the crux of curli fibers. When incorporated into curli fibers, both CsgA and CsgB are detergent insoluble. Cells that do not express CsgB secrete CsgA into the extracellular milieu as a soluble, unpolymerized protein (Fig. 1.2B). Therefore, *in vivo* both CsgA and CsgB are required for curli biogenesis. However, CsgA and CsgB do not have to be expressed by the same cell for curli assembly to occur. In a process called interbacterial complementation, CsgA secreted from a *csgB* mutant, or donating cell, can be polymerized by CsgB produced on the surface of a *csgA* mutant or accepting cell (Fig. 1.2B and C) [2, 71, 72, 74].The ability of CsgB to convert CsgA into an insoluble fiber led it to be designated the curli nucleator protein.

CsgA and CsgB are 30% identical and 51% similar at the amino acid level, and each protein has a domain composed of five glutamine-asparagine rich oligopeptide repeats (Fig. 1.2D) [74-76]. Each glutamine-asparagine rich repeating unit is composed of roughly 20 amino acids and is predicted to form consecutive β–strand loop β–strand motifs that stack perpendicular to the axis of fiber growth (Fig. 1.2D). Peptides composed of the first, third and fifth oligopeptide repeats of CsgA are amyloidogenic [77]. Mature CsgA protein has been purified, and can self-assemble into curli-like amyloid fibers [2]. *In vitro*,

purified CsgA can form amyloid in the absence of CsgB, whereas *in vivo,* CsgA amyloid formation is CsgB-dependent.

CsgA and Aβ *in vitro* polymerization share common features. First, *in vitro* polymerization of both proteins contains three distinct phases: a lag phase, a growth phase, and a stationary phase (Fig.1.1B blue line). Second, in a process called seeding, the lag phase associated with the polymerization of CsgA and Aβ can be abrogated by the addition of preformed fibers composed of CsgA and Aβ respectively (Fig. 1.1B red line) [31, 77]. Lastly, a conformation specific antibody recognizes a folding intermediate formed during the lag phase of each protein's self assembly process [77, 78]. These polymerization features are characteristic of an assembly mechanism that is dependent on nucleus formation. Nucleus formation is the rate limiting step and must occur before the protein can begin self-assembly into an amyloid fiber (Fig. 1.1C). While the role of nucleus formation as it relates to Aβ polymerization and AD has yet to be elucidated, the curli system is unique in that CsgB's function is to serve as a nucleus for CsgA *in vivo*.

A truncated version of CsgB containing the repeating units most similar to those found in CsgA (R1-R4) was recently purified and also demonstrated the ability to self-assemble into an amyloid fiber (Fig. 1.2D) [71]. Similar to CsgA and Aβ polymerization, the polymerization of the truncated CsgB resembled nucleus dependent kinetics displaying a lag phase followed by a polymerization phase, followed by a stationary phase. Fibers composed of the truncated version of CsgB abrogate the CsgA's polymerization lag phase, thus recapitulating *in vivo*

curli biogenesis [71]. These results demonstrate that CsgB acts as a template for CsgA polymerization.

The culmination of the experimental evidence suggests *E. coli* has evolved an elegant strategy to control amyloid fiber biogenesis. Curli biogenesis begins when CsgB is secreted and anchored to the outer membrane where it acts as a template for newly secreted CsgA. In a process called nucleation CsgB converts soluble monomeric CsgA into a β–sheet-rich, detergent insoluble protein. Then, in a process called seeding, the growing fiber tip can act as a folding template for additional soluble CsgA monomers. By strictly regulating the *csg* operons and by separating the nucleation process and seeding process into two separate proteins, the cell ensures amyloid fiber biogenesis occurs at the right place and at the right time. This strategy decreases exposure to potentially cytotoxic folding intermediates by promoting mature amyloid fiber formation. Therefore, understanding the molecular basis of curli nucleation and polymerization may provide new insights into how the toxicity of disease-associated amyloids can be reduced.

Chaplins

The chaplins are extracellular structures produced by the Gram-positive bacterium *Streptomyces coelicolor*. *In vivo*, these amyloid fibers reduce the surface tension at the media/air interface and allow for the development of aerial hyphea [3, 79]. Without the chaplins development of aerial hyphea is impaired [3, 79]. Chaplin biogenesis is dependent upon the translational products of the

chpA-H operon. Like Aβ and CsgA, the chaplins are β–rich insoluble fibers that bind the amyloid specific dye thioflavin T *in vitro* [3].

Like curli, chaplin amyloid biogenesis is temporally and positionally coordinated. Chaplin expression is dependent on the *bldN* developmental sigma factor, ensuring that fiber formation occurs at the proper time [79]. Furthermore, chaplin amyloid formation is localized to the extracellular space, which may limit exposure to cytotoxic intermediates[3, 79].

Microcin E492 and the Harpins

Two examples of bacteria utilizing the cytotoxic properties of amyloid to deter the growth of neighboring cells have been identified. Microcin E492 (also called Mcc), produced by *Klebsiella pneumoniae,* is a potent antibacterial bacteriocin. Mcc is most active during logarithmic growth, losing most of its cytotoxic properties in stationary phase [80, 81]. Bieler and colleagues found that Mcc polymerizes into amyloid fibrils biochemically identical to Aβ and CsgA fibers. Remarkably, the polymerization of Mcc into a mature amyloid fiber coincides with a loss of Mcc antibacterial activity [82]. Thus, a pre-fiber intermediate is proposed to be the cytotoxic species of Mcc [82]. It is also interesting to note that lower concentrations of Mcc are able to induce apoptosis in some human cell lines although the mechanism of Mcc induced apoptosis is currently unknown [83].

The harpins are a second class of bacterial proteins that capitalize on the cytotoxic features of amyloid biogenesis. Produced by plant pathogens, harpins

are type-III secreted proteins that induce the hypersensitive response in plants [84]. The hypersensitive response is a plant defense mechanism that slows intracellular pathogen growth by eliciting plant cell death. The hypersensitive response is similar to apoptosis in animal cells [85-87]. Oh *et al*. discovered that HpaG, a harpin produced by *Xanthomonas axonopodis* pv. *glycines* 8ra, self assembles into amyloid-like fibers. Unlike Mcc, injection of HpaG protofibrils and mature amyloid fibers into plant cells is toxic and results in cell death. Oh *et al.* also demonstrated that a harpin from *E. amylovora*, HrpN, and a harpin from *Pseudomonas syringae* pv. *syringae*, HrpZ, form amyloid fibers [84]. Both of these harpins elicit the hypersensitive response. A harpin unable to induce the hypersensitive response, XopA from *Xanthomonas campestris* pv. *vesicatoria*, did not form amyloid fibers [84]. However, a gain-of-function mutant form of XopA (F48L/M52L) which does induce the hypersensitive response polymerizes into an amyloid fiber, correlating the ability to induce the hypersensitive response to the ability to form amyloid [84]. The harpins are an example of a functional amyloid fiber that is designed to be lethal.

Potential Bacterial Amyloids

Two recently discovered bacterial structures may be composed of amyloid fibers. *M*. *tuberculosis* produces a structure that resembles *E. coli* curli fibers. Like curli and other amyloid fibers, the *M. tuberculosis* pili (MTP) are stable and non-branching fibers [88]. Also like curli, MTP bind host extracellular matrix proteins [88]. Moreover, individuals infected with *M. tuberculosis* have antibodies

that react to MTP, while serum from uninfected healthy individuals do not [88]. Structural and biochemical tests including circular dichroism, the ability to bind the amyloid specific dyes Congo red and thioflavin T, and resistance to proteinase K treatment will determine if these pili are in fact amyloid.

The second potential bacterial structure that might be an amyloid is the bacterial endospore. When confronted with environments limited for nutrients some species of bacteria such as *Bacillus* and *Clostridium* initiate the formation of an endospore, a unique structure that is highly resistant to heat, radiation, pH extremes, and toxic chemicals. High resolution atomic force microcopy has revealed that the spore coat of *Bacillus atrophaeus* is composed of fibrils similar to amyloid [89]. The inner and outer spore coats are composed of over 50 proteins and it is currently unknown which proteins form the fibril species observed and how this structure is assembled [90]. Thus further biochemical characterization of the proteins that form the spore coat, and their amyloidogenicity has not been elucidated. But it makes sense that sporulating bacteria would use the incredibly stable amyloid fiber as protective coat.

Eukaryotic functional amyloids

The Yeast Prion Proteins: Eukaryotic Functional Amyloid Domains

The [*PSI*$^{+}$], [URE3], and [*PIN*$^{+}$] phenotypes of the yeast *Saccharomyces cerevisiae* are defined by non-Mendelian inheritance. These phenotypes are transmitted to daughter cells via a conformationally altered amyloid version of the

yeast proteins Sup35p, Ure2p, and Rnq1p, respectively [91-96]. Sup35p, Ure2p and Rnq1p all undergo a conversion to an aggregative state that can incorporate soluble protein into an insoluble amyloid aggregate [93, 97-106]. These proteins all contain a glutamine/asparagine (Q/N) rich domain and this domain is essential for the propagation of the [*PSI*$^{+}$] and [URE3] prions[97, 100, 103, 105, 107]. In both [*PSI*$^{+}$] and [URE3] this conversion leads to the loss of wild type Sup35p and Ure2p function. The ability to confer a phenotype by converting normally soluble wild type protein into an infectious amyloid aggregate defines these proteins as prions.

[URE3] / Ure2p

Ure2p represses the genetic network needed to utilize poor nitrogen sources [108]. When yeast are provided with good nitrogen sources such as ammonia or glutamine, Ure2p binds to the positive transcriptional regulators Gln3p and Gat1p and prevents their translocation into the nucleus [109-114]. Yeast carrying the [URE3] prion have little Ure2p activity, and no phenotypic advantages have been demonstrated to correlate with the [URE3] prion. In addition, Nakayashiki *et al.* noted that 70 natural isolates of yeast do not carry [URE3], suggesting that the Ure2p prion state is not advantageous in a natural setting [115]. However, recent work by Shewmaker *et al*. demonstrated that Ure2p missing the Q/N domain had substantially reduced stability and activity [116]. Ure2p missing the Q/N domain had reduced steady state levels compared to the wild type protein suggesting the Q/N domain can act to increase Ure2p

stability. These data along with the prevalence of the Q/N domain in the yeast proteome, suggest that the Q/N domain, a domain known to promote amyloidogenesis, may also function as a modular protein-stabilizing domain that also initiates protein-protein interactions.

[PSI$^+$] / Sup35p

The Sup35p protein is an essential component of the translation termination machinery. In [*psi*-] yeast, Sup35p recognizes stop codons and terminates protein synthesis [117]. In [*PSI*$^+$] cells wild type Sup35p is sequestered in self-assembled amyloid aggregates. Aggregated Sup35p is unable to participate in translational termination, resulting in translational read-through at wild type stop codons and C-terminally elongated proteins. As with [URE3], the [*PSI*$^+$] phenotype is propagated through the community as dividing cells transmit the [*PSI*$^+$] phenotype to daughter cells [118, 119]. Novel work done by True and Lindquist demonstrated that the [*PSI*$^+$] prion is advantageous under several growth conditions and may provide an alternative mechanism for phenotypic plasticity during environmental insult by altering the yeast proteome [120]. In addition, the Q/N domain itself has been estimated to be conserved for several hundred million years [121-123]. This suggests a strong selection to retain this amyloidogenic domain despite the possible detrimental effects of decreased translational termination fidelity or amyloid associated toxicity. Because some natural isolates of *S. cerevisiae* do not carry [*PSI*$^+$], it has been proposed that the [*PSI*$^+$] phenotype is not under selective pressure [115].

However, these studies are ongoing and the evolutionary impact of the [*PSI*$^{+}$] phenotype is difficult to assess.

[PIN^{+}] / Rnq1p

The [*PIN*$^{+}$] phenotype is defined by the ability to induce the [*PSI*$^{+}$] phenotype. The Rnq1p protein was discovered to induce [*PSI*$^{+}$] [103]. Interestingly, the only known function of the Rnq1p protein is to induce the [*PSI*$^{+}$] phenotype *de novo*. In addition to Rnq1p, Ure2p and New1p can also can induce [*PSI*$^{+}$] when over-expressed [92, 124]. Having a protein dedicated to the induction [*PSI*$^{+}$] suggests that [*PSI*$^{+}$] maybe advantageous in growth conditions where *rnq1* is expressed. The study determining the prevalence of prions in natural yeast isolates found that the [*PIN*$^{+}$] prion is present in some yeast found within the environment [115].

Regulation and coordination of yeast amyloid formation

Like Aβ and CsgA, Sup35p and Ure2p self assemble into amyloid fibers *in vitro* [106, 125, 126]. Also like CsgA and Aβ, the self assembly process displays a distinct lag phase that can be eliminated by the addition of preformed fibers composed of the respective protein [77, 106, 125, 126]. Moreover, like Aβ and CsgA a conformational specific antibody reacts to an intermediate formed during Sup35 polymerization [106, 127]. The curli proteins, CsgB and CsgA, are also similar to the yeast prion proteins, Sup35p, Ure2p, and Rnq1p, in that they all contain the Q/N rich domains [124, 128]. In fact, the GNNQQNY peptide found

within the Q/N rich domain of Sup35p forms biochemical distinct amyloid fibers [129]. This peptide has been used to examine the cross-beta structure of amyloids at high resolution using X-ray crystallography [130]. Also like CsgA and CsgB, oligopeptide repeats are found within the Q/N domain of Sup35p that aid the propagation and amyloidogenecity of the [*PSI*$^{+}$] phenotype [128, 131]. The Q/N domain of Rnq1p also contains several imperfect oligopeptide repeat sequences that are important for the propagation of [*PIN*$^{+}$] [132]. In addition to Sup35p, Ure2p, and Rnq1p, 104 other polypeptides in the *S. cerevisiae* proteome contain Q/N rich domains [133]. However, their ability to form amyloid has not been demonstrated.

The conversion to the prion state for each of [*PSI*$^{+}$], [URE3] and [*PIN*$^{+}$] occurs at a low rate [96, 134]. Even though the conversion rate to the prion state is low, yeast employ molecular chaperones called heat shock proteins to limit exposure to any toxic intermediates formed during prion propagation. Heat shock proteins, such as heat shock protein 104 (Hsp104), play an essential role in modulating the prion state. Propagation of [*PSI*$^{+}$], [URE3], and [*PIN*$^{+}$] all require Hsp104p as deletion of Hsp104 'cures' (i.e. the prion phenotype no longer propagates to daughter cells) cells from [*PSI*$^{+}$] ,[URE3] and [*PIN*$^{+}$]. However, overexpression of Hsp104p also cures [*PSI*$^{+}$] and overexpression of Ydj1p, a member of the Hsp40 family of proteins, cures cells of the [URE3] prion [103, 135, 136]. Shorter and Lindquist reconciled these seemingly contradictory findings by demonstrating that *in vitro* low concentrations Hsp104 catalyzed the formation of intermediates critical for Sup35p and Ure2p fiber formation, while

high concentrations of Hsp104 completely abrogated the ability of both proteins to form an amyloid [106, 127]. These data suggest that Hsp104 may sequester toxic intermediates as well as decrease the time cells are exposed to such intermediates. These findings also suggests that another mechanism heat shock proteins employ to limit exposure to toxic folding intermediates is to speed the formation of an amyloid fiber to the fiber final product.

Filamentous Fungi Het-S Amyloid

Vegetative cell fusions occur within and between individual cells of the filamentous fungi *Podospora anserina*. These fusion events lead to cytoplasmic mixing and the production of a vegetative heterokaryon or multinucleated cells. The *het* locus controls the viability of the fused fungi, whereby heterokaryons that differ at the *het* locus are destroyed. This process is called heterokaryon incompatibility (For review see [137]). The *het* locus has two alleles, *het-s* and *het-S*. Het-S is the soluble protein product of the *het-S* loci while the protein product of the *het-s* loci, Het-s, has the ability to convert to an aggregated prion state. When fusion between a *het-S* cell and a *het-s* cell occurs the aggregated Het-s interacts with soluble Het-S and this interaction induces the incompatibility reaction. This leads to death of the heterokaryon and prevents any fusion from occurring between the two cells [4]. Maddelein *et al.* demonstrated that the heterokaryon incompatibility reaction is induced when cells are transformed with amyloid fibers composed of recombinant Het-s. The incompatibility reaction is not induced when a soluble version of Het-s was transformed into cells. This result

provided direct experimental evidence that strengthened the protein only prion hypothesis [138]. The molecular mechanisms of Het-s-induced cell death are currently unknown.

CPEB

CPEBs are highly conserved RNA-binding proteins localized at neuronal synapses that stabilize messenger RNA molecules [139]. CPEBs have been found to be important for memory retention due to their ability to activate dormant messenger RNA transcripts near neuronal synapses. These activated messages can then be translated into proteins that stabilize neuronal synapses or help create synaptic connections necessary for long term memory [140]. The CPEB protein of the sea hare, *Aplaysia californica* (ApCPEB), contains a Q/N rich domain. Si *et al*. demonstrated that ApCPEB acts as a prion in yeast and that the aggregative amyloid state of CPEB is the functional, RNA-binding, form of the protein [141]. Thus, ApCPEB is functionally active when polymerized into amyloid aggregates, whereas, the wild type functions of Ure2p and Sup35p are impaired when the proteins are aggregated. It has yet to be elucidated if CPEB folds into an amyloid in neuronal cells, but the ability of the protein to do so in yeast suggests it has the capability to do so in other cell types.

Pmel17

Melanocytes and retinal pigment epithelium are specialized cell types responsible for the production of melanin, a tyrosine based polymer that protects

the mammalian eyes and epidermis from ultra-violet damage and other environmental insults. These cells types synthesize melanin within specialized membrane enclosed vesicles called melanosomes [142-144]. Melanosome maturation and polymerization of melanin are dependent on insoluble fibers composed of the PMEL17 protein [8, 145-148]. Fowler and colleagues demonstrated that fibers composed of PMEL17 contain the biochemical hallmarks of amyloid [6]. PMEL17 amyloid fibers function by kinetically enhancing the polymerization of melanin, presumably by acting as a scaffold for reactive melanin precursors [6]. Mammalian cells have evolved several mechanisms to reduce exposure to toxic folding intermediates produced by PMEL17 amyloid polymerization: (1) polymerizing the amyloid fiber in a membrane enclosed vesicle sequestering folding intermediates from the cytoplasm, (2) regulating the start of polymerization via proteolysis, and (3) using reaction kinetics that skew towards the stability of the mature amyloid fiber [6, 7].

Concluding Remarks

Despite over twenty years of AD research the nature of the toxic species of Aβ has yet to be conclusively identified and little is known about how Aβ polypeptide aggregation begins *in vivo*. Insights into these two critical phenomena will undoubtedly lead to advances in AD treatments. The functional amyloids may hold the key to understanding the molecular mechanisms of amyloid fiber toxicity and initiation of amyloid fiber polymerization because they are naturally occurring directed polymerization processes. Not only are the

amyloid fiber end products in both AD and the functional amyloid systems biochemically similar, but a common intermediate has been identified for CsgA, Sup35p, and Aβ polymerization. This suggests that amyloid biogenesis occurs via a conserved mechanism. Interestingly, most of the directed amyloid synthesis pathways discussed herein polymerize to higher order aggregates/fibers *in vivo* and these fibers have physiological nontoxic roles in most cases. A folding intermediate of Mcc amyloid fibers is cytotoxic but not the mature amyloid fiber itself. Thus, it seems likely that the functional amyloids lend credence to the hypothesis that the fiber end product may not be toxic. The role of the chaperone Hsp104 in yeast prion propagation also supports this idea. At high concentrations the chaperone abrogates amyloid fiber polymerization, but at low concentrations Hsp104 kinetically accelerates fiber formation. These results demonstrate two mechanisms cells use to sequester the build up of toxic intermediates. Chaperones either bind the aberrant toxic intermediate which allows the protein the opportunity to refold or the chaperone forces the protein to fold into an amyloid fiber.

These functional amyloid synthesis pathways will continue to provide novel insights regarding amyloid biogenesis. The functional amyloid systems may even address pivotal questions that remain for Alzheimer's disease progression such as, how does amyloid biogenesis begin *in vivo*, what is the most cytotoxic species produced during amyloid biogenesis, and what are the defining features of proteins that preclude the ability to fold into the amyloid

conformation. The answers to these questions will in turn provide novel therapeutic strategies for treating disease-associated amyloidosis such as AD.

The goal of this dissertation is to demonstrate that CsgB is an amyloidogenic protein and that mediates the conversion of soluble CsgA into an amyloid fiber via a template mediated mechanism. The second chapter demonstrates that a truncated version of CsgB polymerizes into an amyloid fiber that accelerates CsgA polyermization. In Chapter III, I devise a new purification protocol that allows for the purification and biochemical characterization of wild type CsgB. The wild type version of CsgB also polymerizes into an amyloid fiber, but at a much faster rate than CsgA or the truncated CsgB studied in Chapter II. The importance of the repeating units and conserved glutamine and asparagine residues found within the repeating untits is examined using mutagenesis in the third chapter. Finally, inhibitors of fiber polyermization are discussed in the conclusion.

Figure Legends

Figure 1.1. Properties of amyloid polymerization. (A) Negatively stained electron micrograph of polymerized Aβ fibers. The scale bar represents 500 nanometers. (B) A graphic representation of amyloid fiber polymerization displaying nucleus dependent kinetics (blue line). Preformed amyloid fibers can act as seeds to speed the kinetics of fiber polymerization (red line). This process eliminates the lag phase associated with nucleus formation. (C) Model of amyloid fiber polymerization. A build up of monomer occurs which leads to the formation

of multimers and finally the amyloid fiber end product. Large arrows represent processes that are energetically favorable while small arrows represent energetically unfavorable processes.

Figure 1.2. Interaction between the curli subunit proteins CsgA and CsgB. (A) Negative stain electron micrograph of wild type cells producing curli. Scale bar represents 200 nanometers. (B) Model of Interbacterial Complementation. A donor cells secretes soluble CsgA that acts as a substrate for CsgB on an acceptor cells where curli biogenesis takes place. (C) A Congo red indicator plate demonstrating interbacterial complementation. The donor cells and the acceptor cells appear white until the two strains intersect. Once the two cell types intersect Congo red binding occurs demonstrating curli fiber polymerization as taken place. The arrow represents the direction in which the acceptor cells were streaked onto the plate. (D) The oligopeptide repeating units that compose the CsgA and CsgB proteins. The three dimensional structures of CsgA and CsgB are predicted to be composed of five imperfect β-strand-loop-β-strand oligopeptide repeats (R1-R5). Amino acids comprising the ß-strand are located below the arrows, and amino acids predicted to comprise the loops are denoted with italicized blue letters. Bolded letters represent amino acids conserved in CsgB and CsgA at each position relative to the start of each repeating unit. Boxed letters represent amino acids conserved throughout the repeating units in both proteins.

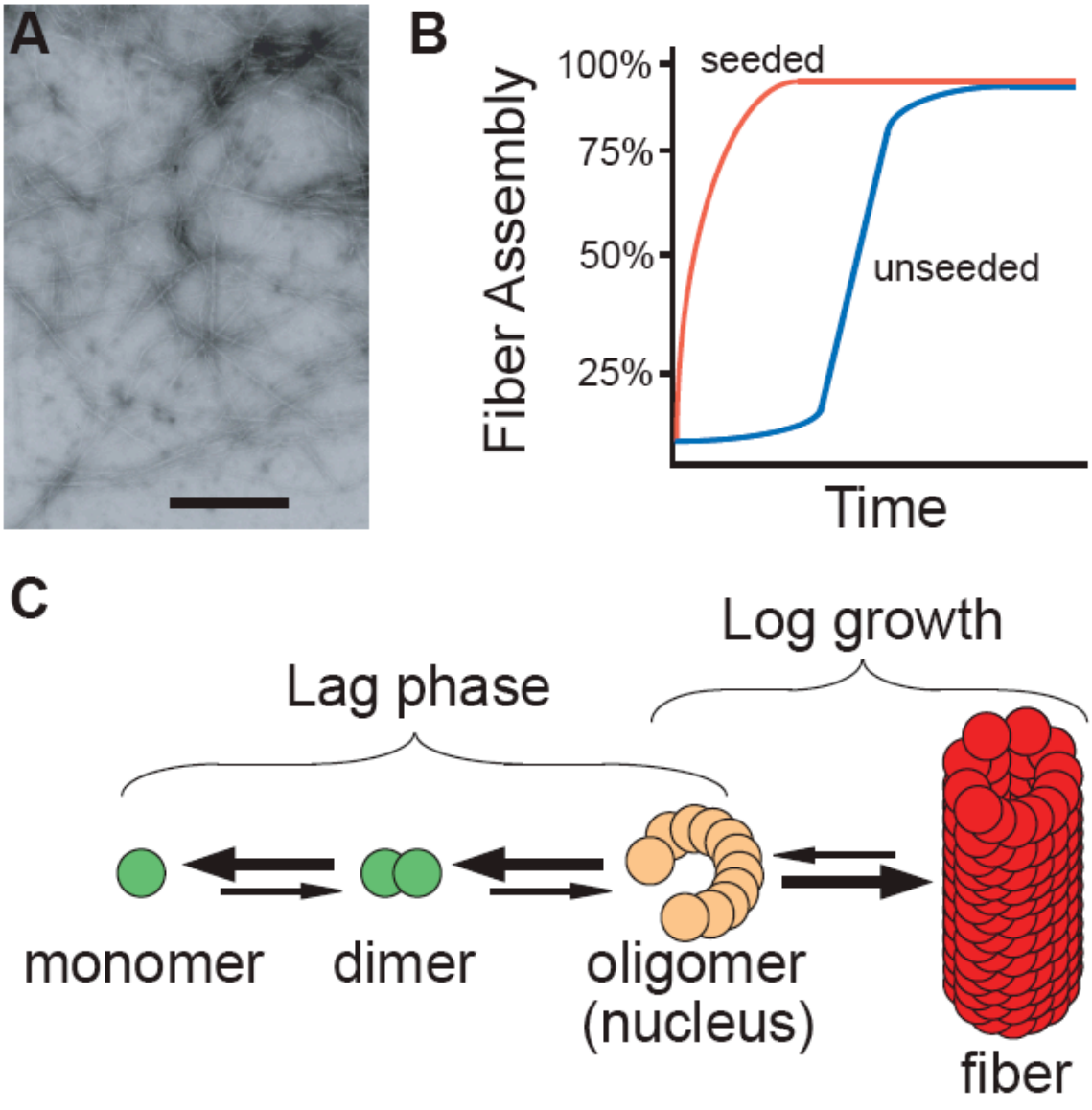

Figure 1.1. Properties of amyloid polymerization.

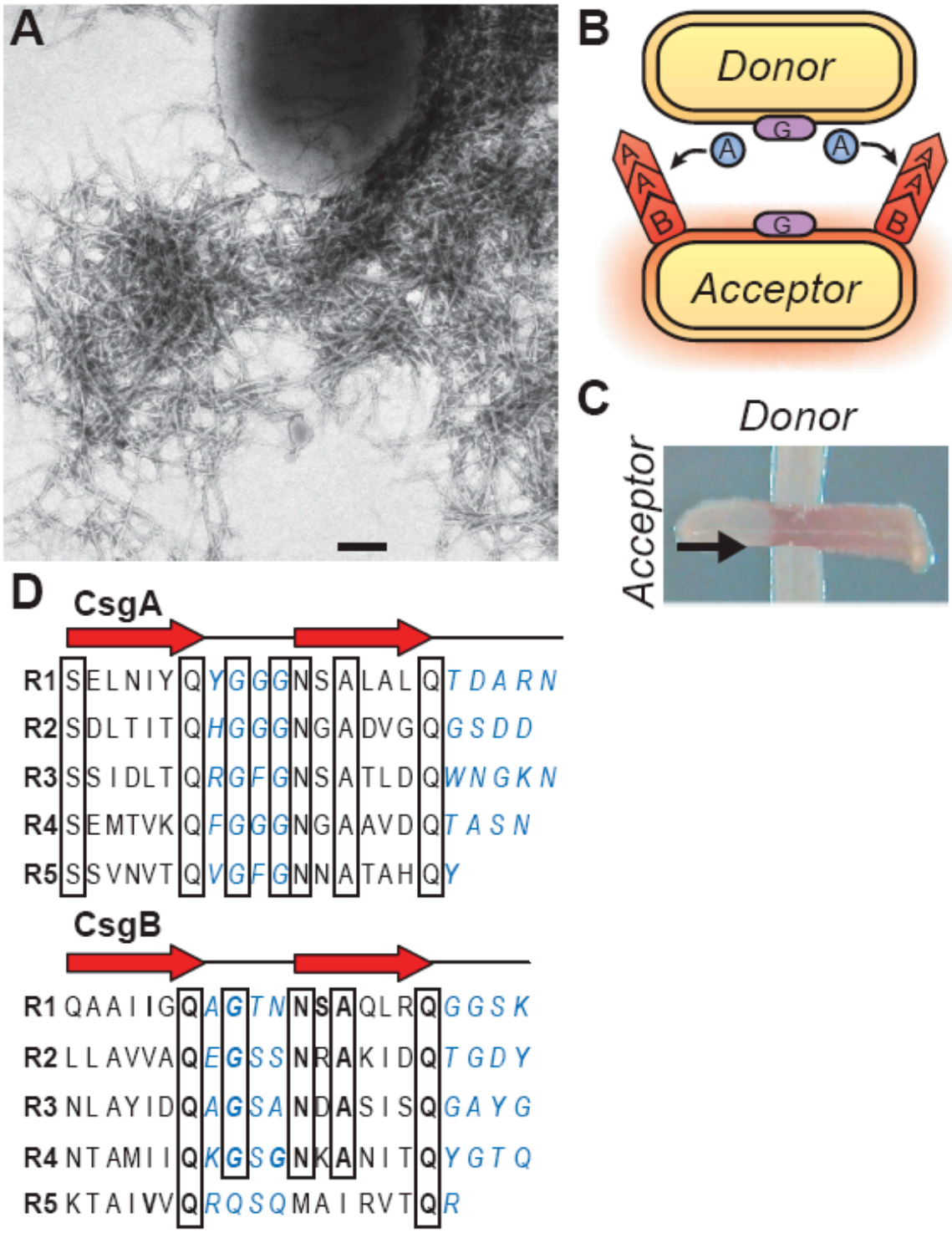

Figure 1.2. Interaction between the curli subunit proteins CsgA and CsgB.

References

1. Smith, J.F., et al., *Characterization of the nanoscale properties of individual amyloid fibrils.* Proc Natl Acad Sci U S A, 2006. **103**(43): p. 15806-11.

2. Chapman, M.R., et al., *Role of Escherichia coli curli operons in directing amyloid fiber formation.* Science, 2002. **295**(5556): p. 851-5.

3. Claessen, D., et al., *A novel class of secreted hydrophobic proteins is involved in aerial hyphae formation in Streptomyces coelicolor by forming amyloid-like fibrils.* Genes Dev, 2003. **17**(14): p. 1714-26.

4. Coustou, V., et al., *The protein product of the het-s heterokaryon incompatibility gene of the fungus Podospora anserina behaves as a prion analog.* Proc Natl Acad Sci U S A, 1997. **94**(18): p. 9773-8.

5. True, H.L., I. Berlin, and S.L. Lindquist, *Epigenetic regulation of translation reveals hidden genetic variation to produce complex traits.* Nature, 2004. **431**(7005): p. 184-7.

6. Fowler, D.M., et al., *Functional amyloid formation within mammalian tissue.* PLoS Biol, 2006. **4**(1): p. e6.

7. Fowler, D.M., et al., *Functional amyloid--from bacteria to humans.* Trends Biochem Sci, 2007. **32**(5): p. 217-24.

8. Kelly, J.W. and W.E. Balch, *Amyloid as a natural product.* J Cell Biol, 2003. **161**(3): p. 461-2.

9. Shorter, J. and S. Lindquist, *Prions as adaptive conduits of memory and inheritance.* Nat Rev Genet, 2005. **6**(6): p. 435-50.

10. Alzheimer, A., *Über eine eigenartige Erkrankung der Hirnrinde.* Allg Zeitschr Psychiatr Psychiatr-Gerichtl Med, 1907. **64**: p. 146.

11. Kidd, M., *Paired helical filaments in electron microscopy of Alzheimer's disease.* Nature, 1963. **197**: p. 192-3.

12. Terry, R.D., N.K. Gonatas, and M. Weiss, *Ultrastructural Studies In Alzheimer's Presenile Dementia.* Am J Pathol, 1964. **44**: p. 269-97.

13. Scherzinger, E., et al., *Huntingtin-encoded polyglutamine expansions form amyloid-like protein aggregates in vitro and in vivo.* Cell, 1997. **90**(3): p. 549-58.

14. Guiroy, D.C., et al., *Amyloid of neurofibrillary tangles of Guamanian parkinsonism-dementia and Alzheimer disease share identical amino acid sequence.* Proc Natl Acad Sci U S A, 1987. **84**(7): p. 2073-7.

15. Glenner, G.G. and C.W. Wong, *Alzheimer's disease: initial report of the purification and characterization of a novel cerebrovascular amyloid protein.* Biochem Biophys Res Commun, 1984. **120**(3): p. 885-90.

16. Wischik, C.M., et al., *Structural characterization of the core of the paired helical filament of Alzheimer disease.* Proc Natl Acad Sci U S A, 1988. **85**(13): p. 4884-8.

17. Haass, C., *Take five--BACE and the gamma-secretase quartet conduct Alzheimer's amyloid beta-peptide generation.* Embo J, 2004. **23**(3): p. 483-8.

18. Zheng, H. and E.H. Koo, *The amyloid precursor protein: beyond amyloid.* Mol Neurodegener, 2006. **1**: p. 5.

19. Hartmann, T., et al., *Distinct sites of intracellular production for Alzheimer's disease A beta40/42 amyloid peptides.* Nat Med, 1997. **3**(9): p. 1016-20.

20. Citron, M., et al., *Mutant presenilins of Alzheimer's disease increase production of 42-residue amyloid beta-protein in both transfected cells and transgenic mice.* Nat Med, 1997. **3**(1): p. 67-72.

21. Raber, J., Y. Huang, and J.W. Ashford, *ApoE genotype accounts for the vast majority of AD risk and AD pathology.* Neurobiol Aging, 2004. **25**(5): p. 641-50.

22. Ye, S., et al., *Apolipoprotein (apo) E4 enhances amyloid beta peptide production in cultured neuronal cells: apoE structure as a potential therapeutic target.* Proc Natl Acad Sci U S A, 2005. **102**(51): p. 18700-5.

23. Bales, K.R., et al., *Apolipoprotein E is essential for amyloid deposition in the APP(V717F) transgenic mouse model of Alzheimer's disease.* Proc Natl Acad Sci U S A, 1999. **96**(26): p. 15233-8.

24. Fryer, J.D., et al., *Human apolipoprotein E4 alters the amyloid-beta 40:42 ratio and promotes the formation of cerebral amyloid angiopathy in an amyloid precursor protein transgenic model.* J Neurosci, 2005. **25**(11): p. 2803-10.

25. Koistinaho, M., et al., *Apolipoprotein E promotes astrocyte colocalization and degradation of deposited amyloid-beta peptides.* Nat Med, 2004. **10**(7): p. 719-26.

26. Zerbinatti, C.V., et al., *Apolipoprotein E and low density lipoprotein receptor-related protein facilitate intraneuronal Abeta42 accumulation in amyloid model mice.* J Biol Chem, 2006. **281**(47): p. 36180-6.

27. Blennow, K., M.J. de Leon, and H. Zetterberg, *Alzheimer's disease.* Lancet, 2006. **368**(9533): p. 387-403.

28. Goedert, M. and M.G. Spillantini, *A century of Alzheimer's disease.* Science, 2006. **314**(5800): p. 777-81.

29. Haass, C. and D.J. Selkoe, *Soluble protein oligomers in neurodegeneration: lessons from the Alzheimer's amyloid beta-peptide.* Nat Rev Mol Cell Biol, 2007. **8**(2): p. 101-12.

30. Hardy, J. and D.J. Selkoe, *The amyloid hypothesis of Alzheimer's disease: progress and problems on the road to therapeutics.* Science, 2002. **297**(5580): p. 353-6.

31. Lomakin, A., et al., *On the nucleation and growth of amyloid beta-protein fibrils: detection of nuclei and quantitation of rate constants.* Proc Natl Acad Sci U S A, 1996. **93**(3): p. 1125-9.

32. Jarrett, J.T. and P.T. Lansbury, Jr., *Seeding "one-dimensional crystallization" of amyloid: a pathogenic mechanism in Alzheimer's disease and scrapie?* Cell, 1993. **73**(6): p. 1055-8.

33. Podlisny, M.B., et al., *Aggregation of secreted amyloid beta-protein into sodium dodecyl sulfate-stable oligomers in cell culture.* J Biol Chem, 1995. **270**(16): p. 9564-70.

34. Podlisny, M.B., et al., *Oligomerization of endogenous and synthetic amyloid beta-protein at nanomolar levels in cell culture and stabilization of monomer by Congo red.* Biochemistry, 1998. **37**(11): p. 3602-11.

35. Walsh, D.M., et al., *Amyloid beta-protein fibrillogenesis. Structure and biological activity of protofibrillar intermediates.* J Biol Chem, 1999. **274**(36): p. 25945-52.

36. Roher, A.E., et al., *Morphology and toxicity of Abeta-(1-42) dimer derived from neuritic and vascular amyloid deposits of Alzheimer's disease.* J Biol Chem, 1996. **271**(34): p. 20631-5.

37. Lorenzo, A. and B.A. Yankner, *Beta-amyloid neurotoxicity requires fibril formation and is inhibited by congo red.* Proc Natl Acad Sci U S A, 1994. **91**(25): p. 12243-7.

38. Yang, F., et al., *Curcumin inhibits formation of amyloid beta oligomers and fibrils, binds plaques, and reduces amyloid in vivo.* J Biol Chem, 2005. **280**(7): p. 5892-901.

39. Pike, C.J., et al., *Neurodegeneration induced by beta-amyloid peptides in vitro: the role of peptide assembly state.* J Neurosci, 1993. **13**(4): p. 1676-87.

40. Pike, C.J., et al., *In vitro aging of beta-amyloid protein causes peptide aggregation and neurotoxicity.* Brain Res, 1991. **563**(1-2): p. 311-4.

41. Bucciantini, M., et al., *Inherent toxicity of aggregates implies a common mechanism for protein misfolding diseases.* Nature, 2002. **416**(6880): p. 507-11.

42. Terry, R.D., et al., *Physical basis of cognitive alterations in Alzheimer's disease: synapse loss is the major correlate of cognitive impairment.* Ann Neurol, 1991. **30**(4): p. 572-80.

43. Lue, L.F., et al., *Soluble amyloid beta peptide concentration as a predictor of synaptic change in Alzheimer's disease.* Am J Pathol, 1999. **155**(3): p. 853-62.

44. Cohen, E., et al., *Opposing activities protect against age-onset proteotoxicity.* Science, 2006. **313**(5793): p. 1604-10.

45. Arrasate, M., et al., *Inclusion body formation reduces levels of mutant huntingtin and the risk of neuronal death.* Nature, 2004. **431**(7010): p. 805-10.

46. Slow, E.J., et al., *Absence of behavioral abnormalities and neurodegeneration in vivo despite widespread neuronal huntingtin inclusions.* Proc Natl Acad Sci U S A, 2005. **102**(32): p. 11402-7.

47. Lambert, M.P., et al., *Diffusible, nonfibrillar ligands derived from Abeta1-42 are potent central nervous system neurotoxins.* Proc Natl Acad Sci U S A, 1998. **95**(11): p. 6448-53.

48. Hartley, D.M., et al., *Protofibrillar intermediates of amyloid beta-protein induce acute electrophysiological changes and progressive neurotoxicity in cortical neurons.* J Neurosci, 1999. **19**(20): p. 8876-84.

49. Nilsberth, C., et al., *The 'Arctic' APP mutation (E693G) causes Alzheimer's disease by enhanced Abeta protofibril formation.* Nat Neurosci, 2001. **4**(9): p. 887-93.
50. Walsh, D.M., et al., *Naturally secreted oligomers of amyloid beta protein potently inhibit hippocampal long-term potentiation in vivo.* Nature, 2002. **416**(6880): p. 535-9.

51. Hoshi, M., et al., *Spherical aggregates of beta-amyloid (amylospheroid) show high neurotoxicity and activate tau protein kinase I/glycogen synthase kinase-3beta.* Proc Natl Acad Sci U S A, 2003. **100**(11): p. 6370-5.

52. Cleary, J.P., et al., *Natural oligomers of the amyloid-beta protein specifically disrupt cognitive function.* Nat Neurosci, 2005. **8**(1): p. 79-84.

53. Lesne, S., et al., *A specific amyloid-beta protein assembly in the brain impairs memory.* Nature, 2006. **440**(7082): p. 352-7.

54. Townsend, M., et al., *Effects of secreted oligomers of amyloid beta-protein on hippocampal synaptic plasticity: a potent role for trimers.* J Physiol, 2006. **572**(Pt 2): p. 477-92.

55. Deshpande, A., et al., *Different conformations of amyloid beta induce neurotoxicity by distinct mechanisms in human cortical neurons.* J Neurosci, 2006. **26**(22): p. 6011-8.

56. Petkova, A.T., et al., *Self-propagating, molecular-level polymorphism in Alzheimer's beta-amyloid fibrils.* Science, 2005. **307**(5707): p. 262-5.

57. Busciglio, J., A. Lorenzo, and B.A. Yankner, *Methodological variables in the assessment of beta amyloid neurotoxicity.* Neurobiol Aging, 1992. **13**(5): p. 609-12.

58. Tsai, J., et al., *Fibrillar amyloid deposition leads to local synaptic abnormalities and breakage of neuronal branches.* Nat Neurosci, 2004. **7**(11): p. 1181-3.

59. Carulla, N., et al., *Molecular recycling within amyloid fibrils.* Nature, 2005. **436**(7050): p. 554-8.

60. Bian, Z., et al., *Expression of and cytokine activation by Escherichia coli curli fibers in human sepsis.* J Infect Dis, 2000. **181**(2): p. 602-12.

61. Bian, Z., et al., *Activation of inducible nitric oxide synthase/nitric oxide by curli fibers leads to a fall in blood pressure during systemic Escherichia coli infection in mice.* J Infect Dis, 2001. **183**(4): p. 612-9.

62. Uhlich, G.A., P.H. Cooke, and E.B. Solomon, *Analyses of the red-dry-rough phenotype of an Escherichia coli O157:H7 strain and its role in biofilm formation and resistance to antibacterial agents.* Appl Environ Microbiol, 2006. **72**(4): p. 2564-72.

63. Wang, X., et al., *Impact of biofilm matrix components on interaction of commensal Escherichia coli with the gastrointestinal cell line HT-29.* Cell Mol Life Sci, 2006. **63**(19-20): p. 2352-63.

64. Vidal, O., et al., *Isolation of an Escherichia coli K-12 mutant strain able to form biofilms on inert surfaces: involvement of a new ompR allele that increases curli expression.* J Bacteriol, 1998. **180**(9): p. 2442-9.

65. White, A.P., et al., *Thin aggregative fimbriae and cellulose enhance long-term survival and persistence of Salmonella.* J Bacteriol, 2006. **188**(9): p. 3219-27.

66. Lawley, T.D., et al., *Genome-wide screen for Salmonella genes required for long-term systemic infection of the mouse.* PLoS Pathog, 2006. **2**(2): p. e11.

67. Barnhart, M.M. and M.R. Chapman, *Curli biogenesis and function.* Annu Rev Microbiol, 2006. **60**: p. 131-47.

68. Hammar, M., et al., *Expression of two csg operons is required for production of fibronectin- and congo red-binding curli polymers in Escherichia coli K-12.* Mol Microbiol, 1995. **18**(4): p. 661-70.

69. Romling, U., et al., *Occurrence and regulation of the multicellular morphotype in Salmonella serovars important in human disease.* Int J Med Microbiol, 2003. **293**(4): p. 273-85.

70. Romling, U., et al., *Multicellular and aggregative behaviour of Salmonella typhimurium strains is controlled by mutations in the agfD promoter.* Mol Microbiol, 1998. **28**(2): p. 249-64.

71. Hammer, N.D., J.C. Schmidt, and M.R. Chapman, *The curli nucleator protein, CsgB, contains an amyloidogenic domain that directs CsgA polymerization.* Proc Natl Acad Sci U S A, 2007.

72. Loferer, H., M. Hammar, and S. Normark, *Availability of the fibre subunit CsgA and the nucleator protein CsgB during assembly of fibronectin-binding curli is limited by the intracellular concentration of the novel lipoprotein CsgG.* Mol Microbiol, 1997. **26**(1): p. 11-23.

73. Robinson, L.S., et al., *Secretion of curli fibre subunits is mediated by the outer membrane-localized CsgG protein.* Mol Microbiol, 2006. **59**(3): p. 870-81.

74. Hammar, M., Z. Bian, and S. Normark, *Nucleator-dependent intercellular assembly of adhesive curli organelles in Escherichia coli.* Proc Natl Acad Sci U S A, 1996. **93**(13): p. 6562-6.

75. Collinson, S.K., et al., *Structural predictions of AgfA, the insoluble fimbrial subunit of Salmonella thin aggregative fimbriae.* J Mol Biol, 1999. **290**(3): p. 741-56.

76. White, A.P., et al., *Structure and characterization of AgfB from Salmonella enteritidis thin aggregative fimbriae.* J Mol Biol, 2001. **311**(4): p. 735-49.

77. Wang, X., et al., *In vitro polymerization of a functional Escherichia coli amyloid protein.* J Biol Chem, 2007. **282**(6): p. 3713-9.

78. Kayed, R., et al., *Common structure of soluble amyloid oligomers implies common mechanism of pathogenesis.* Science, 2003. **300**(5618): p. 486-9.

79. Elliot, M.A., et al., *The chaplins: a family of hydrophobic cell-surface proteins involved in aerial mycelium formation in Streptomyces coelicolor.* Genes Dev, 2003. **17**(14): p. 1727-40.

80. de Lorenzo, V., *Factors affecting microcin E492 production.* J Antibiot (Tokyo), 1985. **38**(3): p. 340-5.

81. de Lorenzo, V., J.L. Martinez, and C. Asensio, *Microcin-mediated interactions between Klebsiella pneumoniae and Escherichia coli strains.* J Gen Microbiol, 1984. **130**(2): p. 391-400.

82. Bieler, S., et al., *Amyloid formation modulates the biological activity of a bacterial protein.* J Biol Chem, 2005. **280**(29): p. 26880-5.

83. Hetz, C., et al., *Microcin E492, a channel-forming bacteriocin from Klebsiella pneumoniae, induces apoptosis in some human cell lines.* Proc Natl Acad Sci U S A, 2002. **99**(5): p. 2696-701.

84. Oh, J., et al., *Amyloidogenesis of type III-dependent harpins from plant pathogenic bacteria.* J Biol Chem, 2007. **282**(18): p. 13601-9.

85. Greenberg, J.T., *Programmed cell death: a way of life for plants.* Proc Natl Acad Sci U S A, 1996. **93**(22): p. 12094-7.

86. Greenberg, J.T., *Programmed Cell Death in Plant-Pathogen Interactions.* Annu Rev Plant Physiol Plant Mol Biol, 1997. **48**: p. 525-545.

87. Pennell, R.I. and C. Lamb, *Programmed Cell Death in Plants.* Plant Cell, 1997. **9**(7): p. 1157-1168.

88. Alteri, C.J., et al., *Mycobacterium tuberculosis produces pili during human infection.* Proc Natl Acad Sci U S A, 2007. **104**(12): p. 5145-50.

89. Plomp, M., et al., *In vitro high-resolution structural dynamics of single germinating bacterial spores.* Proc Natl Acad Sci U S A, 2007. **104**(23): p. 9644-9.

90. Kim, H., et al., *The Bacillus subtilis spore coat protein interaction network.* Mol Microbiol, 2006. **59**(2): p. 487-502.

91. Brachmann, A., U. Baxa, and R.B. Wickner, *Prion generation in vitro: amyloid of Ure2p is infectious.* Embo J, 2005. **24**(17): p. 3082-92.

92. Derkatch, I.L., et al., *Prions affect the appearance of other prions: the story of [PIN(+)].* Cell, 2001. **106**(2): p. 171-82.

93. King, C.Y. and R. Diaz-Avalos, *Protein-only transmission of three yeast prion strains.* Nature, 2004. **428**(6980): p. 319-23.

94. Patel, B.K. and S.W. Liebman, *"Prion-proof" for [PIN+]: infection with in vitro-made amyloid aggregates of Rnq1p-(132-405) induces [PIN+].* J Mol Biol, 2007. **365**(3): p. 773-82.

95. Tanaka, M., et al., *Conformational variations in an infectious protein determine prion strain differences.* Nature, 2004. **428**(6980): p. 323-8.

96. Wickner, R.B., *[URE3] as an altered URE2 protein: evidence for a prion analog in Saccharomyces cerevisiae.* Science, 1994. **264**(5158): p. 566-9.

97. Glover, J.R., et al., *Self-seeded fibers formed by Sup35, the protein determinant of [PSI+], a heritable prion-like factor of S. cerevisiae.* Cell, 1997. **89**(5): p. 811-9.

98. Kimura, Y., S. Koitabashi, and T. Fujita, *Analysis of yeast prion aggregates with amyloid-staining compound in vivo.* Cell Struct Funct, 2003. **28**(3): p. 187-93.

99. Kryndushkin, D.S., et al., *Yeast [PSI+] prion aggregates are formed by small Sup35 polymers fragmented by Hsp104.* J Biol Chem, 2003. **278**(49): p. 49636-43.

100. Masison, D.C. and R.B. Wickner, *Prion-inducing domain of yeast Ure2p and protease resistance of Ure2p in prion-containing cells.* Science, 1995. **270**(5233): p. 93-5.

101. Patino, M.M., et al., *Support for the prion hypothesis for inheritance of a phenotypic trait in yeast.* Science, 1996. **273**(5275): p. 622-6.

102. Paushkin, S.V., et al., *Propagation of the yeast prion-like [psi+] determinant is mediated by oligomerization of the SUP35-encoded polypeptide chain release factor.* Embo J, 1996. **15**(12): p. 3127-34.

103. Sondheimer, N. and S. Lindquist, *Rnq1: an epigenetic modifier of protein function in yeast.* Mol Cell, 2000. **5**(1): p. 163-72.

104. Speransky, V.V., et al., *Prion filament networks in [URE3] cells of Saccharomyces cerevisiae.* J Cell Biol, 2001. **153**(6): p. 1327-36.

105. Taylor, K.L., et al., *Prion domain initiation of amyloid formation in vitro from native Ure2p.* Science, 1999. **283**(5406): p. 1339-43.

106. Shorter, J. and S. Lindquist, *Destruction or potentiation of different prions catalyzed by similar Hsp104 remodeling activities.* Mol Cell, 2006. **23**(3): p. 425-38.

107. Ter-Avanesyan, M.D., et al., *The SUP35 omnipotent suppressor gene is involved in the maintenance of the non-Mendelian determinant [psi+] in the yeast Saccharomyces cerevisiae.* Genetics, 1994. **137**(3): p. 671-6.

108. Cooper, T.G., *Transmitting the signal of excess nitrogen in Saccharomyces cerevisiae from the Tor proteins to the GATA factors: connecting the dots.* FEMS Microbiol Rev, 2002. **26**(3): p. 223-38.

109. Beck, T. and M.N. Hall, *The TOR signalling pathway controls nuclear localization of nutrient-regulated transcription factors.* Nature, 1999. **402**(6762): p. 689-92.

110. Blinder, D., P.W. Coschigano, and B. Magasanik, *Interaction of the GATA factor Gln3p with the nitrogen regulator Ure2p in Saccharomyces cerevisiae.* J Bacteriol, 1996. **178**(15): p. 4734-6.

111. Cardenas, M.E., et al., *The TOR signaling cascade regulates gene expression in response to nutrients.* Genes Dev, 1999. **13**(24): p. 3271-9.

112. Hardwick, J.S., et al., *Rapamycin-modulated transcription defines the subset of nutrient-sensitive signaling pathways directly controlled by the Tor proteins.* Proc Natl Acad Sci U S A, 1999. **96**(26): p. 14866-70.

113. Magasanik, B. and C.A. Kaiser, *Nitrogen regulation in Saccharomyces cerevisiae.* Gene, 2002. **290**(1-2): p. 1-18.

114. Cox, K.H., et al., *Saccharomyces cerevisiae GATA sequences function as TATA elements during nitrogen catabolite repression and when Gln3p is excluded from the nucleus by overproduction of Ure2p.* J Biol Chem, 2000. **275**(23): p. 17611-8.

115. Nakayashiki, T., et al., *Yeast prions [URE3] and [PSI+] are diseases.* Proc Natl Acad Sci U S A, 2005. **102**(30): p. 10575-80.

116. Shewmaker, F., et al., *Ure2p Function Is Enhanced by Its Prion Domain in Saccharomyces cerevisiae.* Genetics, 2007. **176**(3): p. 1557-65.

117. Stansfield, I., et al., *The products of the SUP45 (eRF1) and SUP35 genes interact to mediate translation termination in Saccharomyces cerevisiae.* Embo J, 1995. **14**(17): p. 4365-73.

118. Cox, B.S., M.F. Tuite, and C.J. Mundy, *Reversion from suppression to nonsuppression in SUQ5 [psi+] strains of yeast: the classificaion of mutations.* Genetics, 1980. **95**(3): p. 589-609.

119. Cox, B.S., *[PSI], a cytoplasmic suppressor of super-supression in yeast.* Heredity, 1965. **20**: p. 505-521.

120. True, H.L. and S.L. Lindquist, *A yeast prion provides a mechanism for genetic variation and phenotypic diversity.* Nature, 2000. **407**(6803): p. 477-83.

121. Chernoff, Y.O., et al., *Evolutionary conservation of prion-forming abilities of the yeast Sup35 protein.* Mol Microbiol, 2000. **35**(4): p. 865-76.

122. Jensen, M.A., et al., *Molecular population genetics and evolution of a prion-like protein in Saccharomyces cerevisiae.* Genetics, 2001. **159**(2): p. 527-35.

123. Nakayashiki, T., et al., *Yeast [PSI+] "prions" that are crosstransmissible and susceptible beyond a species barrier through a quasi-prion state.* Mol Cell, 2001. **7**(6): p. 1121-30.

124. Osherovich, L.Z. and J.S. Weissman, *Multiple Gln/Asn-rich prion domains confer susceptibility to induction of the yeast [PSI(+)] prion.* Cell, 2001. **106**(2): p. 183-94.

125. Fay, N., et al., *Assembly of the yeast prion Ure2p into protein fibrils. Thermodynamic and kinetic characterization.* J Biol Chem, 2003. **278**(32): p. 30199-205.

126. Thual, C., et al., *Structural characterization of Saccharomyces cerevisiae prion-like protein Ure2.* J Biol Chem, 1999. **274**(19): p. 13666-74.

127. Shorter, J. and S. Lindquist, *Hsp104 catalyzes formation and elimination of self-replicating Sup35 prion conformers.* Science, 2004. **304**(5678): p. 1793-7.

128. Liu, J.J. and S. Lindquist, *Oligopeptide-repeat expansions modulate 'protein-only' inheritance in yeast.* Nature, 1999. **400**(6744): p. 573-6.

129. Balbirnie, M., R. Grothe, and D.S. Eisenberg, *An amyloid-forming peptide from the yeast prion Sup35 reveals a dehydrated beta-sheet structure for amyloid.* Proc Natl Acad Sci U S A, 2001. **98**(5): p. 2375-80.

130. Nelson, R., et al., *Structure of the cross-beta spine of amyloid-like fibrils.* Nature, 2005. **435**(7043): p. 773-8.

131. Osherovich, L.Z., et al., *Dissection and design of yeast prions.* PLoS Biol, 2004. **2**(4): p. E86.

132. Vitrenko, Y.A., et al., *Propagation of the [PIN+] prion by fragments of Rnq1 fused to GFP.* Curr Genet, 2007. **51**(5): p. 309-19.

133. Michelitsch, M.D. and J.S. Weissman, *A census of glutamine/asparagine-rich regions: implications for their conserved function and the prediction of novel prions.* Proc Natl Acad Sci U S A, 2000. **97**(22): p. 11910-5.

134. Lund, P.M. and B.S. Cox, *Reversion analysis of [psi-] mutations in Saccharomyces cerevisiae.* Genet Res, 1981. **37**(2): p. 173-82.

135. Chernoff, Y.O., et al., *Role of the chaperone protein Hsp104 in propagation of the yeast prion-like factor [psi+].* Science, 1995. **268**(5212): p. 880-4.

136. Moriyama, H., H.K. Edskes, and R.B. Wickner, *[URE3] prion propagation in Saccharomyces cerevisiae: requirement for chaperone Hsp104 and curing by overexpressed chaperone Ydj1p.* Mol Cell Biol, 2000. **20**(23): p. 8916-22.

137. Saupe, S.J., *Molecular genetics of heterokaryon incompatibility in filamentous ascomycetes.* Microbiol Mol Biol Rev, 2000. **64**(3): p. 489-502.

138. Maddelein, M.L., et al., *Amyloid aggregates of the HET-s prion protein are infectious.* Proc Natl Acad Sci U S A, 2002. **99**(11): p. 7402-7.

139. Mendez, R. and J.D. Richter, *Translational control by CPEB: a means to the end.* Nat Rev Mol Cell Biol, 2001. **2**(7): p. 521-9.

140. Si, K., et al., *A neuronal isoform of CPEB regulates local protein synthesis and stabilizes synapse-specific long-term facilitation in aplysia.* Cell, 2003. **115**(7): p. 893-904.

141. Si, K., S. Lindquist, and E.R. Kandel, *A neuronal isoform of the aplysia CPEB has prion-like properties.* Cell, 2003. **115**(7): p. 879-91.

142. Hearing, V.J., *The melanosome: the perfect model for cellular responses to the environment.* Pigment Cell Res, 2000. **13 Suppl 8**: p. 23-34.

143. Land, E.J., C.A. Ramsden, and P.A. Riley, *Quinone chemistry and melanogenesis.* Methods Enzymol, 2004. **378**: p. 88-109.

144. Marks, M.S. and M.C. Seabra, *The melanosome: membrane dynamics in black and white.* Nat Rev Mol Cell Biol, 2001. **2**(10): p. 738-48.

145. Berson, J.F., et al., *Pmel17 initiates premelanosome morphogenesis within multivesicular bodies.* Mol Biol Cell, 2001. **12**(11): p. 3451-64.

146. Berson, J.F., et al., *Proprotein convertase cleavage liberates a fibrillogenic fragment of a resident glycoprotein to initiate melanosome biogenesis.* J Cell Biol, 2003. **161**(3): p. 521-33.

147. Chakraborty, A.K., et al., *Polymerization of 5,6-dihydroxyindole-2-carboxylic acid to melanin by the pmel 17/silver locus protein.* Eur J Biochem, 1996. **236**(1): p. 180-8.

148. Lee, Z.H., et al., *Characterization and subcellular localization of human Pmel 17/silver, a 110-kDa (pre)melanosomal membrane protein associated with 5,6,-dihydroxyindole-2-carboxylic acid (DHICA) converting activity.* J Invest Dermatol, 1996. **106**(4): p. 605-10.

Chapter II

The curli nucleator protein, CsgB, contains an amyloidogenic domain that directs CsgA polymerization

[This chapter is a modified version of Hammer, N.D., Schmidt, J.C., and Chapman M.R. accepted for publication to the Proceedings of the National Academy of Sciences July, 2007]

Abstract

Curli are functional amyloid fibers assembled by enteric bacteria such as *Escherichia coli* and *Salmonella* spp. In *E. coli*, the polymerization of the major curli fiber subunit protein CsgA into an amyloid fiber is dependent on the minor curli subunit protein, CsgB. The outer membrane-localized CsgB protein shares nearly 30% sequence identity with the amyloid-forming protein CsgA, suggesting that CsgB might also have amyloidogenic properties. Here, we characterized the biochemical properties of CsgB and the molecular basis for CsgB-mediated nucleation of CsgA. Deletion analysis revealed that a CsgB molecule missing 19 amino acids from its C-terminus ($CsgB_{trunc}$) was not outer membrane-associated, but secreted away from the cell. $CsgB_{trunc}$ was overexpressed and purified from the extracellular milieu of cells as a SDS-soluble, non-aggregated protein. Soluble $CsgB_{trunc}$ assembled into fibers that bound to the amyloid specific dyes

Congo red and thioflavin-T. $CsgB_{trunc}$ fibers were able to seed soluble CsgA polymerization *in vitro*. $CsgB_{trunc}$ displayed modest nucleator activity *in vivo*, as demonstrated by its ability to convert extracellular CsgA into an amyloid fiber. Unlike WT CsgB, $CsgB_{trunc}$ was only able to act as a nucleator when cells were genetically manipulated to secrete higher concentrations of CsgA. This work represents the first demonstration of functional amyloid nucleation and it suggests an elegant model for how *E. coli* guides efficient amyloid fiber formation on the cell surface.

Introduction

Enteric bacteria such as *Escherichia coli* and *Salmonella* spp. produce amyloid fibers called curli that are the major proteinacious component of a complex extracellular matrix. The extracellular matrix participates in many aspects of *E. coli* and *Salmonella* spp. physiology and pathogenicity. For example, curli and the extracellular matrix convey resistance to desiccation and long-term survival, host cell adhesion and invasion, and immune system activation [1-7]. Curli are also critical determinants of biofilm formation where they most likely mediate the initial step of surface attachment [6, 8, 9]. Curliated bacteria colonize chemically diverse surfaces such as plant tissues, stainless steel and glass [10-12].

Curli are assembled by a unique and highly regulated extracellular nucleation/precipitation pathway. At least six proteins, encoded by the divergently transcribed *csgBA* and *csgDEFG* operons (*csg*, curli specific genes), are dedicated to curli formation in *E. coli* [8, 13]. The major curli subunit protein, CsgA is nucleated

into a fiber by the minor fiber subunit, CsgB [14, 15]. As a result, both subunits are incorporated into the fiber [16]. Polymerization is thought to occur after secretion of the subunits to the extracellular space, as CsgA and CsgB do not have to be expressed from the same cell in order to assemble curli. In a process called 'interbacterial complementation', CsgA secreted from a *ΔcsgB* donor cell can be assembled into a fiber on the surface of an CsgB-producing acceptor cell [8, 15, 17]. Once polymerized, curli fibers exhibit the biochemical and structural properties of amyloids [17].

Amyloid fiber formation is traditionally associated with human neurodegenerative conditions including Alzheimer's, Parkinson's, and the prion diseases [18]. The proteins associated the eukaryotic amyloid diseases transition from natively soluble conformations into SDS insoluble, non-branching, β-sheet fibers. This conformational change is preceded by a lag phase during which cytotoxic intermediates are formed [19, 20].

Curli represent a novel twist to the conventional view of amyloidogenesis because typical disease-associated amyloid formation is considered an off-pathway protein folding event, whereas, curli are the product of a highly regulated and directed process. However, the fundamental similarities between curli and disease-associated amyloid biogenesis suggest that amyloid fiber polymerization in general occurs via a conserved protein folding process. Thus, understanding how functional amyloids, such as curli, mediate efficient amyloid nucleation on the cell surface will provide insight into disease-associated amyloidogenesis and cytotoxicity.

Like disease-associated amyloids, curli are non-branching, β-sheet rich fibers that are resistant to protease digestion and denaturation by 1% SDS [17, 21-24]. Amyloid fibers, including curli, are propagated by the addition of soluble precursors to the growing fiber tip in a process called seeding [25-27]. For example, the polymerization of purified CsgA *in vitro* is characterized by a 1-2 hour lag phase that precedes rapid fiber elongation (33). The lag phase can be significantly shortened by the addition of preformed CsgA fibers [27]. The CsgA fiber seeds are predicted to provide a specific template that guides fiber elongation and allows polymerization to proceed with a shorter lag phase. Amyloid seeding is usually observed between proteins and fibers with identical or nearly identical amino acid sequences [28].

Although CsgA polymerization can be ameliorated by fiber seeds *in vitro*, assembly of CsgA polymers on the bacterial cell surface is dependent on the CsgB nucleator protein. The molecular and structural mechanisms of CsgB-mediated nucleation are not known; although we hypothesize that CsgB may be an amyloidogenic protein that provides a seed or template to CsgA that promotes curli formation. Consistent with this hypothesis, CsgA and CsgB are nearly 30% identical at the amino acid level and *in silico* molecular modeling predicts that they adopt a similar cross β-strand structure [16, 24]. Both CsgB and CsgA contain a conserved five-fold sequence homology within their amino acid sequences [8, 15, 16, 24]. In CsgA these regions of homology, called repeating units, have recently been demonstrated to be amyloidogenic [27].

In order to determine the molecular mechanism of curli fiber nucleation, we have biochemically and genetically characterized CsgB. For the first time, we demonstrate CsgB-mediated nucleation *in vitro* and show that CsgB is itself an amyloidogenic protein, providing insight into how these functional amyloid fibers are assembled.

Results

$CsgB_{trunc}$ forms amyloid-like fibers in vitro. The similarity in amino acid content and the *in silico* structural predictions of CsgA and CsgB suggest that these proteins may share biochemical properties (Fig. 2.1A). Numbering from the indicated serine residues, the first four repeating units from CsgA and CsgB contain at least five identical amino acids: a glutamine at position seven, a glycine at position nine, an asparagine at position twelve, an alanine at position fourteen, and another glutamine at position eighteen (Fig. 2.1A). Thus, the consensus sequence of the β-strand-loop-β-strand structure for each CsgA repeating unit would be Ser X_5 Gln X_1 Gly X_1 Gly Asn X_1 Ala X_3 Gln, while the consensus sequence of the first four repeating units of CsgB are X_6 Gln X_1 Gly X_2 Asn X_1 Ala X_3 Gln (Fig. 2.1A). Although sequence alignments comparing CsgA to CsgB reveal a high degree of amino acid conservation between the first four repeating units, the fifth repeating unit (amino acids 133-151) of CsgB is less conserved (Fig. 2.1A). The fifth repeating unit of CsgB does not complete the medial glycine, asparagine, or alanine stacks conserved in all five CsgA repeating units or in the first four repeating units of CsgB. Furthermore, four of

the nineteen amino acids in the C-terminal domain of CsgB are positively charged amino acids, a higher percent of charged amino acids than any of the other repeating units found within either protein (Fig. 2.1A). Because the imperfect repeating units of CsgA are amyloidogenic and the first four repeating units of CsgB share a high degree of conservation to CsgA we hypothesized that the first four repeating units of CsgB may also be amyloidogenic.

To test the hypothesis that the first four repeating units of CsgB contained amyloid-like properties, a *csgB* allele missing the C-terminal repeating unit (called $csgB_{trunc}$; containing a C-terminal deletion of amino acids from 133-151) was cloned into the expression vector, pNH2. WT *csgB* and $csgB_{trunc}$ were expressed in the Δ*csg* strain LSR12 that contained a plasmid encoding CsgG, the proposed curli outer membrane secretion protein [29, 30]. Western blot analysis revealed that WT CsgB was cell associated, but $CsgB_{trunc}$ was secreted away from the cells in a CsgG dependent manner (Fig. 2.1B). Both WT CsgB and $CsgB_{trunc}$ were SDS soluble when expressed in the absence of CsgA (Fig. 2.1B). However, WT *csgB* expression was considerably reduced compared to $csgB_{trunc}$ and repeated attempts to purifiy WT CsgB were unsuccessful. Because outer membrane-associated WT CsgB was not amendable to purification, we focused on characterizing the biochemical properties of $CsgB_{trunc}$.

$CsgB_{trunc}$ was affinity purified from cell free supernatants. Immediately after purification, $CsgB_{trunc}$ was SDS soluble and migrated to its predicted molecular weight in an SDS-PAGE gel **(**Fig. 2.1C). However, after incubation at room temperature for 24 hours a precipitate appeared in $CsgB_{trunc}$-containing samples,

and $CsgB_{trunc}$ no longer migrated into an SDS-PAGE gel, indicating that $CsgB_{trunc}$ had assembled into SDS-insoluble aggregates. $CsgB_{trunc}$ migrated into an SDS-PAGE gel when the aggregates were pre-treated with 90% formic acid (FA) (Fig. 2.1D).

The ultrastructure of $CsgB_{trunc}$ aggregates was investigated by transmission electron microscopy (TEM) and with the amyloid specific dyes thioflavin T and Congo red [31-34]. TEM analysis of purified $CsgB_{trunc}$ revealed the presence of highly ordered, amyloid-like fibers (Fig. 2.2A). When freshly purified $CsgB_{trunc}$ was mixed with the amyloid-specific dye, thioflavin T fluorescence increased in a concentration dependent manner after an approximately 100 minute lag phase (Fig. 2.2B). Amyloid formation was also assessed using the diazo dye Congo red, which produces a unique spectral pattern in the presence of an amyloid fiber called a 'red shift' [35]**.** $CsgB_{trunc}$ aggregates mixed with Congo red had a maximum absorbance at 501 nanometers (nm). The maximum absorbance of freshly purified $CsgB_{trunc}$ was 485 nm while the maximum absorbance of the non-amyloid protein bovine serum albumin mixed with Congo red was 491 nm (Fig. 2.2C).

The structural changes that occur during $CsgB_{trunc}$ polymerization were measured using circular dichroism (CD). The CD spectra of freshly purified $CsgB_{trunc}$ displayed a trough at 198 nm, which is characteristic of proteins that adopt a random coil structure (Fig. 2.2D open circles). Following incubation of $CsgB_{trunc}$ at room temperature for 24 hours the CD spectrum revealed a trough at 212 nm (Fig. 2.2D open squares). Upon prolonged incubation, the CD analysis of

$CsgB_{trunc}$ revealed a trough at 218 nm, indicative of a β-sheet rich conformation (Fig. 2.2D closed squares). Collectively, the $CsgB_{trunc}$ aggregates are: SDS insoluble, β-sheet-rich fibers that interact with the amyloid specific dyes thioflavin T and Congo red. These biochemical features are consistent with the hypothesis that $CsgB_{trunc}$ forms amyloid-like aggregates.

$CsgB_{trunc}$ can Nucleate CsgA in vitro. The biochemical analysis of $CsgB_{trunc}$ demonstrated that the first four repeating units of CsgB contained an amyloidogenic domain. We next asked if $CsgB_{trunc}$ fibers provided a nucleation surface for CsgA polymerization. CsgA's transition into an amyloid fiber in vitro is characterized by distinguishable lag, growth, and stationary phases. The lag phase can be shortened by the addition of preformed CsgA fibers [27]. When mixed with thioflavin T, the relative fluorescence units of a 30 μM solution of freshly purified CsgA increased after a 100 minute lag phase (Fig. 2.3A closed circles). The lag phase of CsgA polymerization was dramatically shortened when 10% w/w or 6% w/w $CsgB_{trunc}$ aggregates were added to the reaction (Fig. 2.3A open squares and circles, respectively). As a control for non-specific seeding of CsgA, we used amyloid fibers derived from the IAPP protein [36]. The lag phase of CsgA was not reduced when 17% w/w of IAPP seeds were added (Fig. 2.3B), suggesting that CsgA seeding is a phenomena specific to the proteins that compose the curli fiber, CsgB and CsgA. TEM analysis of the aggregates produced when CsgA was seeded by $CsgB_{trunc}$ revealed fibers with a similar structure to those produced by CsgA self-polymerization (Compare Fig. 2.3C to Fig. 2.3D). These results suggest that $CsgB_{trunc}$ promotes the conversion of

soluble CsgA into an insoluble fiber in a specific manner, a process defined as nucleation.

$CsgB_{trunc}$ is secreted from the cell and is sufficient for nucleation in vivo. To determine if $CsgB_{trunc}$ had retained nucleator activity *in vivo*, *$csgB_{trunc}$* was expressed under the control of the *csgBA* promoter in plasmid pNH1. Colonies of *E. coli* producing curli fibers stain red when grown on Congo red indicator plates. The *csgB* deletion strain harboring pNH1 (*$csgB_{trunc}$*), pLR8 (WT *csgB*), or pLR2 (empty vector) were streaked on Congo red indicator plates and incubated at 26° C. After 48 hours of growth on Congo red indicator plates WT and *csgB*/pLR8 cells stained red, while *csgB*/pNH1 (*$csgB_{trunc}$*) cells were light red (Fig. 2.4A compare #1, #3 and #4). Western blotting was used to localize $CsgB_{trunc}$ expressed by cells grown under curli-inducing conditions. WT CsgB was detected in whole cell samples by western analysis, while $CsgB_{trunc}$ was not (Fig. 2.4B compare top panel whole cell lanes 2, 5 and 6). However, $CsgB_{trunc}$ was detected in samples in which the underlying agar was collected along with the whole cells (Fig. 2.4B compare bottom panel agar plug lanes 2, 5 and 6). Therefore, $CsgB_{trunc}$ is not cell associated, confirming our previous finding in Fig. 2.1B that, unlike WT CsgB, $CsgB_{trunc}$ is secreted away from the cell as an SDS-soluble protein.

The localization defect of $CsgB_{trunc}$ might account for its inability to nucleate CsgA into a fiber *in vivo*. Since the local concentration of CsgA would be predicted to be highest close to the cell surface, and $CsgB_{trunc}$ is secreted

away from cells into the extracellular space, we reasoned that $CsgB_{trunc}$ would have a decreased chance of interacting with CsgA. To increase the probability that $CsgB_{trunc}$ would interact with CsgA, we utilized two genetically modified *csgB* strains that secrete more CsgA. The first strain overexpressed CsgG, proposed to be a central component of the curlin secretion apparatus [29]. Overexpression of CsgG has been demonstrated to increase the secretion of CsgA [30]. When grown under curli expressing conditions on Congo red indicator plates, *csgB* cells containing pNH1 (*csgB*$_{trunc}$) and pMC1 (*csgG*) stained darker red than *csgB* cells containing pNH1 (*csgB*$_{trunc}$) or pMC1 (*csgG*) alone (Fig. 2.4A). The second strain we utilized was a *csgF* mutant. A *csgF* mutant secretes more CsgA, although the precise role of this protein is still unresolved [17]. A *csgBF* mutant was transformed with pNH1 (*csgB*$_{trunc}$). $CsgB_{trunc}$ was able to partially restore Congo red-binding to a *csgBF* strain (Fig. 2.4B #5). Congo red binding was dependent on the expression of $CsgB_{trunc}$ as the *csgBF*/pLR2 (empty vector) remained white on Congo red indicator plates (Fig. 2.4B #8). Congo red binding was also dependent on CsgA as a *csgFBA*/pNH1 did not bind Congo red (data not shown).

Another measure of fiber formation is the SDS solubility of both CsgA and CsgB. CsgA and CsgB that have assembled into an amyloid fiber are resistant to depolymerization by SDS and need to be treated with formic acid (FA) in order to liberate the monomers [22]. At 48 hours CsgA became SDS insoluble in *csgBF* /pNH1 (*csgB*$_{trunc}$) cells (Fig. 2.4D; compare top panel whole cell lanes 9 and 10). $CsgB_{trunc}$ was also SDS insoluble at 48 hours when expressed in *csgBF* cells

(Fig. 2.4C; compare top panel whole cell lanes 9 and 10). However, a substantial amount of both $CsgB_{trunc}$ and CsgA were SDS soluble when the underlying agar was collected along with the cells (Fig. 2.4C and 4D bottom panel agar plugs lanes 9 and 10). In contrast, CsgB and CsgA were completely SDS insoluble in WT cells (Fig. 2.4C and Fig. 2.4D compare bottom panel agar plug lanes 1 and 2). TEM was used to visualize the fibers produced in *csgB*/pLR8 (WT *csgB*) and *csgBF*/pNH1 (*csgB*$_{trunc}$). The *csgBF*/pNH1 (*csgB*$_{trunc}$) cells consistently produced fibers that were more diffuse and extended further away from the cell than *csgB*/pLR8 (WT *csgB*) cells (compare Fig. 2.5A and 2.5B). To summarize, the *csgBF*/pNH1 (*csgB*$_{trunc}$) cells stained light red on Congo red indicator plates, produced SDS insoluble $CsgB_{trunc}$ and CsgA, and assembled curli-like fibers, indicating that the first four repeating units of CsgB are sufficient for nucleator activity. Although $CsgB_{trunc}$ clearly mediates CsgA nucleation *in vivo*, it does so less efficiently than WT CsgB.

We further investigated the Congo red binding phenotype of the *csgBF*/pNH1 (*csgB*$_{trunc}$) strain as it compared to WT by mechanically scraping the cells off the Congo red YESCA plate after 48 hours of growth. When scraped off the plate, WT cells were stained a deep red color (Fig. 2.5C #1). In contrast, the *csgBF*/pNH1 (*csgB*$_{trunc}$) appeared pink (Fig. 2.5C #2). The non-fiber producing *csgFBA*/pNH1 (*csgB*$_{trunc}$) appeared light brown (Fig. 2.5C #3). The portion of the plate where the WT cells had grown was white/very light red (Fig. 2.5D #1). The cell-associated fibers produced by the WT cells bound the Congo red dye leaving little dye in the agar plate. Surprisingly, the portion of the Congo red agar plate

where the *csgBF*/pNH1 (*csgB*$_{trunc}$) grew appeared bright red, outlining the areas of cellular growth (Fig. 2.5D #2). These data suggest a portion of the fibers produced by the *csgBF*/pNH1cells were localized to the agar plate.

Discussion

Nucleus formation is proposed to be the rate limiting step during amyloid fiber formation [37]. Despite years of research on the eukaryotic amyloids, curli are the only known amyloid pathway to have a dedicated nucleator protein *in vivo*. Mounting evidence suggests that amyloid precursors are cytotoxic, while the fibers are an innocuous final product of the misfolding event [38-46]. Functional amyloidosis may have evolved specialized mechanisms to eliminate the build up the cytotoxic intermediates. For example, PMEL17, a mammalian functional amyloid, self aggregates so quickly that no toxic intermediates are hypothesized to form [47]. Utilizing a dedicated nucleator may be an alternative strategy to decrease exposure to cytotoxic intermediates. In the curli system, CsgA polymerization *in vitro* contains a lag phase that can be shortened by CsgB$_{trunc}$, consistent with the idea that CsgB$_{trunc}$ facilitates the direct conversion of CsgA to a mature amyloid fiber.

Curli assembly on the cell surface of *E. coli* is a highly regulated and elegant process. In a simple model of curli formation, the major curli subunit CsgA is secreted from the cell as a soluble, unpolymerized protein. CsgA would remain unpolymerized unless it contacts a CsgB-expressing cell. In a process called nucleation, CsgB mediates the conversion of CsgA from a soluble protein

to an insoluble fiber. This marks the first step of curli fiber biogenesis. Once fiber formation is initiated, CsgA can then use the growing fiber tip as a template for additional polymerization in a process called seeding. We propose CsgB-mediated 'nucleation' and fiber mediated 'seeding' of CsgA polymerization to be mechanistically similar processes.

A refined model of extracellular nucleation/precipitation is suggested based on our work. The mature CsgB protein contains five imperfect repeating units that share similarities with the five repeating units in CsgA, and which have been shown to be amyloidogenic [24, 27]. We found that a C-terminal CsgB truncation mutant lacking the fifth repeating unit ($CsgB_{trunc}$) no longer associates with the outer membrane and is secreted into the cellular milieu (Fig. 2.1B, Fig. 2.4C, and Fig. 2.5D). $CsgB_{trunc}$ contains an amyloidogenic domain (Fig. 2.2), which is sufficient to nucleate soluble CsgA *in vitro* (Fig. 2.3A). However, $CsgB_{trunc}$ does not complement a *csgB* mutant *in vivo*, possibly because $CsgB_{trunc}$ is not optimally positioned on the cell surface to act on newly secreted CsgA molecules. This defect is overcome when $CsgB_{trunc}$ is expressed in *csgB* genetic backgrounds manipulated to secrete increased levels of CsgA (Fig. 2.4). Thus, $CsgB_{trunc}$ is sufficient to perform nucleation in a *csgB* background when presented with increased levels of CsgA.

Our model predicts that the fifth repeating unit of CsgB may not be essential for nucleation, but might be required for outer membrane association such that it is optimally localized to nucleate CsgA monomers as they are secreted. However, *in vitro* polymerization studies with full length CsgB protein

may reveal that the C-terminal repeating unit contributes, either negatively or positively, to the kinetics of fiber formation and is not simply an outer membrane anchor. Therefore, it remains to be seen whether the C-terminus of CsgB similarly modulates fiber formation directly, or is merely a localization factor that indirectly aids the nucleation process (i.e. retaining CsgB near the highest concentrations of CsgA). However, these two functions of the CsgB C-terminus are not necessarily mutually exclusive, and this would not be the first example of a functional amyloid having a repeating unit(s) that serves two functions. Studies investigating the effect of deleting repeating units from the C-terminus of the yeast prion protein Sup35 showed that some repeating units contribute directly to fiber growth, some contribute to the inheritance phenotype, and some contribute to both [48, 49]. In our curli model, the C-terminal repeating unit of CsgB anchors the protein to the outer membrane, the optimum locale for interaction with CsgA monomers.

An inherent problem in functional amyloid systems is maintaining control of a self-propagating reaction such that it does not occur at the wrong time or in the wrong place. We propose that the curli system has achieved control by separating the nucleation and elongation properties into two distinct proteins (CsgB and CsgA, respectively) and then dictating when and where those proteins interact. The separation of nucleation and polymerization may be a general mechanism to harness functional amyloid formation. This makes curli an ideal system to study the initial stages of amyloid fiber formation from both an *in vivo* and *in vitro* perspective.

Experimental Procedures

Bacterial growth. To induce curli production, bacteria were grown at 26^{o} C on YESCA plates (17). Curli production was monitored using Congo red-YESCA plates (17). Antibiotics were added to the growth media in the following concentrations, kanamycin 50 μg/ml, chloramphenicol 25 μg/ml, or ampicillin 100 μg/ml.

Bacterial strains and plasmids. Strains used in this study are found in Table 2.1. Plasmids used in this study are found in Table 2.2. Primer sequences used in this study can be found in Table 2.3. Plasmid pNH1, containing $csgB_{trunc}$ under the control of the *csgBA* promoter was constructed by amplifying $csgB_{trunc}$ using the NDH7 and NDH8 primers, digesting the PCR product with *Nco*I and *BamH*I, and ligation into pLR2. Plasmid pNH2 contains a C-terminally his-tagged version of $csgB_{trunc}$. The $csgB_{trunc}$ insert was amplified using the NDH9 and NDH10 primers, and was ligated into the *Nde*I and *EcoR*I sites of the IPTG inducible plasmid pMC3. WT *csgB* was his-tagged and cloned into pMC3 using the NDH11 and NDH12 primers resulting in plasmid pNH4. The pNH3 empty vector plasmid was constructed by gel purifying the *Nco*I - *BamH*I double digestion product of pNH2. The digestion product was blunt ended, ligated, and transformed into LSR12. The *csgFBA* mutant was constructed in the MHR 592 background and the *csgBA* operon was deleted using the Lambda Red system and the following

primers: NDH14 and NDH15 [50]. Strain LSR12 is the *flp*-mediated deletion of the curli operon in LSR6.

$CsgB_{trunc}$ purification. An overnight culture of LSR12 containing pMC1 (p*csgG*) and pNH2 (p*$csgB_{trunc}$*), was subcultured 1:40 in 2 L of Luria-Burtani (LB) broth supplemented with chloramphenicol and ampicillin and grown to an OD_{600} of 0.6. An additional 1 L of room temperature LB was added to the culture which was then grown to OD_{600} 0.9. IPTG was added to a final concentration of 250 μM and was incubated for 45 minutes at 37° C. The culture was centrifuged for 15 minutes at 7,500 x g at 4° C. The supernatant was filtered though a 0.22 μm PES bottle-top filter (Corning, Acton, MA) before loading onto a HIS-Select™ HF NiNTA (Sigma Aldrich, Atlanta, GA) column. The column was washed with 10 volumes of 10 mM potassium phosphate buffer (KPi) pH 7.2, and eluted with 10 mM KPi 100 mM imidazole pH 7.2. Protein-containing fractions (as measured byOD_{280}) were combined, desalted using Sephadex G-25 Fine (Amersham Biosiences, Uppsala, Sweden), and buffer exchanged into 50 mM KPi pH 7.2. OD_{280} was used to determine fractions containing $CsgB_{trunc}$. Protein-containing fractions were combined, filtered through a 0.2 μm filter (Corning Incorporated, Lowell, Massachusettes), and analyzed by SDS-PAGE. The final protein concentration was determined by the BCA assay (Pierce, Rockford, Illinois).

CsgA purification. CsgA was purified as previously described (27).

IAPP preperation. Lyophilized IAPP peptides were disaggregated by resuspension in a 1:1 mixture of 100 % HFIP and 100 % TFA as in Chen S and Wetzel R. *Protein Sci.* 2001 and O´Nuallain, B., and Wetzel, R. *PNAS*. 2002 (51, 52). This suspension was incubated at RT for two hours and vortexed every 30 min. The solvent mixture was then evaporated in a desiccator. Ice cold 2 mM KOH was used to dissolve the peptide (62.5 µM) and neutralize any residual acid. Residual aggregates and contaminations within the solution were removed by centrifugation at 70,000 x g for 1 hour at 4° C (Sorvall Discovery 90, SW55ti-Rotor). After centrifugation the top 80 % of the solution was transferred into a fresh tube on ice. Ice cold 5 x buffer (250 mM KPi pH 7.2, 0.25 % NaN3) was added to the peptide solution to adjust the final buffer concentration to 50 mM KPi pH 7.2 and 0.05 % NaN3. The final protein concentration was determined using the BCA assay.

Thioflavin T assay. Thioflavin T assays were done as previously described (27). To create $CsgB_{trunc}$ seeds, freshly purified $CsgB_{trunc}$ was incubated at room temperature for at least 24 hours with shaking. Prior to use, seed samples were sonicated using a sonic dismembrator (Fisher Model 100, Fisher, Pittsburg, PA) for three 15-second bursts on ice.

Circular Dichroism (CD) spectroscopy. $CsgB_{trunc}$ samples were assayed in a Jasco J-810 spectropolarimeter from 190 nm to 250 nm in a quartz cell with 1-mm path length at 25° C.

Electron microscopy. Philips CM12 Scanning Transmission Electron Microscope was used to visualize the fiber aggregates. Samples were absorbed onto formvar coated copper grids (Ernest F. Fullam, Inc, Latham, NY) for 2 min, washed with deionized water, and negatively stained with 2% uranyl acetate for 90 seconds.

Congo red binding assay. Freshly purified $CsgB_{trunc}$ (0.3 mg/ml) was incubated at room temperature overnight, mixed with 67 µg/ml Congo red, incubated at room temperature for ten minutes before absorbance was measured from 400 nm to 700 nm using a DU800 spectrophotometer (Beckman Coulter, Fullerton, California). Bovine serum albumin (Pierce, Rockford, Illinois) was diluted to a concentration to a concentration of 0.3 mg/ml in 50 mM KPi pH7.2.

SDS-PAGE and western blotting. Bacteria whole cell lysates were prepared and probed for both CsgB and CsgA using previously described methods (29). Blots were probed for CsgB first, developed, and then stripped using 100 mM betamercaptoethanol, 2% SDS, and 62.5 mM Tric-HCl, pH6.7 before reprobing for CsgA.

Figure Legends

Figure 2.1. Biochemical characterization of CsgB and $CsgB_{trunc}$. (A) The imperfect repeating units in CsgA and CsgB (R1-R5) are predicted to form β-strand-loop-β-strand structures. Amino acids comprising the ß-strand are located below the arrows, and amino acids predicted to comprise the loops are italicized. Bolded letters represent amino acids conserved in CsgB and CsgA at each position relative to the start of each repeating unit. Boxed letters represent amino acids conserved throughout the repeating units in both proteins. Positively charged amino acids in the fifth repeating unit of CsgB are marked with asterisks. (B) Western analysis of WT CsgB (*) and $CsgB_{trunc}$ (**) expressed in the Δ*csg* strain LSR12. The *csgB* constructs were co-expressed with the IPTG inducible *csgG* containing plasmid pMC1 or the corresponding empty vector, pTrc99A. Cultures were grown in LB to an OD_{600} of 0.9 and induced with 250 μM IPTG. Post-induction cell suspensions were normalized by OD_{600} and separated by centrifugation into cell (C) and supernatant fractions (S). The blot was probed using αCsgB peptide antisera. Lane 1 contains LSR12/pTrc99A/pNH3 cells and lane 2 contains corresponding supernatant; lanes 3 (C) and 5 (S) LSR12/pTrc99A/pNH4; lanes 4 (C) and 6 (S) LSR12/pMC1/pNH4; lanes 7 (C) and 9 (S) LSR12/pTrc99A/pNH2; and lanes 8 (C) and 10 (S) LSR12/pMC1/pNH2. (C) Coomassie stained SDS-PAGE of $CsgB_{trunc}$ containing fractions after purification. Lane one represents total $CsgB_{trunc}$ eluted from the Nickel NTA column before desalting with the Sephadex G-25 Fine column. Lanes 2 through 12 represent 1 ml fractions containing $CsgB_{trunc}$ collected after elution in 50 mM KPi from the Sephadex G-25 Fine column. Lane 13 represents an

equal volume mixture of the buffer exchanged, fractions 11 through 16. (D) Western blot of purified $CsgB_{trunc}$ probed with αCsgB peptide antibody. Two samples containing equal concentrations of purified soluble $CsgB_{trunc}$ were incubated at room temperature overnight prior to centrifugation for 1 minute in an Eppendorf microcentrifuge. The supernatant was decanted and the pellet was resuspended in 2x SDS loading buffer (lane 1) or pretreated with 90% formic acid (FA) and dried before resuspension in 2x SDS loading buffer (lane 2).

Figure 2.2. Amyloid-like properties of $CsgB_{trunc}$ aggregates. (A) TEM analysis of soluble $CsgB_{trunc}$ incubated at room temperature overnight reveals fibrous aggregates. Scale bars equal 500 nm. (B) Freshly purified $CsgB_{trunc}$ was mixed with the amyloid-specific dye, thioflavin T, and incubated at room temperature for 600 minutes at the following concentrations: 43 μM (open diamonds), 33 μM (open circles), 22 μM (closed diamonds), 16 μM (closed circles), 11 μM (open triangles), 8 μM (x), 5 μM (Closed triangles), 0 μM (solid line). Relative fluorescence emitted at 495 nm was measured every ten minutes after excitation at 438 nm. (C) Congo red absorbance spectra of purified $CsgB_{trunc}$ (open circles) and $CgsB_{trunc}$ that had been incubated for 24 hrs at room temperature following purification (closed circles). An equivalent concentration of bovine serum albumin (BSA) protein mixed with Congo red (open squares). (D) Far UV spectral analysis of 22 μM $CsgB_{trunc}$ immediately after purification (open circles), after incubation for 24 hours (open squares) at room temperature, or after incubation

at room temperature for 15 days (closed squares). The KPi buffer only control is represented by a solid black line.

Figure 2.3. $CsgB_{trunc}$ can nucleate CsgA *in vitro*. (A) Thioflavin T kinetic plot monitoring the polymerization of 30 μM CsgA (closed circles) and 30 μM CsgA in the presence of 10% w/w (open squares) or 6% w/w (open circles) $CsgB_{trunc}$ aggregates. (B) Thioflavin T kinetic plot of 18 uM CsgA (closed circles) and 18 uM CsgA incubated in the presence of 8.8% w/w CsgA seeds (open circles) or 17.2% w/w IAPP seeds (open squares). (C) TEM of 30 μM CsgA. (D) TEM of the fibers produced by polymerization of 30 μM CsgA seeded by 10% $CsgB_{trunc}$. Scale bars equal 500 nm.

Figure 2.4. *In vivo* nucleation properties of $CsgB_{trunc}$. (A) Congo red-containing YESCA plates comparing the Congo red binding phenotypes of *csgB* cells harboring the plasmids pNH1 (*$csgB_{trunc}$*), pMC1, the multiple copy vector containing *csgG*, or the corresponding empty vector, pTrc99A. (B) Congo red-containing YESCA plates comparing the Congo red binding phenotypes of *csgB* and *csgBF* harboring an empty vector control (pLR2), WT *csgB* on a plasmid (pLR8), or *$csgB_{trunc}$* (pNH1). Cells in (B): 1 WT/pLR2, 2 *csgB*/ pLR2, 3 *csgB*/ pLR8, 4 *csgB*/pNH1, 5 *csgBF*/pNH1, 6 *csgBF*/pNH1, 7 *csgBF*/pLR8, 8 *csgBF*/pLR2. All strains contain pTrc99A except, #6 which contain pCsgF. (C, top panel) Whole cell lysate (WC) samples probed with αCsgB peptide antiserum reveal WT CsgB (*) and $CsgB_{trunc}$ (**). Samples were treated with (+) or without (-

) formic acid (FA). (C, bottom panel) Whole cells and the underlying agar (plugs) were collected from YESCA plates and probed for CsgB. (D, top panel) Western blots of whole cells (WC) using αCsgA antiserum. (D, bottom panel) Western blots of whole cells and underlying agar (plug) samples probing for CsgA. The WT cells in lanes 1 and 2 contain empty vectors pLR2 and pTrc99A. All other strains in A and B also contain the empty vector pTrc99A in addition to either pLR2 (pEmpty) or pNH1 ($pCsgB_{trunc}$).

Figure 2.5. Characterization of fibers nucleated by $CsgB_{trunc}$ *in vivo.* (A) TEM of *csgB*/pLR8. (B) TEM of *csgBF*/pNH1. Scale bars represent 500 nm. (C) Cells were mechanically scraped off of a Congo red-containing YESCA plate using disposable inoculating loops to compare the Congo red binding phenotypes of (1) WT/pLR2 (empty vector), (2) *csgBF*/pNH1 ($csgB_{trunc}$) and (3) *csgFBA*/pNH1 ($csgB_{trunc}$) or (4) *csgFBA*/pLR2 (empty vector). (D) The Congo red-containing YESCA plate used to cultivate cells in Fig. 2. 5C after cells have been removed. In panel (D), the numbers indicate the region of the Congo red plate where the following strains had grown: 1 WT/pLR2, 2 *csgBF*/pNH1, 3 *csgFBA*/pNH1 and 4 *csgFBA*/pLR2.

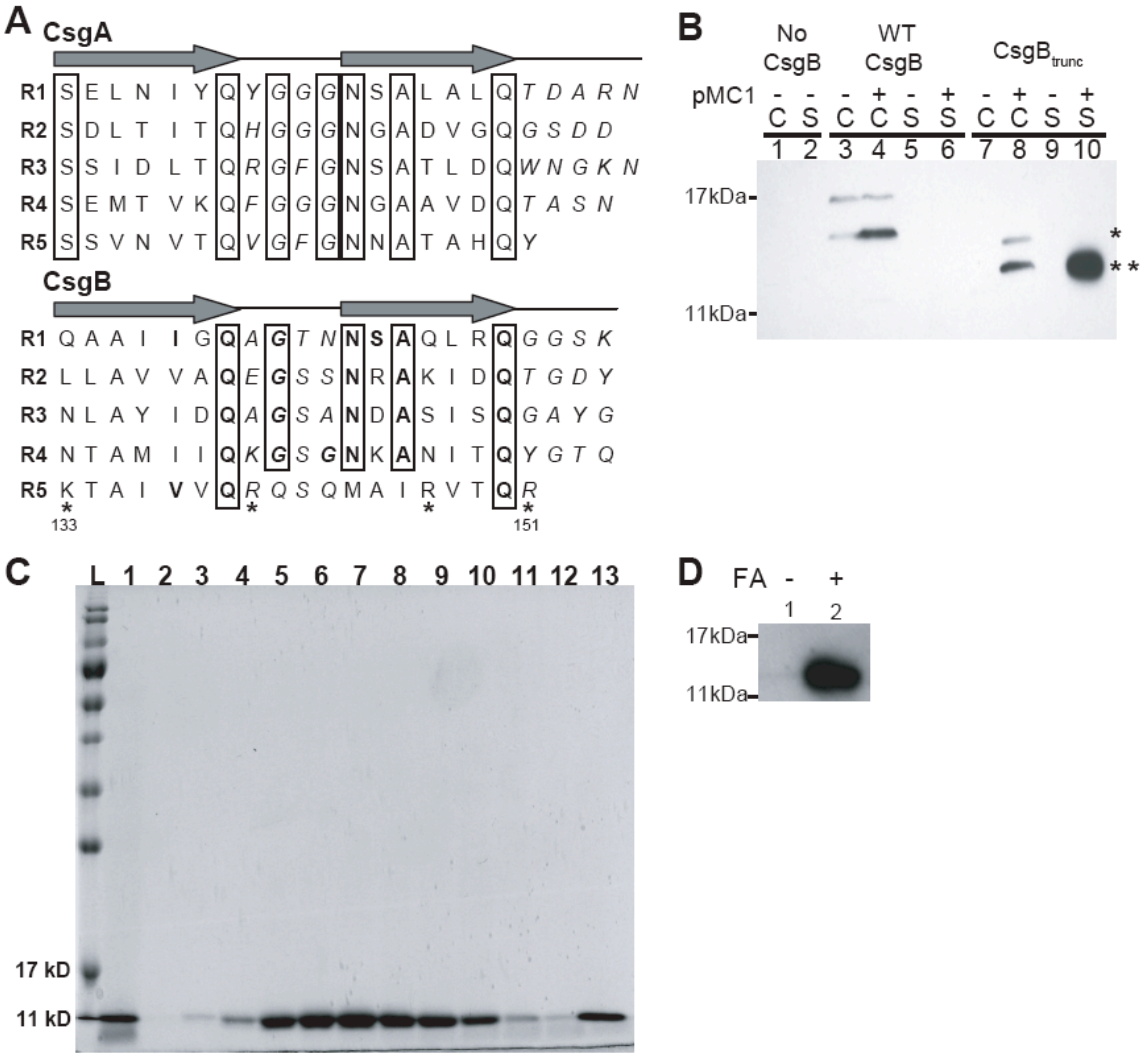

Figure 2.1. Biochemical characterization of CsgB and $CsgB_{trunc}$.

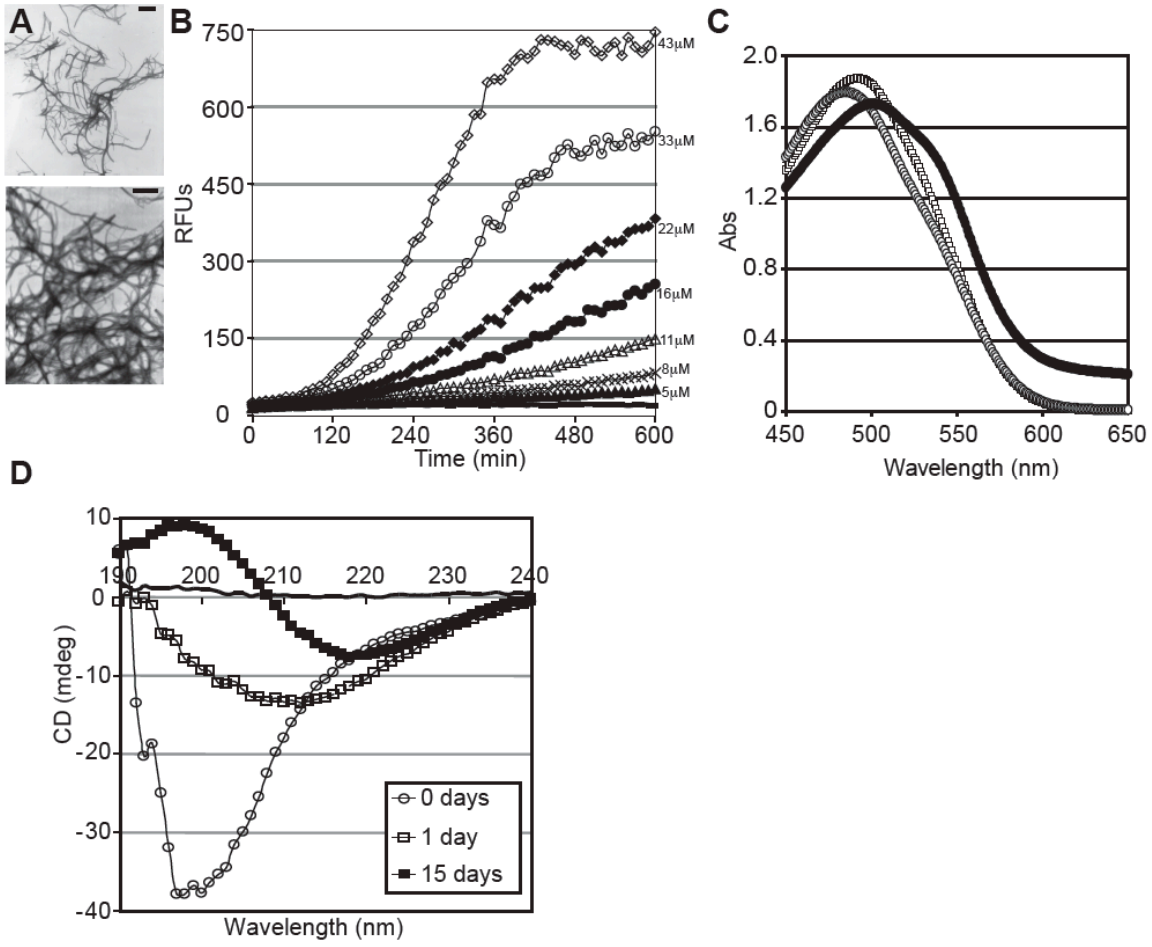

Figure 2.2. Amyloid-like properties of $CsgB_{trunc}$ aggregates.

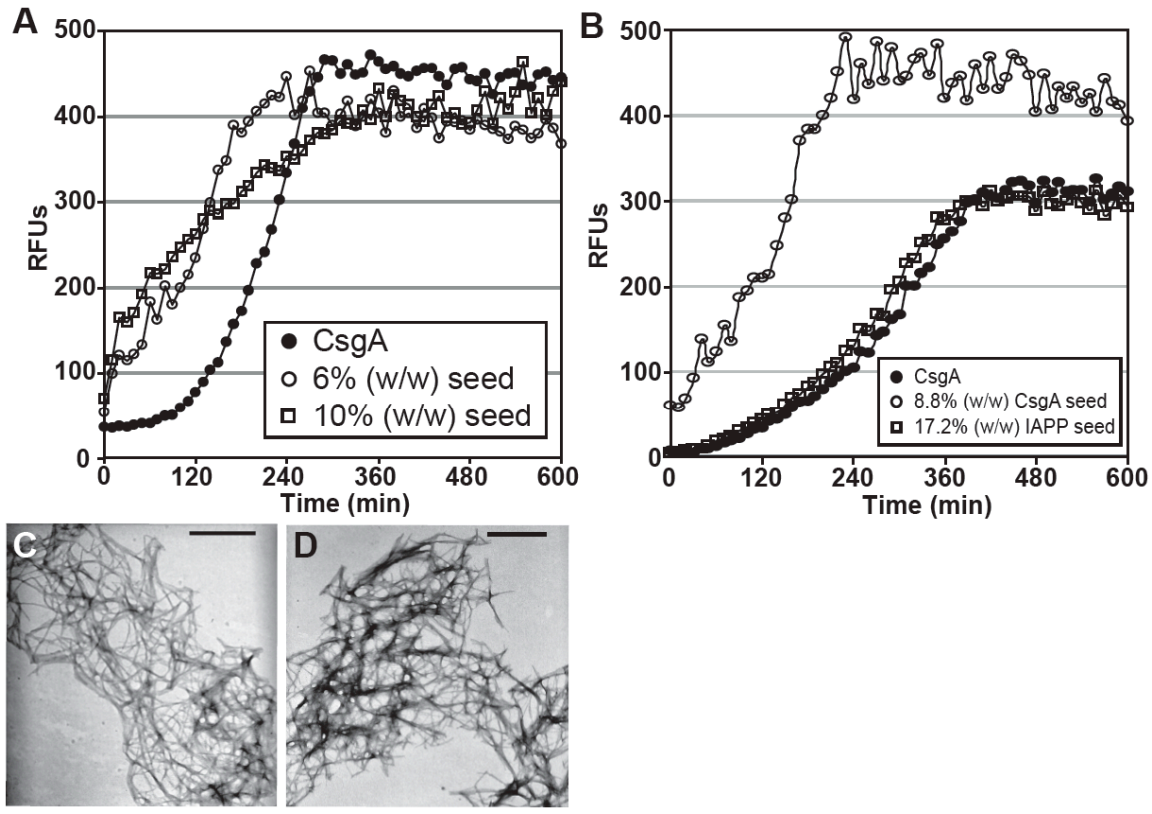

Figure 2.3. $CsgB_{trunc}$ can nucleate CsgA *in vitro*.

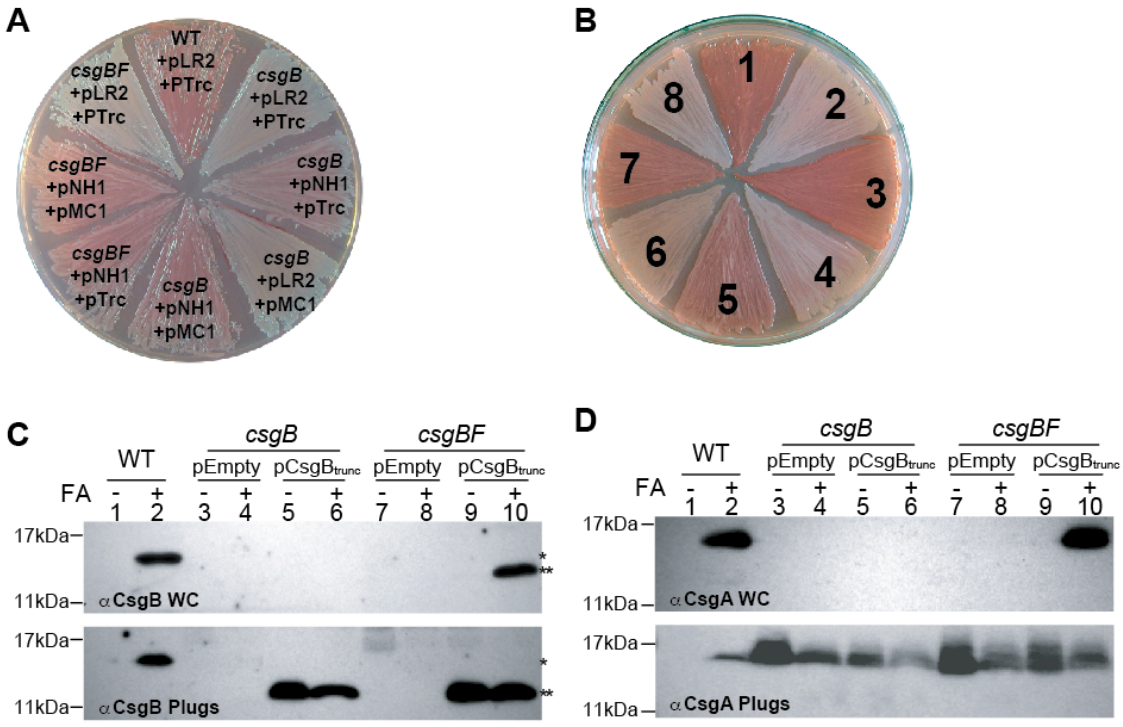

Figure 2.4. *In vivo* nucleation properties of $CsgB_{trunc}$.

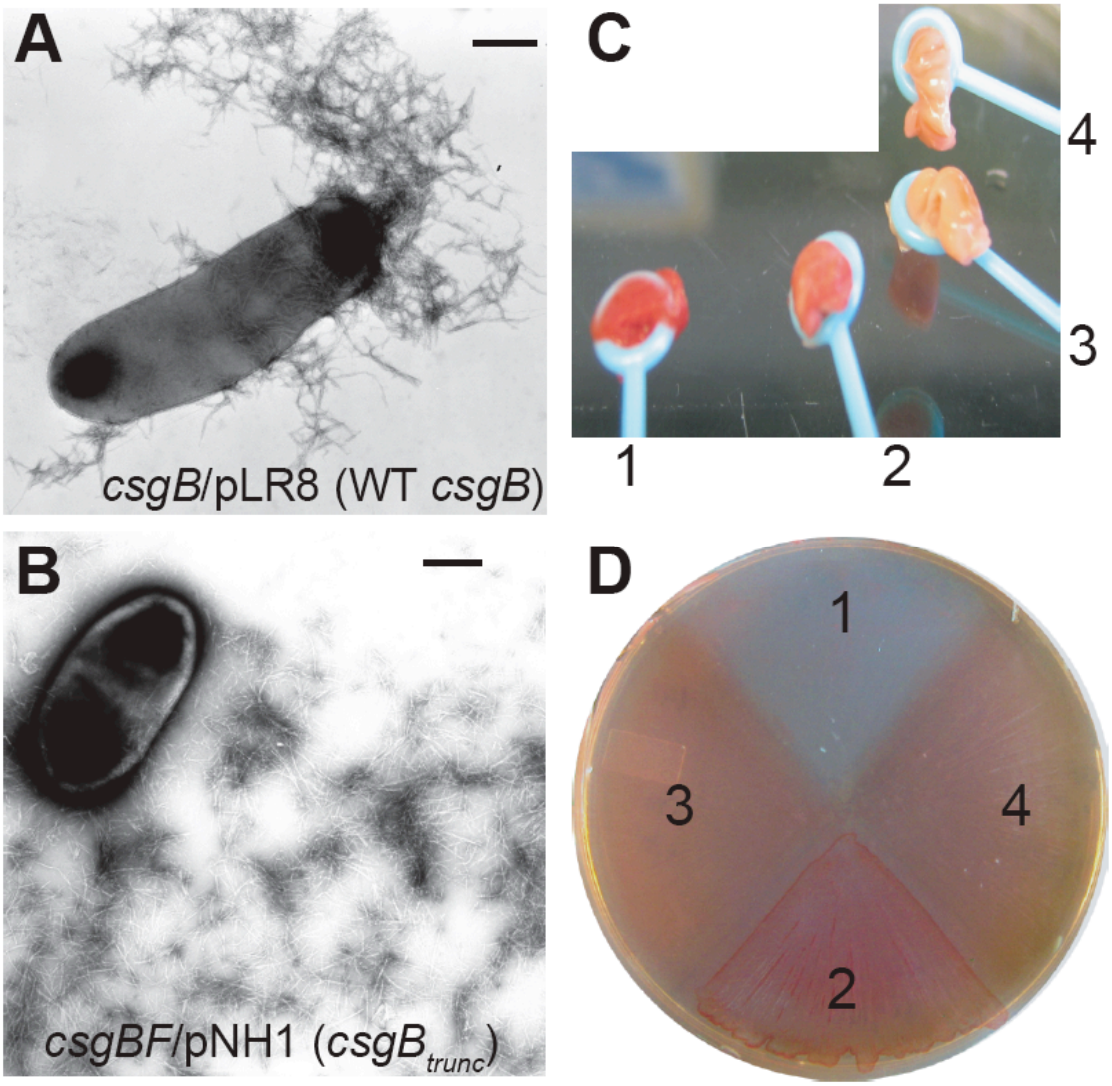

Figure 2.5. Characterization of fibers nucleated by $CsgB_{trunc}$ *in vivo.*

Strains	Relevant characteristics	References
MC4100 and derivatives:		
MC4100	F- *araD*139 Δ(*argF-lac*) U169 *rpsL*150(*strR*) *relA*1 *fibB*5301 *deoC*1 *ptsF*25 *rbsB*	51
MHR261	*csgB*	15
MHR442	*csgBF*	17
MHR592	*csgF*	17
LSR10	Δ*csgA*	17
LSR13	Δ*csgBA*	This study
NDH108	*csgF* Δ*csgBA*	This study
C600 and derivatives:		
C600	F- *thr leu thi lac tonA*	52
LSR6	Δ*csg*::KanR	17
LSR12	Δ*csgDEFG* Δ*csgBA*	This study

Table 2.1. Strains used in this study.

Plasmids	Relevant characteristics	References
pTrc99A	Expression vector	Pharmacia
pMC1	*csgG* cloned into pTrc99A	17
pMC3	His-tagged *csgA* cloned into the IPTG inducible plasmid pHL3	17
pCsgF	His-tagged *cgsF* cloned into pTrc99A	This study
pNH2	His-tagged $csgB_{trunc}$cloned into pMC3	This study
pNH3	Empty expression vector	This study
pNH4	His tagged *csgB* cloned into pMC3	This study
pLR2	Empty vector containing the *csgBA* promoter	29
pLR8	*csgB* cloned into pLR2	This study
pNH1	$csgB_{trunc}$ cloned into pLR2	This study

Table 2.2. Plasmids used in this study.

Primer	Sequence
NDH7	5’-GCGCCATGGGGAAAAACAAATTGTTATTTATG-3’
NDH8	5’-GCGGGATCCTTATTGAGTACCATACTGTGTAATATT–3’
NDH9	5’-GCGCATATGAAAAACAAATTGTTATTTATGATG-3’
NDH10	5’-GCGGAATTCTTAGTGATGGTGATGGTGATGTTGAGTACCATACTGT GTAATATT-3’
NDH11	5’- GCGGAGCTCATATGAAAAACAAATTGTTATTTATGATG -3’
NDH12	5’- GCGCTGCAGAATTCTTAGTGATGGTGATGGTGATGA CGT TGTGTC ACGCG -3’
NDH14	5’-ATTTCTTAAATGTACGACCAGGTCCAGGGTGACAACATGAAAAACGT GTGTAGGCTGGAGCTGCTTC-3’
NDH 14	5’-GGCTTGCGCCCTGTTTCTGTAATACAAATGATGTATTAGTACTGCATA TGAATATCCTCCTT AG-3’

Table 2.3 Primers used in this study.

References

1. Kikuchi, T., et al., *Curli fibers are required for development of biofilm architecture in Escherichia coli K-12 and enhance bacterial adherence to human uroepithelial cells.* Microbiol Immunol, 2005. **49**(9): p. 875-84.

2. Wang, X., et al., *Impact of biofilm matrix components on interaction of commensal Escherichia coli with the gastrointestinal cell line HT-29.* Cell Mol Life Sci, 2006. **63**(19-20): p. 2352-63.

3. Gophna, U., et al., *Curli fibers mediate internalization of Escherichia coli by eukaryotic cells.* Infect Immun, 2001. **69**(4): p. 2659-65.

4. Bian, Z., et al., *Expression of and cytokine activation by Escherichia coli curli fibers in human sepsis.* J Infect Dis, 2000. **181**(2): p. 602-12.

5. Bian, Z., et al., *Activation of inducible nitric oxide synthase/nitric oxide by curli fibers leads to a fall in blood pressure during systemic Escherichia coli infection in mice.* J Infect Dis, 2001. **183**(4): p. 612-9.

6. Uhlich, G.A., P.H. Cooke, and E.B. Solomon, *Analyses of the red-dry-rough phenotype of an Escherichia coli O157:H7 strain and its role in biofilm formation and resistance to antibacterial agents.* Appl Environ Microbiol, 2006. **72**(4): p. 2564-72.

7. Vidal, O., et al., *Isolation of an Escherichia coli K-12 mutant strain able to form biofilms on inert surfaces: involvement of a new ompR allele that increases curli expression.* J Bacteriol, 1998. **180**(9): p. 2442-9.

8. Barnhart, M.M. and M.R. Chapman, *Curli biogenesis and function.* Annu Rev Microbiol, 2006. **60**: p. 131-47.

9. Gerstel, U. and U. Romling, *The csgD promoter, a control unit for biofilm formation in Salmonella typhimurium.* Res Microbiol, 2003. **154**(10): p. 659-67.

10. Barak, J.D., et al., *Salmonella enterica virulence genes are required for bacterial attachment to plant tissue.* Appl Environ Microbiol, 2005. **71**(10): p. 5685-91.

11. Jeter, C. and A.G. Matthysse, *Characterization of the binding of diarrheagenic strains of E. coli to plant surfaces and the role of curli in the interaction of the bacteria with alfalfa sprouts.* Mol Plant Microbe Interact, 2005. **18**(11): p. 1235-42.

12. Ryu, J.H., et al., *Attachment and biofilm formation on stainless steel by Escherichia coli O157:H7 as affected by curli production.* Lett Appl Microbiol, 2004. **39**(4): p. 359-62.

13. Hammar, M., et al., *Expression of two csg operons is required for production of fibronectin- and congo red-binding curli polymers in Escherichia coli K-12.* Mol Microbiol, 1995. **18**(4): p. 661-70.

14. Bian, Z. and S. Normark, *Nucleator function of CsgB for the assembly of adhesive surface organelles in Escherichia coli.* Embo J, 1997. **16**(19): p. 5827-36.

15. Hammar, M., Z. Bian, and S. Normark, *Nucleator-dependent intercellular assembly of adhesive curli organelles in Escherichia coli.* Proc Natl Acad Sci U S A, 1996. **93**(13): p. 6562-6.

16. White, A.P., et al., *Structure and characterization of AgfB from Salmonella enteritidis thin aggregative fimbriae.* J Mol Biol, 2001. **311**(4): p. 735-49.

17. Chapman, M.R., et al., *Role of Escherichia coli curli operons in directing amyloid fiber formation.* Science, 2002. **295**(5556): p. 851-5.

18. Cohen, F.E. and J.W. Kelly, *Therapeutic approaches to protein-misfolding diseases.* Nature, 2003. **426**(6968): p. 905-9.

19. Lashuel, H.A., et al., *Neurodegenerative disease: amyloid pores from pathogenic mutations.* Nature, 2002. **418**(6895): p. 291.

20. Lesne, S., et al., *A specific amyloid-beta protein assembly in the brain impairs memory.* Nature, 2006. **440**(7082): p. 352-7.

21. Olsen, A., A. Jonsson, and S. Normark, *Fibronectin binding mediated by a novel class of surface organelles on Escherichia coli.* Nature, 1989. **338**(6217): p. 652-5.

22. Collinson, S.K., et al., *Purification and characterization of thin, aggregative fimbriae from Salmonella enteritidis.* J Bacteriol, 1991. **173**(15): p. 4773-81.

23. Collinson, S.K., et al., *Thin, aggregative fimbriae mediate binding of Salmonella enteritidis to fibronectin.* J Bacteriol, 1993. **175**(1): p. 12-8.

24. Collinson, S.K., et al., *Structural predictions of AgfA, the insoluble fimbrial subunit of Salmonella thin aggregative fimbriae.* J Mol Biol, 1999. **290**(3): p. 741-56.

25. Naiki, H., et al., *Apolipoprotein E and antioxidants have different mechanisms of inhibiting Alzheimer's beta-amyloid fibril formation in vitro.* Biochemistry, 1998. **37**(51): p. 17882-9.

26. Serio, T.R., et al., *Nucleated conformational conversion and the replication of conformational information by a prion determinant.* Science, 2000. **289**(5483): p. 1317-21.

27. Wang, X., et al., *In Vitro Polymerization of a Functional Escherichia coli Amyloid Protein.* J Biol Chem, 2007. **282**(6): p. 3713-9.

28. O'Nuallain, B., et al., *Seeding specificity in amyloid growth induced by heterologous fibrils.* J Biol Chem, 2004. **279**(17): p. 17490-9.

29. Robinson, L.S., et al., *Secretion of curli fibre subunits is mediated by the outer membrane-localized CsgG protein.* Mol Microbiol, 2006. **59**(3): p. 870-81.

30. Loferer, H., M. Hammar, and S. Normark, *Availability of the fibre subunit CsgA and the nucleator protein CsgB during assembly of fibronectin-binding curli is limited by the intracellular concentration of the novel lipoprotein CsgG.* Mol Microbiol, 1997. **26**(1): p. 11-23.

31. Vassar, P.S. and C.F. Culling, *Fluorescent stains, with special reference to amyloid and connective tissues.* Arch Pathol, 1959. **68**: p. 487-98.

32. Klunk, W.E., J.W. Pettegrew, and D.J. Abraham, *Quantitative evaluation of congo red binding to amyloid-like proteins with a beta-pleated sheet conformation.* J Histochem Cytochem, 1989. **37**(8): p. 1273-81.

33. LeVine, H., 3rd, *Thioflavine T interaction with synthetic Alzheimer's disease beta-amyloid peptides: detection of amyloid aggregation in solution.* Protein Sci, 1993. **2**(3): p. 404-10.

34. LeVine, H., 3rd, *Quantification of beta-sheet amyloid fibril structures with thioflavin T.* Methods Enzymol, 1999. **309**: p. 274-84.

35. Klunk, W.E., R.F. Jacob, and R.P. Mason, *Quantifying amyloid by congo red spectral shift assay.* Methods Enzymol, 1999. **309**: p. 285-305.

36. Kayed, R., et al., *Conformational transitions of islet amyloid polypeptide (IAPP) in amyloid formation in vitro.* J Mol Biol, 1999. **287**(4): p. 781-96.

37. Rochet, J.C. and P.T. Lansbury, Jr., *Amyloid fibrillogenesis: themes and variations.* Curr Opin Struct Biol, 2000. **10**(1): p. 60-8.

38. Sousa, M.M., et al., *Deposition of transthyretin in early stages of familial amyloidotic polyneuropathy: evidence for toxicity of nonfibrillar aggregates.* Am J Pathol, 2001. **159**(6): p. 1993-2000.

39. Lue, L.F., et al., *Soluble amyloid beta peptide concentration as a predictor of synaptic change in Alzheimer's disease.* Am J Pathol, 1999. **155**(3): p. 853-62.

40. McLean, C.A., et al., *Soluble pool of Abeta amyloid as a determinant of severity of neurodegeneration in Alzheimer's disease.* Ann Neurol, 1999. **46**(6): p. 860-6.

41. Wang, J., et al., *The levels of soluble versus insoluble brain Abeta distinguish Alzheimer's disease from normal and pathologic aging.* Exp Neurol, 1999. **158**(2): p. 328-37.

42. Moechars, D., et al., *Early phenotypic changes in transgenic mice that overexpress different mutants of amyloid precursor protein in brain.* J Biol Chem, 1999. **274**(10): p. 6483-92.

43. Larson, J., et al., *Alterations in synaptic transmission and long-term potentiation in hippocampal slices from young and aged PDAPP mice.* Brain Res, 1999. **840**(1-2): p. 23-35.

44. Bucciantini, M., et al., *Inherent toxicity of aggregates implies a common mechanism for protein misfolding diseases.* Nature, 2002. **416**(6880): p. 507-11.

45. Sirangelo, I., et al., *Fibrillogenesis and cytotoxic activity of the amyloid-forming apomyoglobin mutant W7FW14F.* J Biol Chem, 2004. **279**(13): p. 13183-9.

46. Malisauskas, M., et al., *Does the cytotoxic effect of transient amyloid oligomers from common equine lysozyme in vitro imply innate amyloid toxicity?* J Biol Chem, 2005. **280**(8): p. 6269-75.

47. Fowler, D.M., et al., *Functional amyloid formation within mammalian tissue.* PLoS Biol, 2006. **4**(1): p. e6.

48. Osherovich, L.Z., et al., *Dissection and design of yeast prions.* PLoS Biol, 2004. **2**(4): p. E86.

49. Parham, S.N., C.G. Resende, and M.F. Tuite, *Oligopeptide repeats in the yeast protein Sup35p stabilize intermolecular prion interactions.* Embo J, 2001. **20**(9): p. 2111-9.

50. Datsenko, K.A. and B.L. Wanner, *One-step inactivation of chromosomal genes in Escherichia coli K-12 using PCR products.* Proc Natl Acad Sci U S A, 2000. **97**(12): p. 6640-5.

51. Casadaban, M.J. *Transposition and fusion of the lac genes to selected promoters in Escherichia coli using bacteriophage lambda and Mu*. J Mol Biol, 1976. **104**(3): p. 541-55.

52. Campbell, A. *Sensitive mutants of bacteriophage lambda*. Virology, 1961. **14**: p.22-32.

Chapter III

Defining the molecular basis of curli amyloid nucleation

Abstract

Curli fibers are functional amyloid fibers produced by enteric bacteria. The major curli fiber subunit, CsgA, self assembles into an amyloid fiber *in vitro*. However, the minor curli subunit protein, CsgB, is required for CsgA polymerization *in vivo*. Both CsgA and CsgB are composed of five β–sheet-loop-β–sheet-loop-repeating units that feature conserved glutamine and asparagine residues. Because of this similarity, we hypothesize that CsgB drives the polymerization of CsgA into an amyloid *in vivo* via a template-mediated mechanism. This would suggest that CsgB also has the capability to polymerize into an amyloid fiber. In this work, we purified full-length WT CsgB, and found that WT CsgB self-polymerized into an amyloid fiber *in vitro*. Additionally, preformed CsgB fibers seeded CsgA polymerization into an amyloid fiber. To define the molecular basis of CsgB nucleation we generated repeating unit deletion mutants. N-terminally truncated CsgB mutants were able convert CsgA into a detergent insoluble fiber *in vivo*, however these mutants were unable to complement a *csgB* strain for formation of a pellicle biofilm. CsgB mutants missing either the 4th or 5th repeating units were not localized to the outer membrane like WT CsgB, but were secreted into the extracellular milieu. Due to this mislocalization, these C-

terminal CsgB deletion mutants were unable to support *in vivo* polymerization of CsgA. However, all of the repeating unit deletion mutants were capable of self-assembly *in vitro*. Finally, we found that the conserved glutamines and asparagines in the second and fourth repeating units: Q73, N78, Q117, and N122, were required for CsgB function *in vivo*. Our results demonstrate the modular nature of CsgB and illustrate that *in vivo* nucleator activities are more sensitive to mutation than the ability of CsgB to polymerize into an amyloid fiber *in vitro*.

Introduction

Amyloid fibers are a common pathology of many neurodegenerative diseases such as Alzheimer's disease and Parkinson's disease [1]. These diseases have classically been referred to as protein misfolding diseases because amyloidogenesis results from an aberrant aggregation process where a normally soluble protein self assembles into a highly ordered, structurally stable fiber. Biochemically, amyloid fibers are defined by unique tinctorial properties, resistance to proteases and detergents, and a β-sheet rich secondary structure [2]. Typically there are three phases to *in vitro* amyloid polymerization: a lag phase, a phase of rapid fiber growth, and a stationary phase [3-8]. Rapid fiber growth is dependent on the formation of a nucleus [9]. A common feature of nucleus dependent polymerization reactions is that preformed fibers can act to seed the polymerization of soluble monomers. It is proposed that preformed fibers provide a template for monomer polymerization, and this interaction

mediates the exit from the lag phase. Although amyloid nucleation and polymerization have been extensively studied *in vitro*, robust *in vivo* models that distinguish these processes have not been developed.

Curli fibers are extracellular amyloid fibers produced by *E. coli* and other enteric bacteria [10, 11]. The discovery of these fibers produced a paradigm shift in the amyloid field, because curli assembly is the result of a dedicated biogenesis pathway and not the result of a misfolding event. Curli fibers are part of the extracellular matrix that are required for biofilm formation and for mediating host-bacterial interactions [12-16]. Curli fibers are composed of two proteins CsgA, the major subunit, and CsgB, the minor subunit [17-19]. Purified CsgA polymerizes into an amyloid fiber *in vitro*, but CsgB is required for the formation of curli fibers *in vivo* [6, 20]. In the absence of CsgB, CsgA is secreted away from the cell as a soluble protein [17, 21]. In a process referred to as interbacterial complementation, CsgB expressed on the surface of a *csgA* mutant grown in close proximity to CsgA secreting *csgB* mutants can convert the soluble CsgA into an ordered amyloid fiber [10, 17]. The CsgB expressed on the surface of *csgA* mutants can also nucleate exogenously added purified CsgA [22, 23]. CsgB becomes incorporated into the fiber after initiating the polymerization of CsgA, yet the sequences or domains of CsgB that guide nucleation have yet to be elucidated.

In silico structural predictions suggest that both CsgA and CsgB contain a β-sheet rich domain that can be further divided into five β-sheet-loop-β-sheet motifs repeated in succession [17, 24]. We call these motifs repeating units. The

CsgA and CsgB repeating units contain a high degree of glutamines and asparagines. The amino acids sequence of CsgA and CsgB are 51% similar [18]. This similarity and the *in silico* structural predictions led us to hypothesize that CsgB, like CsgA, may also adopt an amyloid like fold and that this feature of CsgB is the mechanism used to template CsgA polymerization. We previously purified a truncated version of CsgB missing the fifth repeating unit. The truncated CsgB mutant self assembled into β-sheet rich amyloid fibers that could template CsgA polymerization *in vitro*. Truncated CsgB was not able to complement a *csgB* mutant due to a mislocalization defect, but could polymerize CsgA *in vivo* if cells were genetically altered to secrete an increased amount of CsgA [25].

We report here that full length, WT CsgB polymerizes faster than CsgA and the truncated CsgB we previously characterized. Purified CsgB was able to template CsgA polymerization *in vitro* and when applied to *csgB* mutants. We also assessed the contribution of each CsgB repeating unit to nucleator function *in vivo* and to CsgB polymerization *in vitro*. We found that the fourth repeating unit of CsgB is required for cell association suggesting that both the fourth and fifth repeating units function to anchor CsgB to the cell. Synthetic peptides composed of the amino acids found in repeating units 1, 2, or 4 of CsgB can form amyloid *in vitro*. Mutating conserved glutamines and asparagines found in these repeating units impair CsgB function *in vivo*. Our results suggest a model where CsgB quickly adopts a β-sheet rich amyloid fold that templates the conversion of CsgA into an amyloid fiber at the cell surface.

Results

Purified CsgB forms amyloid fibers that can seed CsgA polymerization. Previously, we purified a mutated CsgB molecule that lacked the C-terminal repeating unit by harvesting the supernatant of cells expressing the truncated protein. Attempts to purify full-length CsgB from the extracellular milieu in a similar fashion were thwarted by relatively low expression levels [25]. Expression of full length, mature CsgB (*sec*-signal sequence minus) was induced in the cytoplasm of cells. After induction, cells contained significant amounts of SDS insoluble CsgB protein (Fig. 3.1A lane 2 and 3). Soluble CsgB was recovered by affinity purification after pellets of induced cells were resuspended in 8 M guanidine hydrochloride (GndHCl) pH 7.2 (Fig. 3.1A lane 4).

CsgB polymerization was monitored using the amyloid specific dye thioflavin-T (ThT). CsgB rapidly increased the ThT fluorescent signal after a short lag phase (Fig. 3.1B). The increase in ThT fluorescence was concentration dependent (Fig. 3.1B). Both CsgA and CsgB polymerization curves contained a lag phase, a fast phase, and a stationary phase (Fig. 3.1B). However, the CsgB lag phase was shorter than the CsgA lag phase at equivalent concentrations of protein (Fig. 3.1B). Electron microscopy (EM) analysis of fractions containing CsgB revealed an ordered fibrous structure, similar to what has been observed for CsgA (Fig. 3.1C) [6]. The fibrous CsgB aggregates were not soluble in SDS

and pretreatment with formic acid was required to visualize monomeric protein on an SDS PAGE gel (Fig. 3.1D lane 2).

To test whether CsgB fibers could template CsgA polymerization *in vitro*, we measured the polymerization of soluble CsgA in the presence of preformed CsgB fibers. In the absence of CsgB, CsgA polymerization had a lag phase of about two hours. When 5% w/w preformed CsgB fibers were added to the reaction mix a 1-hour lag phase was observed. CsgA polymerization proceeded without an apparent lag phase when the amount of CsgB seeds was increased to 12% (Fig. 3.1E). Taken together, these results suggested that WT CsgB rapidly polymerizes into an amyloid fiber that templates CsgA polymerization.

The ability of CsgB to template CsgA under more physiologically relevant conditions was tested by adding purified, soluble CsgB to *csgA* and *csgB* mutant cells grown on YESCA plates. We used a similar assay to measure the ability of cell-presented CsgB to stimulate the polymerization of purified and exogenously added CsgA [22, 23]. Purified CsgB was overlaid on the surface of *csgA* or *csgB* cells grown under curli-inducing conditions, followed by overnight incubation as described in the materials and methods. The cells were then stained with Congo red as described [22, 23]. In comparison to the *csgA* mutant cells, the *csgB* mutants incubated with CsgB had a pronounced Congo red staining phenotype where the purified CsgB had been added (Fig. 3.1F). The purified CsgB complemented a *csgB* mutant for Congo red binding when the purified protein was added to the cells exogenously. To confirm fiber formation, we prepared electron micrographs of the *csgB* mutant incubated with CsgB and found that

fibers were visible when CsgB was incubated with the *csgB* mutants (Fig. 3.1G). The presence of fibers and the increased Congo red staining when CsgB was added to the *csgB* mutant is consistent with the hypothesis that purified CsgB is able to stimulate CsgA polymerization on the cell surface. To determine if CsgA secreted from the *csgB* mutants had formed detergent insoluble fibers, the *csgB* cells that were incubated in the presence of purified CsgB were harvested and resuspended in the presence or absence of formic acid. More CsgA was detected when *csgB* mutants that were incubated in the presence of CsgB were collected than when no protein was added to the cells (Fig. 3.1H). An increased amount of CsgA was seen if the *csgB* mutant cells incubated in the presence of CsgB were pretreated with formic acid (Fig. 3.1H). These data confirm that the fibers produced when exogenous CsgB is added to *csgB* mutants are detergent insoluble. Collectively, these results suggest purified CsgB adopts an amyloid conformation that can template CsgA polymerization.

In vivo contribution of the repeating units to CsgB function. CsgB contains a glutamine-asparagine rich domain that can be divided into five repeat sequences called r1, r2, r3, r4, and r5 (Fig. 3.2A) [18, 20]. Each repeating unit is predicted to contain two β-sheets. The repeating unit structure of CsgA and CsgB contain a high degree similarity (Fig. 3.2A). In order to determine the contribution of each repeating units to CsgB function *in vivo* we constructed inframe deletions of each repeating unit. When *csgB* mutants harboring deletions of CsgB r1, r2, or r3 ($CsgB^{\Delta r1\text{-}\Delta r3}$) were grown under curli-inducing

conditions on Congo red-containing agar plates, the mutants bound as much Congo red as WT cells and a *csgB* mutant complemented with WT *csgB* (Fig. 3.2B). Both CsgB$^{\Delta r1}$ and CsgB$^{\Delta r3}$ could be detected by western blot and an increased amount of CsgB$^{\Delta r1}$ and CsgB$^{\Delta r3}$ monomer were seen when the whole cells samples were pretreated with FA (Fig. 3.2C top panel). The CgsB$^{\Delta r2}$ protein was not detected by western, because the CsgB antibody used for the western blot was raised using a peptide fragment found within r2 [26]. However, like the CsgB$^{\Delta r1}$ and CsgB$^{\Delta r3}$ constructs, CsgA could only be detected when the CsgB$^{\Delta r2}$ samples were pretreated with FA (Fig. 3.2C bottom panel). These results suggest that the CsgB$^{\Delta r1}$, CsgB$^{\Delta r2}$, and CsgB$^{\Delta r3}$ constructs function to convert soluble CsgA into an SDS insoluble fiber. To confirm the presence of fibers, we prepared EM samples of *csgB* mutants harboring each deletion. Consistent with the Congo red and western blot data, fibers were seen when *csgB* mutants harboring the CsgB$^{\Delta r1}$, CsgB$^{\Delta r2}$, and CsgB$^{\Delta r3}$ constructs were viewed by EM and the fibers were morphologically similar to WT fibers (Fig. 3.2D).

Unlike the N-terminal deletions, both the r4 and r5 deletion constructs were unable to complement a *csgB* mutant for Congo red binding (Fig. 3.2B). To test for the stability of CsgB$^{\Delta r4}$ and CsgB$^{\Delta r5}$, cell lysates were probed with α-CsgB serum and no cell-associated CsgB$^{\Delta r4}$ or CsgB$^{\Delta r5}$ protein could be detected (Fig. 3.2C top panel). However, when whole cells and the underlying agar were collected, bands corresponding to the CsgB$^{\Delta r4}$ and CsgB$^{\Delta r5}$ constructs were observed (Fig. 3.2C middle panel). This indicated that both CsgB$^{\Delta r4}$ and

CsgB$^{\Delta r5}$ were not cell associated, but were instead secreted into the underlying agar. These results are consistent with what we published for CsgB$^{\Delta r5}$ (CsgB$_{trunc}$) [25]. Soluble CsgA was only detected when the underlying agar was collected along with the *csgB* cells harboring CsgB$^{\Delta r4}$ or CsgB$^{\Delta r5}$ (data not shown). Thus the CsgB$^{\Delta r4}$ and CsgB$^{\Delta r5}$ constructs do not alter CsgA stability. No fibers could be detected when *csgB* cells expressing *csgB*$^{\Delta r4}$ were observed by EM (Fig. 3.2D). Likewise, fibers were not detected when *csgB* cells expressing *csgB*$^{\Delta r5}$ were examined by EM [25]. These results suggest the C-terminal portion of CsgB is required for nucleator function *in vivo*.

The Congo red binding phenotype, assessing CsgA solubility, and visualizing mutants by EM help us determine if fibers are present, but these assays do not address if these mutant fibers are functional. Curli fibers promote biofilm development in enteric bacteria such as *E. coli*. To test the ability of the fibers produced by the CsgB$^{\Delta r1}$, CsgB$^{\Delta r2}$, and CsgB$^{\Delta r3}$ constructs to form biofilms, cells were grown under curli-inducing conditions and the ability of each strain to form a pellicle was assessed. None of the deletion constructs were able to complement a *csgB* mutant for pellicle formation (Fig. 3.2E). The N-terminal deletion constructs CsgB$^{\Delta r1}$, CsgB$^{\Delta r2}$, and CsgB$^{\Delta r3}$, promoted the conversion of CsgA into an SDS insoluble fiber, however the fibers produced by these mutant constructs were not functional. All five repeating units of CsgB were required to form functional curli fibers.

The repeating unit deletion mutants form amyloid in vitro. A possible explanation for the *in vivo* defect of the CsgB$^{\Delta r4}$ construct was that the fourth repeating unit is required for interaction with CsgA. To determine if CsgB$^{\Delta r4}$ could act as a template for CsgA polymerization and to characterize the *in vitro* characteristics of the other repeating unit mutants, we constructed expression plasmids for each of the CsgB repeating unit deletion mutants. All the repeating unit deletions, with the exception of CsgB$^{\Delta r4}$, formed SDS insoluble cytoplasmic aggregates after induction (Fig. 3.3A). To purify soluble protein for each mutant we lysed the cells in 8 M GndHCl as described in the Materials and Methods. The CsgB$^{\Delta r2}$, CsgB$^{\Delta r3}$, CsgB$^{\Delta r4}$, and CsgB$^{\Delta r5}$ mutants could be purified as SDS soluble proteins (data not shown). We were unable to purify CsgB$^{\Delta r1}$ (materials and methods).

We monitored the *in vitro* polymerization of CsgB$^{\Delta r2}$, CsgB$^{\Delta r3}$, CsgB$^{\Delta r4}$, and CsgB$^{\Delta r5}$ using the ThT assay. We previously reported that the polymerization curve of truncated CsgB$^{\Delta r5}$ contained a two-hour lag phase and a similar lag phase was observed here (Fig. 3.3B). The lag phase for CsgB$^{\Delta r5}$ was longer than that of WT, CsgB$^{\Delta r2}$, CsgB$^{\Delta r3}$, and CsgB$^{\Delta r4}$. This suggests CsgB repeating unit r5 promotes CsgB-CsgB interactions *in vitro*.

The normalized CsgB$^{\Delta r2}$ ThT polymerization profile demonstrated that CsgB$^{\Delta r2}$ polymerized as quickly as WT CsgB (Fig. 3.3B). However, the relative fluorescent units (RFUs) recorded for CsgB$^{\Delta r2}$ after twelve hours of polymerization was lower than WT CsgB at the same time point (Fig. 3.3B inset). In fact, CsgB$^{\Delta r2}$ consistently induced less ThT fluorescence than WT,

suggesting that CsgB$^{\Delta r2}$ adopts an altered amyloid conformation. We observed the fibers produced by CsgB$^{\Delta r2}$ after incubation at room temperature by EM, and found were no gross morphological differences between CsgB$^{\Delta r2}$ fibers and WT CsgB fibers (Fig. 3.1C and Fig. 3.3C top panel). We tested the ability of the CsgB$^{\Delta r2}$ fibers to seed CsgA polymerization. Indicative of a low CsgA concentration (14 μM) a five-hour lag phase was seen. At this lower concentration of CsgA, only 3.5% (w/w) seed of WT CsgB was needed to eliminate the lag phase (Fig. 3.3D). A short lag phase of roughly 30 minutes was seen when 3.5% (w/w) CsgB$^{\Delta r2}$ fiber was added to the reaction mix, but no lag phase was observed when the amount of seed was increased to 9% (w/w) CsgB$^{\Delta r2}$ fiber (Fig. 3.3D). CsgB$^{\Delta r2}$ was able to seed CsgA polymerization and this result is consistent with the *in vivo* results that demonstrated that CsgB$^{\Delta r2}$ complemented a *csgB* mutant (Fig. 3.2).

The CsgB$^{\Delta r4}$ mutant was defective *in vivo*, but had a ThT fluorescence profile similar to WT CsgB (Fig. 3.3B). Fractions containing CsgB$^{\Delta r4}$ were incubated overnight and viewed by EM to assess aggregate morphology. CsgB$^{\Delta r4}$ fibers appeared similar to WT CsgB fibers (Fig. 3.3C bottom panel). To determine if the *in vivo* defect of CsgB$^{\Delta r4}$ could be attributed to an inability of CsgB$^{\Delta r4}$ to seed CsgA polymerization *in vitro* CsgB$^{\Delta r4}$ fibers were added to a CsgA polymerization reaction. A short lag phase of about 30 minutes was observed when 3.5% (w/w) CsgB$^{\Delta r4}$ fibers were added to CsgA, but when the amount of preformed fiber was increased to 8% (w/w), CsgA polymerization proceeded without an apparent lag phase (Fig. 3.3D). These results revealed

that CsgB$^{\Delta r4}$ formed amyloid fibers *in vitro* and that these CsgB$^{\Delta r4}$ fibers could template CsgA polymerization. Therefore, the mislocalization of this mutant *in vivo* plays a dominant role in the inability of CsgB$^{\Delta r4}$ to complement a *csgB* mutant.

The conserved glutamine and asparagines residues in the amyloidogenic repeating units of CsgB drive nucleator function in vivo. The repeating units of both CsgA and CsgB contain conserved glutamine and asparagine residues [17, 18, 22, 25]. A site-directed mutagenesis screen was performed on CsgA to determine which conserved glutamines and asparagines were required for CsgA polymerization (Fig. 3.2A). Polymerization of CsgA was most impaired when the glutamines found at the end of the first β-sheet and the asparagines found at the beginning of the second β-sheet in r1 and r5 were mutated to alanines [22]. Synthetic peptides composed of the amino acids in CsgA r1 or r5 also have increased ThT fluorescence over time and amyloid fibers were visualized by EM [22, 23]. CsgB has conserved glutamines and asparagines at the same positions in r1, r2, r3, and r4 (Fig. 3.2A). We wanted to assess the contribution of the glutamines and asparagines in the amyloidogenic repeating units of CsgB to nucleator function *in vivo*.

Since CsgA r1 and CsgA r5 were found to be required for CsgA polymerization and peptides composed of CsgA r1 or CsgA r5 are responsive to ThT we reasoned we could narrow our mutagenesis to the repeating units of CsgB that fluoresce ThT after a 24-hour incubation. Peptides composed of

amino acids in CsgB r1, r2, or r4 displayed higher ThT fluorescence after a 24-hour incubation (Fig. 3.4A). This result suggests that r1, r2, and r4 all contribute to the overall amyloidogenicity of CsgB. Using the ThT data to guide our mutagenesis, the glutamines that conclude the first β-sheet and the asparagines that mark the beginning of the second β-sheet in r1 (Q51 N56), r2 (Q73 N78), and r4 (Q117 N122) were mutated to alanines. These mutants are referred to *r1mut, r2mut*, and *r4mut* respectively (Fig. 3.2A). We tested the ability of each of the mutants to complement a *csgB* mutant for Congo red binding. Cells expressing the *r1mut* had a modest decrease in Congo red staining, while *r2mut* expressing cells had a dramatic decrease in Congo red staining compared to *csgB* harboring WT *csgB* (Fig. 3.4B). No Congo red staining was detected when *csgB* cells harboring *r4mut* were grown on Congo red-containing agar plates (Fig. 3.4B). Like WT CsgB, CsgB *r1mut* could be detected when whole cells were analyzed by western blot (Fig. 3.4C top panel). CsgA was predominantly SDS insoluble in whole cell samples of *csgB* mutants containing *r1mut* (Fig. 3.4C bottom panel). Consistent with the Congo red phenotype and the western blot analysis, fibers were observed when visualized by EM (Fig. 3.4C). When cells expressing *r2mut* were analyzed by western blot, CsgB *r2mut* was stable, but could only be detected in samples containing both the cells and underlying agar (Fig. 3.4C). This suggests that the partial Congo red binding defect could be due to mislocalization. Fibers were present when the *r2mut* mutant was visualized by EM (Fig. 3.4D). However, fewer fibers were observed than what was visualized for the *r1mut* mutant. The *r4mut* mutant had the most dramatic

influence on Congo red binding (Fig. 3.4B). The stability of *r4mut* was tested by western blot, and similar to what was observed for $CsgB^{\Delta r4}$, a band corresponding to *r4mut* was only seen when we collected the cells along with the underlying growth medium (Fig. 3.4C). CsgA remained SDS soluble when whole cells expressing *r4mut* were collected for western blot, and no fibers were seen when *csgB* mutants expressing *r4mut* were visualized by EM (data not shown and Fig. 3.4D).

Since both the CsgB r1 and r2 synthetic peptides increased ThT fluorescence over time we hypothesized that *r1mut* still functioned because CsgB r2 was able to provide an amyloid template for CsgA polymerization. If CsgB r1 and CsgB r2 each provide a template for CsgA polymerization, we reasoned mutating the conserved glutamines and asparagines in both r1 and r2 would abolish nucleator function. We constructed a quadruple point mutant (Q51A N56A Q73A N78A) called *r12mut* (Fig. 3.2A). The Congo red binding phenotype of *csgB* mutants harboring *r12mut* was similar to the Congo red binding phenotype of *csgB* mutants harboring *r2mut* (Fig. 3.4B). Also similar to *r2mut*, *r12mut* could only be detected by western blot if the underlying agar along was collected along with cells (Fig. 3.4C). These results suggest the contribution of CsgB r2 to nucleator function is dominant to CsgB r1. Unlike *r2mut*, an ordered fibrous structure could not be observed when *csgB* mutants containing *r12mut* were visualized by EM (Fig. 3.4D). Instead the fibers that could be seen were sparse, thin and not densely packed together. Therefore,

mutating the four conserved glutamines and asparagines in CsgB r1 and CsgB r2 severely hindered fiber biogenesis.

Discussion

The self-assembly of soluble proteins into amyloid fibers is a hallmark of many neurodegenerative diseases. This link to disease prompted a surge of studies looking for the toxic species associated with amyloid fiber biogenesis. Recent evidence suggests that amyloid fiber precursors are the cytotoxic component of amyloid polymerization. Proteins associated with amyloid diseases aggregate relatively slowly *in vitro*, and the longer lag phases associated with the polymerization of these proteins have led to the idea that cytotoxic amyloid precursors accumulate *in vivo* [27-35]. These precursors have been shown to compromise membrane integrity, leading to cell death [36-39]. Therefore, strategies that minimize amyloidogenesis intermediates promise to provide therapeutic solutions for many amyloid-mediated disorders.

Functional amyloid biogenesis pathways need to proceed without compromising the physiology of the cell. One strategy cells employ to reduce the accumulation of cytotoxic precursors is to promote the rapid conversion of inert monomers to stable amyloid fibrils. One such example of this is the mammalian functional amyloid protein Pmel that polymerizes without a lag phase *in vitro* [40]. Bacteria expressing curli, utilize a dedicated nucleator protein that speeds the conversion of soluble CsgA into an amyloid fiber. Our previous studies have demonstrated that CsgA polymerization *in vitro* has a

consistent two-hour lag phase [6]. A potentially toxic intermediate is formed during the lag phase, but the addition of preformed CsgA fibers to freshly purified CsgA eliminated the lag phase [6]. This suggests the process of seeding helps increase the rate of polymerization and bypasses the accumulation of toxic intermediates.

CsgA and CsgB have similar primary amino acid sequences and are β-sheet rich amyloidogenic proteins. We hypothesized that CsgB mediated nucleation is similar to CsgA mediated seeding, and recently demonstrated that preformed fibers composed of a truncated CsgB molecule, called $CsgB_{trunc}$ (referred to here as $CsgB^{\Delta r5}$), also eliminated the CsgA lag phase. However, $CsgB^{\Delta r5}$ was unable to complement a *csgB* strain for nucleator function *in vivo* (Fig. 3.3B) [25].

Here, we discovered that wild type CsgB polymerizes more rapidly than CsgA. In fact purified wild type CsgB began to fluoresce in the presence of ThT after only 20 to 30 minutes of incubation at room temperature (Fig. 3.1B). This lag phase is substantially shorter than the two-hour lag phases observed with both CsgA and $CsgB^{\Delta r5}$ (Fig. 3.1B and Fig. 3.3B). CsgB amyloid fibers also seeded CsgA polymerization *in vitro* (Fig. 3.1 E). More importantly, freshly purified, soluble CsgB applied to *csgB* mutant cells was able to nucleate the CsgA secreted from these *csgB* mutants (Fig. 3.1F-H). Collectively, this data supports the notion that CsgB quickly adopts an amyloid confirmation that templates CsgA polymerization.

The β–sheet rich domain of CsgA and CsgB contain five regions of imperfect homology referred to as repeating units. Mutagenesis was used to determine that CsgA requires both its N-terminal (CsgA r1) and C-terminal (CsgA r5) repeating units to polymerize *in vivo* [23]. Mutating the conserved glutamines and asparagines in repeating units r1 and r5 greatly hindered CsgA polymerization [22]. In a similar fashion, we assessed the importance of CsgB repeating units to nucleator function. CsgB$^{\Delta r1,}$ CsgB$^{\Delta r2}$, and CsgB$^{\Delta r3}$ were all able to complement a *csgB* mutant for Congo red binding, and CsgA was SDS insoluble in all these mutant backgrounds (Fig. 3.2B and C). Only when the conserved glutamines and asparagines in both CsgB r1 and CsgB r2 were mutated was nucleator function completely lost (Fig. 3.4). The C-terminal CsgB repeating units were sensitive to mutagenesis. CsgB mutants deleted for either CsgB r4 or CsgB r5 could not complement a *csgB* mutant for Congo red binding and fibers could not be observed when these mutants were viewed by EM (Fig. 3.2B and C) [25]. The defect of the CsgB$^{\Delta r5}$ mutant was attributed to the fact the protein was no longer anchored to the cell (Fig. 3.2C) [25]. The CsgB$^{\Delta r4}$ mutant was also not associated with the cell (Fig. 3.2C).

Even though both CsgB$^{\Delta r4}$ and CsgB$^{\Delta r5}$ were defective *in vivo*, both mutant proteins polymerized *in vitro*. In fact, all of the CsgB deletion mutants polymerized into amyloid fibers *in vitro* (Fig. 3B). These results suggest the *in vivo* molecular parameters for nucleation are more stringent than the parameters for CsgB polymerization *in vitro*. CsgB is soluble in the absence of CsgA *in vivo* [17, 21]. Anchoring CsgB to the membrane seems to be required

for efficient nucleator function and may also keep CsgB from polymerizing in the absence of CsgA *in vivo*. Determining the molecular details of the CsgB-membrane interaction will increase our understanding of how *E. coli* keeps CsgB from polymerizing at the membrane without compromising physiology. These details could also lead to novel insights into amyloid biology, because the membrane is particularly sensitive to the accumulation of cytotoxic intermediates produced during amyloid fiber biogenesis.

The molecular events that initiate amyloid biogenesis *in vivo* are not understood. Curli biogenesis represents an elegant functional amyloid biosynthesis pathway that prevents the accumulation of toxic precursors. Our results provide support for the model of curli biogenesis where CsgB quickly adopts an amyloid-like fold that templates the folding of soluble CsgA as it comes in contact with the cell surface. Further study of curli biogenesis proceeds without the accumulation of toxic intermediates, from both *in vivo* and *in vitro* perspectives, may provide alternative approaches for inhibiting disease associated amyloid biogenesis.

Experimental Procedures

Bacterial Growth. For protein expression and general strain propagation bacteria were cultured in L broth [41]. To induce curli production, bacteria were grown at 26° C on yeast extract casamino acids (YESCA) plates [10]. Curli production was monitored by using Congo red-containing YESCA plates [10]. To promote biofilm development cells were incubated for 30 days in liquid YESCA broth at

26° C. When necessary growth media was supplemented with antibiotics at the following concentrations: kanamycin 50 μg/ml or ampillicin, 100 μg/ml.

Bacterial Strains and Plasmids. MC4100 was the WT strain used [42]. The other strains and plasmids used in this study can be found in table 1. Primers used to construct the plasmids in this study can be found in table 2. The repeating unit deletions and point mutants were constructed using synthesis by overlapping ends (SOEing) PCR. PCR was preformed using standard techniques. To test the ability of the *csgB* mutants to complement *csgB* cells the mutated sequences were all subcloned into pLR2, a plasmid that contains the native *csgBA* promoter, using NcoI and BamHI restriction sites found a the 5' and 3' end respectively [26]. To express and purify *sec*-signal minus WT CsgB and the repeating unit deletions, PCR-amplified sequences including 6 histidine residues at the C-terminus were subcloned into pET11d (New England Biolabs, Ipswich, MA) using NcoI and BamHI restriction sites. Our attempts to purify proteins using a denaturing protocol described below were hindered by a contaminating protein of approximately 30 kDa. We identified this protein as SlyD, a protein enriched with histidine residues at the C-terminus, by mass spectrophotometry analysis (Michigan Proteome Consortium). In order to eliminate this contamination we P1 transduced the *slyD::aph* allele from the Keio collection strain, JW3311, into our expression strain NEB 3016 [43, 44]. We named the resulting strain NDH 471.

CsgA and CsgB Protein purification. NDH 471 (NEB 3016 *slyD::aph*) cells harboring a pET11d vector containing polyhistidine-tagged mature versions of CsgA, CsgB, or the CsgB repeating unit deletions mutants were grown at 37° C to 0.9 OD_{600}. At this point the cells were induced with 0.5 mM isopropyl-β-D-thiogalactoside (IPTG) and induction proceeded at 37° C for an hour. Cells were collected by centifugation and the pellets were stored at -80° C. The cells were chemically lysed using 8 M guanidine hydrochloride (GndHCl) buffered with 50 mM potassium phosphate buffer (KPi) pH7.2. A total of 75 ml of lysis solution was used per pellet generated from a 500 ml culture. The lysate was incubated at room temperature with magnetic stirring for 24 hours. The insoluble portion of the lysate was removed by centrifuging at 10,500 x g for 15 minutes and the resulting supernatant was sonicated 5 times, each time for 15 seconds. Sonication was applied at 5 amplitudes. The samples were incubated for 2 minutes on ice in between bursts. The supernatant was then centrifuged again at 10,5000 x g for 15 min. HIS-Select™ HF NiNTA (Sigma Aldrich, Atlanta, GA) was added to the supernatant and this mixture was incubated for 1 hour at room temperature with rocking. The polyhistidine-tagged proteins were affinity purified by collecting the nickel beads as the mixture passed through a Kontes column. The beads were washed with 50 mM KPi pH7.2 to eliminate the GndHCl and then washed with 50 mM KPi containing 12.5 mM immidazole pH7.2 to elute contaminating proteins that bound to the nickel beads. The proteins were eluted from the column using 125 mM immidazole in 50 mM KPi pH 7.2. Fractions were collected and analyzed for the presence of protein by SDS PAGE. Protein

concentration was determined by the BCA assay (Thermo Scientific, Rockford, IL). We were not able to purify $CsgB^{\Delta r1}$. A significant amount of $CsgB^{\Delta r1}$ protein was found to be SDS insoluble even after the cells were resuspended in 8 M GndHCl (data not shown).

Thioflavin-T (ThT) Assay. Proteins were mixed with 20 μM thioflavin-T (ThT) in 96-well plates and incubated at room temperature. Every 10 minutes samples were excited at 438 nm and fluorescence emitted 495 nm with a 475 nm cutoff was measured using a Spectramax M2 plate reader (Molecular Devices, Sunnyvale, CA). Samples were shaken for 5 seconds before each read. Due to the differences in preparation–to-preparation protein yield, a representative ThT kinetic graph taken from a series of ThT assays is shown. The net RFUs generated by a protein at a specific concentration from a given preparation were remarkably consistent with the net RFUs generated from a similar concentration of the same protein purified from a different preparation. ThT fluorescence was normalized using $(F_i - F_o)/(F_{max} - F_o)$ were F_o was the ThT background intensity (fluorescence arbitrary unit), F_i was the ThT intensity of samples, and F_{max} was the maximum ThT intensity of the reaction. Samples used to seed CsgA were sonicated using a sonic dismembrator (Fisher Model 100; Fisher, Pittsburg, PA) for three 15-second bursts on ice.

Overlay assay. Cells were grown under curli inducing conditions as previously described for 24 hours on YESCA plates. Purified CsgB (10 ul) was pipetted

onto the bacterial lawn and incubated at 26° C for an additional 24 hours. Congo red dye (10mg/ml) was then applied to the bacterial lawn-CsgB mixture. The dye was decanted and the bacterial lawns were carefully washed with 50 mM KPi buffer pH 7.2.

Transmission Electron Microscopy (TEM). Samples (10 μL) were placed on Formvar-coated copper grids (Ernest F. Fullman, Inc., Latham, NY) for 2 minutes, washed twice briefly (10 seconds) with deionized water, and negatively stained with 2% uranyl acetate for 90 seconds. Samples were viewed using a Phillips CM-100 transmission electron microscope.

SDS/PAGE and Western Blotting. Bacteria whole cell lysates and agar plugs were prepared and probed for both CsgA and CsgB by using previously described methods [25, 26].

Peptide preparation. Peptides were chemically synthesized (Proteintech Group, Chicago, IL). Purity was greater that 90% by high pressure liquid chromatography, and size was confirmed by mass spectroscopy (Proteintech Group, Chicago, IL). Lyophilized peptide (1 mg) was dissolved in 8 M GndHCl (1ml) buffered by 50 mM potassium phosphate pH 7.2. The suspension was incubated at room temperature for 1 hour with rocking. In order to remove the 8 M GndHCl and collect the soluble peptide, the sample was passed through a Sephadex G10 column that was balanced in 50 mM potassium phosphate pH

7.2. The BCA assay was used to assess peptide concentration and polymerization was monitored by ThT.

Figure legends

Figure 3.1. Biochemical and physiological properties of WT CsgB. (A) Coomassie stained SDS-PAGE of normalized cell lysates pre-induction (IPTG -) or post-induction (IPTG +) lanes 1 through 3. Cells were resuspended in SDS loading buffer (-) or pretreated with formic acid (FA)(+). CsgB was solubilized post purification by incubation in 8 M guanidine HCl (Lane 4). (B) Representative ThT kinetic plot of 70 μM (○), 35 μM (□), or 17.5 μM (◇) purified CsgB and 27 μM purified CsgA (X). Relative fluorescent units (RFUs) emitted at 495 nm were recorded every 10 min. after excitation at 438 nm. (C) TEM of 65 μM CsgB incubated at room temperature. The scale bar represents 500nm. (D) Coomassie stained SDS-PAGE of 65 μM CsgB polymerized into fibers, centrifuged and resuspended in SDS loading buffer with (+) or without (-) prior formic acid (FA) treatment (E) Representative ThT kinetic plot of 27 μM CsgA (X), 27 μM CsgA and 5% (●) or 12 % (■) w/w WT CsgB seeds. (F) 10 ul of 37 μM purified CsgB was overlaid on *csgA* and *csgB* mutants and stained with Congo red dye after a 24-hour incubation at 26° C. (G) TEM of *csgB* cells that were incubated with 37 μM purified CsgB and stained with Congo red dye. The scale bar represents 500nm. (H) CsgA western blot analysis of the *csgB* cells in (F) that were incubated in the absence of CsgB (Lanes 1 and 2) or

presence of CsgB (lanes 3 and 4). Samples were resuspended in SDS loading buffer with (+) or without (-) formic acid (FA) pretreatment.

Figure 3.2. Contribution of each repeating unit to CsgB function *in vivo*. (A) Amino acid sequence alignment of the CsgA and CsgB repeating units. Arrows represent each repeating unit. Boxed amino acids indicate the conserved glutamines and asparagines that were mutated to alanine for each mutant. (B) Congo red binding phenotype of MC4100 (WT), or *csgB* harboring a vector control plasmid (vector), WT *csgB*, CsgB$^{\Delta r1}$ (Δr1), CsgB$^{\Delta r2}$ (Δr2), CsgB$^{\Delta r3}$ (Δr3), CsgB$^{\Delta r4}$ (Δr4), or CsgB$^{\Delta r5}$ (Δr5). Scale bar represents 500 nm. (C) Western blot analysis, using α-CsgB or α-CsgA antibodies, of *csgB* harboring a vector control (vector lanes 1 and 2), WT *csgB* (lanes 3 and 4), CsgB$^{\Delta r1}$ (Δr1 lanes 5 and 6), CsgB$^{\Delta r2}$ (Δr2 lanes 7 and 8), CsgB$^{\Delta r3}$ (Δr3 lanes 9 and 10), CsgB$^{\Delta r4}$ (Δr4 lanes 11 and 12), or CsgB$^{\Delta r5}$ (Δr5 lanes 13 and 14). Prior to loading the gel, samples were resuspended in SDS loading buffer with (+) or without (-) formic acid (FA) pretreatment. The top two panels are samples blotted using anti-CsgB antibody. The bottom panel is a blot probed with anti-CsgA antibody. Whole cells samples are represented in the first and third panel, while samples containing whole cells and the underlying agar are represented in the second panel. (D) TEM of *csgB* mutants harboring CsgB$^{\Delta r1}$ (Δr1), CsgB$^{\Delta r2}$ (Δr2), CsgB$^{\Delta r3}$ (Δr3), or CsgB$^{\Delta r4}$ (Δr4) grown under curli-inducing conditions. The scale bars represent 500 nm. (E) Comparison of MC4100 (WT test tube 1), and *csgB* harboring WT CsgB (test tube 2), CsgB$^{\Delta r1}$ (Δr1 test tube 3), CsgB$^{\Delta r2}$ (Δr2 test tube 4), CsgB$^{\Delta r3}$ (Δr3 test

tube 5), CsgB$^{\Delta r4}$ (Δr4 test tube 6), or CsgB$^{\Delta r5}$ (Δr5 test tube 7) for pellicle formation after 30 days of growth in YESCA broth at 26° C.

Figure 3.3. *In vitro* characterization of the repeating unit deletions. (A) Coomassie stained SDS-PAGE of normalized cell lysates of cells harboring pET11d (EV lanes 1 and 2), WT CsgB (lanes 3 and 4), CsgB$^{\Delta r1}$ (Δr1 lanes 5 and 6), CsgB$^{\Delta r2}$ (Δr2 lanes 7 and 8), CsgB$^{\Delta r3}$ (Δr3 lanes 9 and 10), CsgB$^{\Delta r4}$ (Δr4 lanes 11 and 12), or CsgB$^{\Delta r5}$ (Δr5 lanes 13 and 14) after 1 hour incubation with 0.5 mM IPTG. Prior to loading the gel, samples were resuspended in SDS loading buffer with (+) or without (-) formic acid (FA) pretreatment. (B) Representative ThT kinetic plot of the WT CsgB (○), CsgB$^{\Delta r2}$ (Δr2 □), CsgB$^{\Delta r3}$ (Δr3 △), CsgB$^{\Delta r4}$ (Δr4 X), and CsgB$^{\Delta r5}$ (Δr5 ◇). The inset is a representative bar graph the RFUs for each protein after 12 hours of incubation at room temperature with ThT. (C) TEM of purified CsgB$^{\Delta r2}$ (Δr2 top panel) or purified CsgB$^{\Delta r4}$ (Δr4 bottom panel) after 24 hours of incubation at room temperature. The scale bars represent 500nm. (D) Representative thioflavin-T kinetic plot monitoring the polymerization of 14 μM CsgA (X), 14 μM seeded with 9% w/w WT CsgB (●), seeded with 3.5% w/w WT CsgB (○), seeded with 9% w/w CsgB$^{\Delta r2}$ (Δr2 ■), seeded with 3.5% w/w CsgB$^{\Delta r2}$ (Δr2 □), seeded with 8% w/w CsgB$^{\Delta r4}$ (Δr4 ▲), or seeded with 3.5% w/w CsgB$^{\Delta r4}$ (Δr4 △).

Figure 3.4. *In vivo* functional analysis of the conserved glutamines and asparagines in the amyloidogenic repeating units of CsgB. (A) Relative

fluorescent units produced by synthetic peptides composed of the amino acids in r1 (145 μM), r2 (102 μM), r3 (138 μM), r4 (176 μM), and r5 (167 μM) after incubation at room temperature for 24 hours in the presence of ThT. (B) Congo red binding phenotype of MC4100 (WT) or *csgB* harboring vector control (vector), WT *csgB*, *csgB r1mut*, *csgB r2mut*, *csgB r4mut*, or *csgB r12mut*. (C) Western blot analysis, using either α-CsgB or α-CsgA antibodies, of *csgB* harboring WT *csgB* (lanes 1 and 2), *csgB r1mut* (lanes 3 and 4), *csgB r2mut* (lanes 5 and 6), *csgB r4mut* (lanes 7 and 8), or *csgB r12mut* (lanes 9 and 10). Samples were resuspended in SDS loading buffer with (+) or without (-) prior treatment with formic acid (FA). Top two panels were blotted with anti-CgsB antibody. Bottom two panels were blotted with anti-CsgA antibody. Whole cell samples are represented in the first and third panel, while samples containing whole cells and the underlying agar are represented in the second and fourth panel. (D) TEM of *csgB* complemented with *csgB r1mut*, *csgB r2mut*, *csgB r4mut*, or *csgB r12mut*. Cells were collected after growth in curli inducing-conditions. The scale bar represents 500nm.

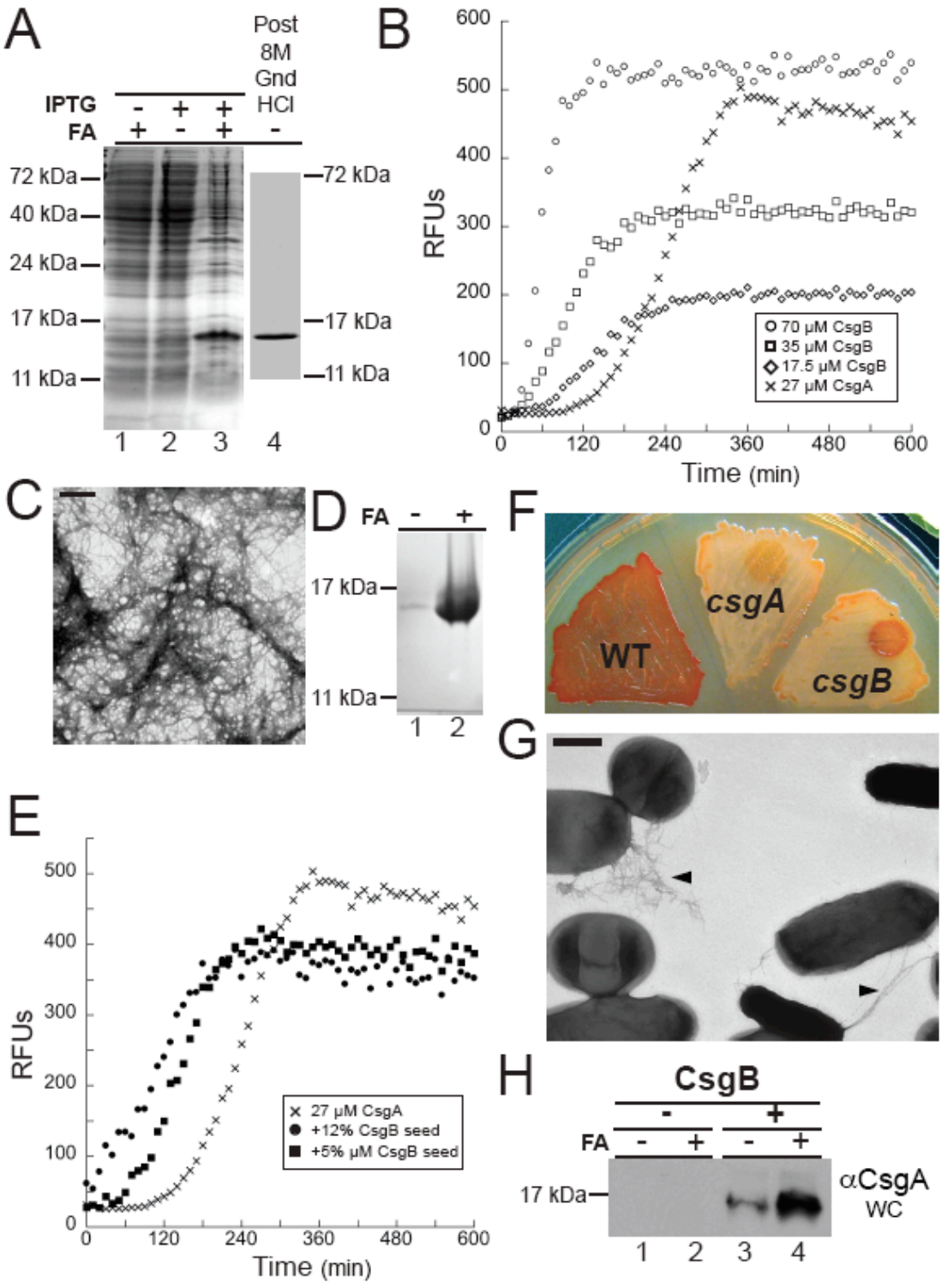

Figure 3.1. Biochemical and physiological properties of WT CsgB.

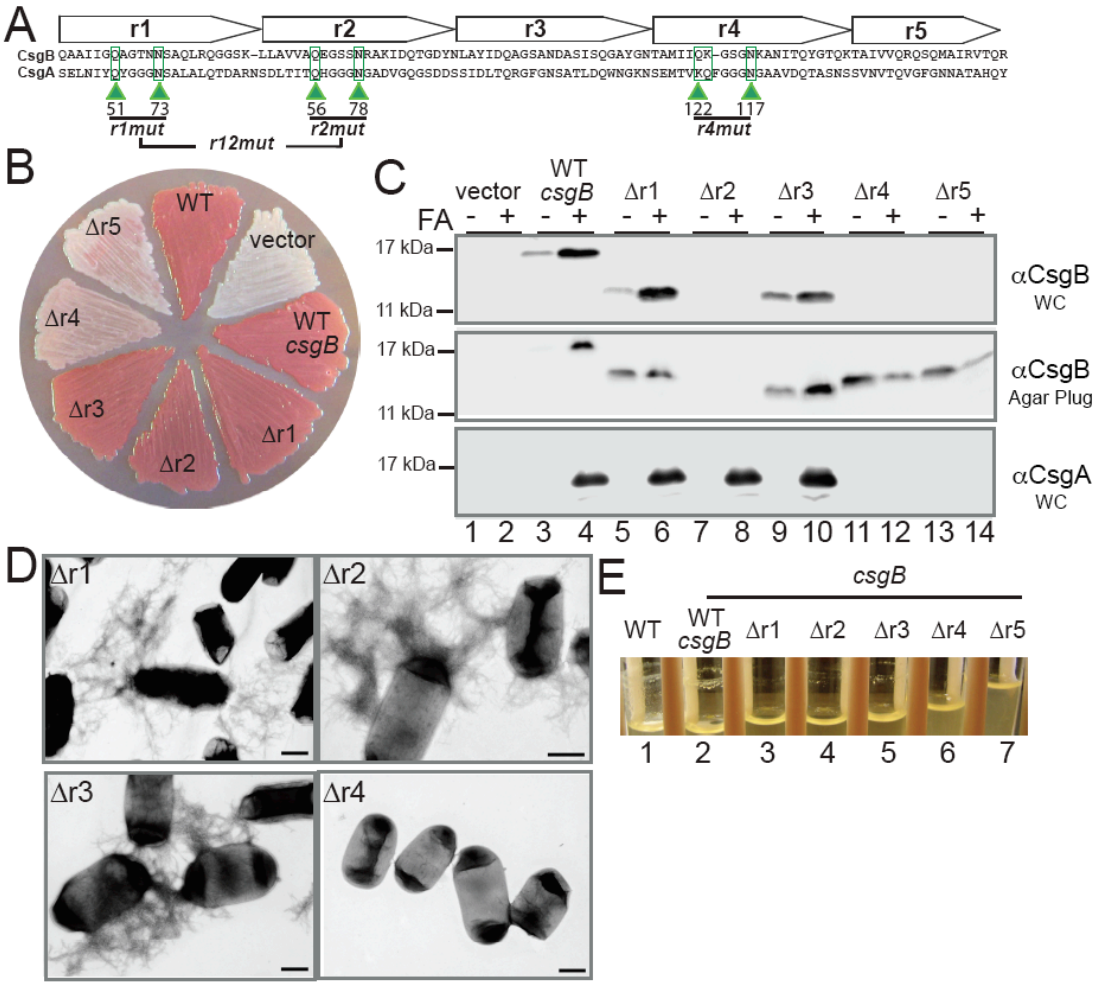

Figure 3.2. Contribution of each repeating unit to CsgB function *in vivo*.

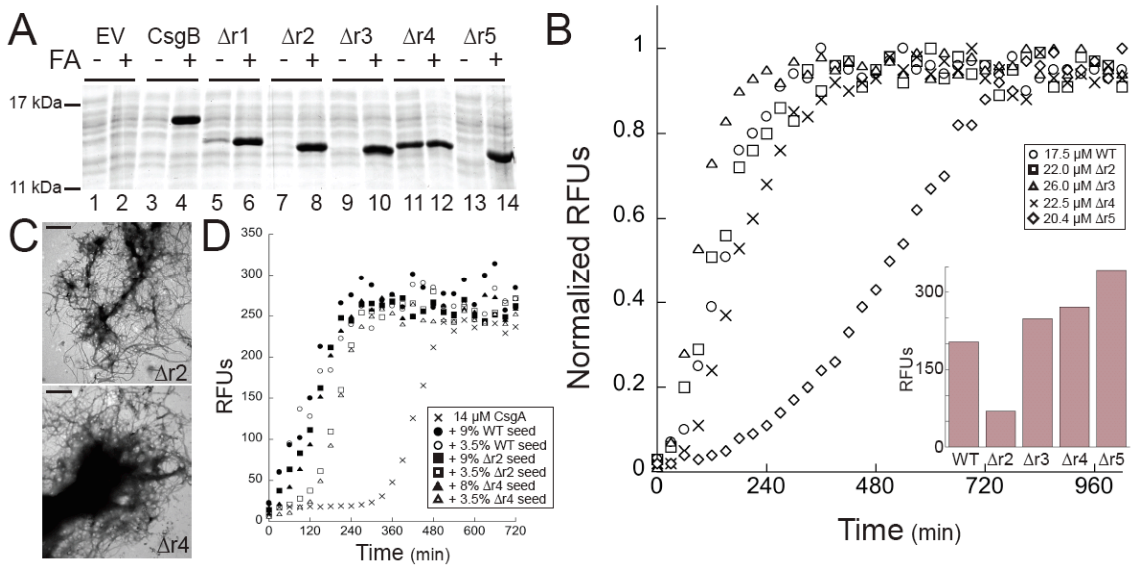

Figure 3.3. *In vitro* characterization of the repeating unit deletions.

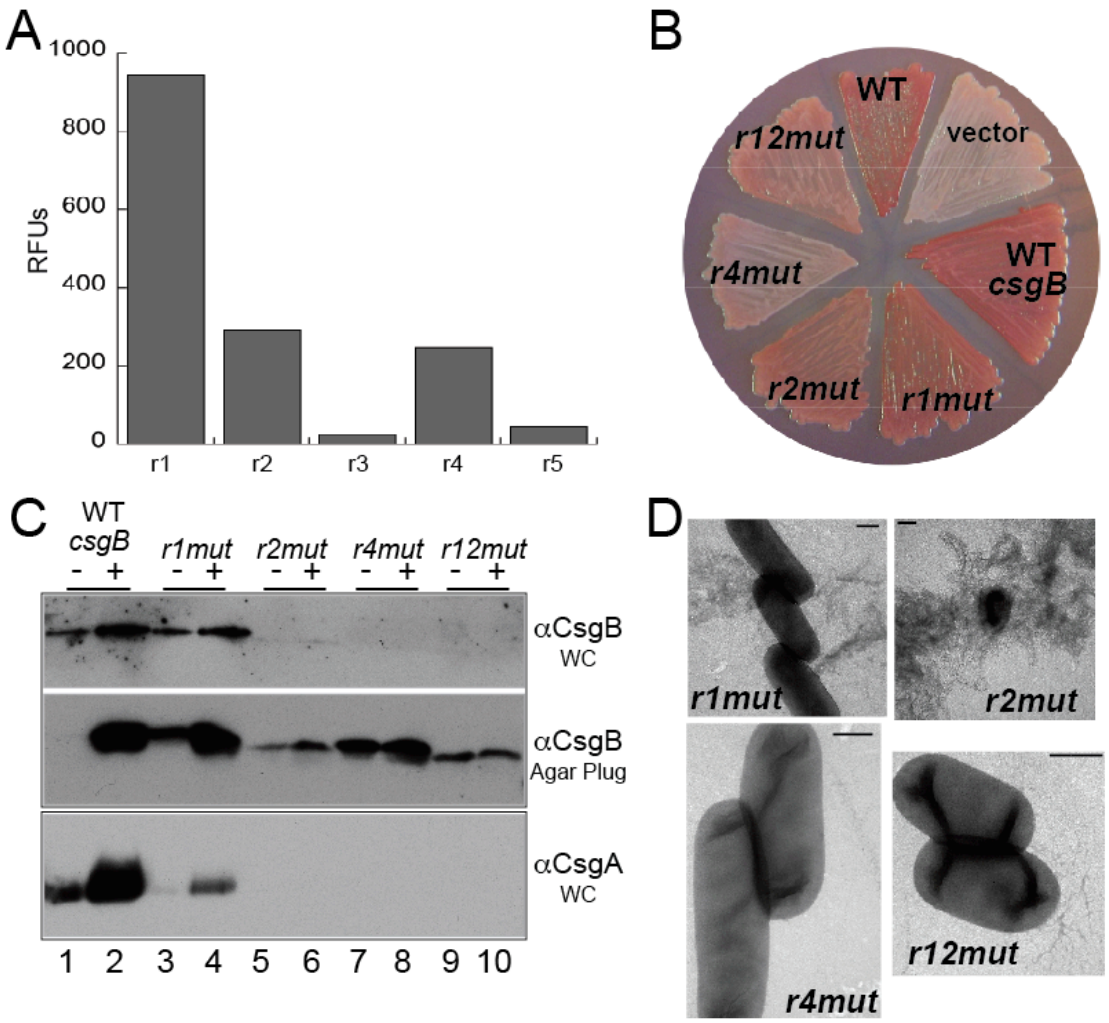

Figure 3.4. *In vivo* functional analysis of the conserved glutamines and asparagines in the amyloidogenic repeating units of CsgB

Strains	Relevant characteristics	Refs.
MC4100	F- *araD*139 Δ(*argF-lac*) U169 *rpsL*150(*strR*) *relA*1 *fibB*5301 *deoC*1 *ptsF*25 *rbsB*	42
MHR261	*csgB*	17
LSR10	Δ*csgA*	10
NEB 3016	*fhuA2 lacZ::T7 gene1 [lon] ompT gal sulA11 R(mcr-73::miniTn10--*Tet^S*)2 [dcm] R(zgb-210::Tn10--*Tet^S*) endA1 Δ(mcrC-mrr)114::IS10 [mini-lacI^q (*Cam^R*)]*	NEB
JW3311	*slyD::aph*	44
NDH471	NEB 3016 *slyD::aph*	This Study

Table 3.1. Strains used in this study

Plasmids	Relevant characteristics	References
pLR2	Vector containing the *csgBA* promoter	26
pLR8	*csgB* cloned into pLR2	Hammer
pNH1	$csgB^{\Delta r5}$ cloned into pLR2	Hammer
pBM1	$csgB^{\Delta r1}$ cloned into pLR2	This study
pBM2	$csgB^{\Delta r2}$ cloned into pLR2	This study
pBM3	$csgB^{\Delta r3}$ cloned into pLR2	This study
pBM4	$csgB^{\Delta r4}$ cloned into pLR2	This study
pNH38	$csgB^{Q51A\ N56A}$ cloned into pLR2 (*r1mut)*	This study
pNH39	$csgB^{Q73A\ N78A}$ cloned into pLR2 (*r2mut)*	This study
pNH40	$csgB^{Q117A\ N122A}$ cloned into pLR2 (*r4mut)*	This study
pNH45	$csgB^{Q51A\ N56A\ Q73A\ N78A}$ cloned into pLR2 (*r12mut)*	This study
pET11d	Expression vector	NEB
pAN1	WT *csgB* cloned into pET11d	This study
pNH20	$csgB^{\Delta r1}$ cloned into pET11d	This study
pNH21	$csgB^{\Delta r2}$ cloned into pET11d	This study
pNH22	$csgB^{\Delta r3}$ cloned into pET11d	This study
pNH23	$csgB^{\Delta r4}$ cloned into pET11d	This study
pNH28	$csgB^{\Delta r5}$ cloned into pET11d	This study

Table 3.2. Plasmids used in this study

Primer	Primer Sequence	Construct
NDH7[a]	5'-GCG*CCATGG*GGAAAAACAAATTGTTATTTATG-3'	ORFs cloned into pLR2
BAM2*	5'- AAGTCTTCATTTAATCTTTTGGCGGTTGTT –3'	pBM1 (CsgB$^{\Delta r1}$)
BAM4*	5'- CAGGGAGGCTCAAAAAACCTTGCATATATT -3'	pBM2 (CsgB$^{\Delta r2}$)
BAM6*	5'- CAGACAGGAGATTATAATACTGCGATGATT -3'	pBM3 (CsgB$^{\Delta r3}$)
BAM8*	5'- CAAGGTGCTTATGGTAAAACGGCAATTGTA -3'	pBM4 (CsgB$^{\Delta r4}$)
NDH67*	5'-ATAATTGGTGCGGCTGGGACTAATGCGAGTGCTCAG-3'	pNH38 (*r1mut*)
NDH69*	5'-GTTGTTGCGGCTGAAGGTAGTAGCGCTCGGGCAAAG-3'	pNH39 (*r2mut*)
NDH71*	5'-ATGATTATCGCTAAAGGTTCTGGTGCTAAAGCAAAT-3'	pNH40 (*r4mut*)
BAM11[a]	5'- GCG*GGATCC*TTAACGTTGTGTCACGCG-3'	ORFs cloned into pLR2
NDH46 [b]	5'-GCGTTT*CCATGG*CAGGTTATGATTTAGCTAATTCAG-3'	ORFs cloned into pET11d
NDH47[b]	5'-GTTTAAAGCTT*GGATCC*TTAGTGGTGGTGGTGGTGGTGACGT TGTGTCACGCGAATAGCC -3'	ORFs cloned into pET11d
NDH50	5'-GCG*GGATCC*TTAGTGATGGTGATGGTGATGTTGAGTACCATA CTGTGTATTATT-3'	pNH28 (CsgB$^{\Delta r5}$)
FpLR5[c]	5'-CATGCCATGGCGAAACTTTTAAAAGTAGC-3'	Sequencing
RpLR5 [c]	5'-CGGGATCCTGTATTAGTACTGAT -3'	Sequencing

Table 3.3. Primers used in this study.

Restriction sites used for cloning are italicized and underlined. Point mutations generated by the primers are underlined.

[a] NDH7 and BAM11 were used as the forward and reverse primers to clone into pLR2 respectively.

[b] NDH46 and NDH47 were the forward and reverse primers used to amplify the *sec*-signal sequence minus CsgB and mutant variants that were cloned into pET11d. Plasmids pBM1, pBM2, pBM3, and pBM4 were used as the templates to generate pNH20, pNH21, pNH22, and pNH23 respectively. The T7 primer provided by the University of Michigan DNA Sequencing Core was used to confirm the sequence of each ORF.

[c] Primers FpLR5 and RpLR5 were used to sequence the mutants cloned into pLR2.

*Primers BAM2, BAM4, BAM6, BAM8, NDH67, NDH69, and NDH71 were used to amplify one of the two PCR products needed for the fusion PCR. The reverse complement of these primers was used to amplify the other PCR product needed for fusion PCR.

References

1. Cohen, F.E. and J.W. Kelly, *Therapeutic approaches to protein-misfolding diseases.* Nature, 2003. **426**(6968): p. 905-9.

2. Chiti, F. and C.M. Dobson, *Protein misfolding, functional amyloid, and human disease.* Annu Rev Biochem, 2006. **75**: p. 333-66.

3. Pedersen, J.S., G. Christensen, and D.E. Otzen, *Modulation of S6 fibrillation by unfolding rates and gatekeeper residues.* J Mol Biol, 2004. **341**(2): p. 575-88.

4. Serio, T.R., et al., *Nucleated conformational conversion and the replication of conformational information by a prion determinant.* Science, 2000. **289**(5483): p. 1317-21.

5. Uversky, V.N., et al., *Biophysical properties of the synucleins and their propensities to fibrillate: inhibition of alpha-synuclein assembly by beta- and gamma-synucleins.* J Biol Chem, 2002. **277**(14): p. 11970-8.

6. Wang, X., et al., *In vitro polymerization of a functional Escherichia coli amyloid protein.* J Biol Chem, 2007. **282**(6): p. 3713-9.

7. Jarrett, J.T. and P.T. Lansbury, Jr., *Seeding "one-dimensional crystallization" of amyloid: a pathogenic mechanism in Alzheimer's disease and scrapie?* Cell, 1993. **73**(6): p. 1055-8.

8. Lomakin, A., et al., *On the nucleation and growth of amyloid beta-protein fibrils: detection of nuclei and quantitation of rate constants.* Proc Natl Acad Sci U S A, 1996. **93**(3): p. 1125-9.

9. Rochet, J.C. and P.T. Lansbury, Jr., *Amyloid fibrillogenesis: themes and variations.* Curr Opin Struct Biol, 2000. **10**(1): p. 60-8.

10. Chapman, M.R., et al., *Role of Escherichia coli curli operons in directing amyloid fiber formation.* Science, 2002. **295**(5556): p. 851-5.

11. Wang, X., et al., *Impact of biofilm matrix components on interaction of commensal Escherichia coli with the gastrointestinal cell line HT-29.* Cell Mol Life Sci, 2006. **63**(19-20): p. 2352-63.

12. Uhlich, G.A., P.H. Cooke, and E.B. Solomon, *Analyses of the red-dry-rough phenotype of an Escherichia coli O157:H7 strain and its role in biofilm formation and resistance to antibacterial agents.* Appl Environ Microbiol, 2006. **72**(4): p. 2564-72.

13. Barnhart, M.M. and M.R. Chapman, *Curli biogenesis and function.* Annu Rev Microbiol, 2006. **60**: p. 131-47.

14. Gerstel, U. and U. Romling, *The csgD promoter, a control unit for biofilm formation in Salmonella typhimurium.* Res Microbiol, 2003. **154**(10): p. 659-67.

15. Vidal, O., et al., *Isolation of an Escherichia coli K-12 mutant strain able to form biofilms on inert surfaces: involvement of a new ompR allele that increases curli expression.* J Bacteriol, 1998. **180**(9): p. 2442-9.

16. Olsen, A., A. Jonsson, and S. Normark, *Fibronectin binding mediated by a novel class of surface organelles on Escherichia coli.* Nature, 1989. **338**(6217): p. 652-5.

17. Hammar, M., Z. Bian, and S. Normark, *Nucleator-dependent intercellular assembly of adhesive curli organelles in Escherichia coli.* Proc Natl Acad Sci U S A, 1996. **93**(13): p. 6562-6.

18. White, A.P., et al., *Structure and characterization of AgfB from Salmonella enteritidis thin aggregative fimbriae.* J Mol Biol, 2001. **311**(4): p. 735-49.

19. Bian, Z. and S. Normark, *Nucleator function of CsgB for the assembly of adhesive surface organelles in Escherichia coli.* Embo J, 1997. **16**(19): p. 5827-36.

20. Hammar, M., et al., *Expression of two csg operons is required for production of fibronectin- and congo red-binding curli polymers in Escherichia coli K-12.* Mol Microbiol, 1995. **18**(4): p. 661-70.

21. Loferer, H., M. Hammar, and S. Normark, *Availability of the fibre subunit CsgA and the nucleator protein CsgB during assembly of fibronectin-binding curli is limited by the intracellular concentration of the novel lipoprotein CsgG.* Mol Microbiol, 1997. **26**(1): p. 11-23.

22. Wang, X. and M.R. Chapman, *Sequence determinants of bacterial amyloid formation.* J Mol Biol, 2008. **380**(3): p. 570-80.

23. Wang, X., N.D. Hammer, and M.R. Chapman, *The molecular basis of functional bacterial amyloid polymerization and nucleation.* J Biol Chem, 2008. **283**(31): p. 21530-9.

24. Collinson, S.K., et al., *Structural predictions of AgfA, the insoluble fimbrial subunit of Salmonella thin aggregative fimbriae.* J Mol Biol, 1999. **290**(3): p. 741-56.

25. Hammer, N.D., J.C. Schmidt, and M.R. Chapman, *The curli nucleator protein, CsgB, contains an amyloidogenic domain that directs CsgA polymerization.* Proc Natl Acad Sci U S A, 2007. **104**(30): p. 12494-9.

26. Robinson, L.S., et al., *Secretion of curli fibre subunits is mediated by the outer membrane-localized CsgG protein.* Mol Microbiol, 2006. **59**(3): p. 870-81.

27. Bucciantini, M., et al., *Inherent toxicity of aggregates implies a common mechanism for protein misfolding diseases.* Nature, 2002. **416**(6880): p. 507-11.

28. Larson, J., et al., *Alterations in synaptic transmission and long-term potentiation in hippocampal slices from young and aged PDAPP mice.* Brain Res, 1999. **840**(1-2): p. 23-35.

29. Lue, L.F., et al., *Soluble amyloid beta peptide concentration as a predictor of synaptic change in Alzheimer's disease.* Am J Pathol, 1999. **155**(3): p. 853-62.

30. Malisauskas, M., et al., *Does the cytotoxic effect of transient amyloid oligomers from common equine lysozyme in vitro imply innate amyloid toxicity?* J Biol Chem, 2005. **280**(8): p. 6269-75.

31. McLean, C.A., et al., *Soluble pool of Abeta amyloid as a determinant of severity of neurodegeneration in Alzheimer's disease.* Ann Neurol, 1999. **46**(6): p. 860-6.

32. Moechars, D., et al., *Early phenotypic changes in transgenic mice that overexpress different mutants of amyloid precursor protein in brain.* J Biol Chem, 1999. **274**(10): p. 6483-92.

33. Sirangelo, I., et al., *Fibrillogenesis and cytotoxic activity of the amyloid-forming apomyoglobin mutant W7FW14F.* J Biol Chem, 2004. **279**(13): p. 13183-9.

34. Sousa, M.M., et al., *Deposition of transthyretin in early stages of familial amyloidotic polyneuropathy: evidence for toxicity of nonfibrillar aggregates.* Am J Pathol, 2001. **159**(6): p. 1993-2000.

35. Wang, J., et al., *The levels of soluble versus insoluble brain Abeta distinguish Alzheimer's disease from normal and pathologic aging.* Exp Neurol, 1999. **158**(2): p. 328-37.

36. Cecchi, C., et al., *Insights into the molecular basis of the differing susceptibility of varying cell types to the toxicity of amyloid aggregates.* J Cell Sci, 2005. **118**(Pt 15): p. 3459-70.

37. Stefani, M. and C.M. Dobson, *Protein aggregation and aggregate toxicity: new insights into protein folding, misfolding diseases and biological evolution.* J Mol Med, 2003. **81**(11): p. 678-99.

38. Bokvist, M., et al., *Two types of Alzheimer's beta-amyloid (1-40) peptide membrane interactions: aggregation preventing transmembrane anchoring versus accelerated surface fibril formation.* J Mol Biol, 2004. **335**(4): p. 1039-49.

39. Kayed, R., et al., *Permeabilization of lipid bilayers is a common conformation-dependent activity of soluble amyloid oligomers in protein misfolding diseases.* J Biol Chem, 2004. **279**(45): p. 46363-6.

40. Fowler, D.M., et al., *Functional amyloid formation within mammalian tissue.* PLoS Biol, 2006. **4**(1): p. e6.

41. Miller, J.H., *Experiments in molecular genetics*. 1972, [Cold Spring Harbor, N.Y.]: Cold Spring Harbor Laboratory. xvi, 466 p.

42. Casadaban, M.J., *Transposition and fusion of the lac genes to selected promoters in Escherichia coli using bacteriophage lambda and Mu.* J Mol Biol, 1976. **104**(3): p. 541-55.

43. Goldberg, R.B., R.A. Bender, and S.L. Streicher, *Direct selection for P1-sensitive mutants of enteric bacteria.* J Bacteriol, 1974. **118**(3): p. 810-4.

44. Baba, T., et al., *Construction of Escherichia coli K-12 in-frame, single-gene knockout mutants: the Keio collection.* Mol Syst Biol, 2006. **2**: p. 2006 0008.

Chapter IV

Conclusions

Amyloid fibers are a common pathology of many neurodegenerative diseases such as Alzheimer's disease, Parkinson's disease, and the spongiform encephalopathies [1]. Due to this association with neurodegeneration, amyloid fiber biogenesis was exclusively believed to be the result of protein misfolding. It is thought that normally soluble proteins aggregate into amyloid fibers in these diseases. This has led to the current models of amyloid cytotoxicity, where the accumulation of amyloid fiber precursors leads to cell death [1]. However, a paradigm shift has recently occurred in the amyloid field based on the discoveries that bacteria, yeast, and even mammalian cells produce amyloid fibers under physiological conditions. These organisms utilize the amyloid fold to carry out specific functions and the amyloid fibers are produced without compromising the physiology of the cell [2-4]. Instead of the random, sporadic *in vivo* polymerization of the disease associated amyloids, the functional amyloids are the result of dedicated biogenesis pathways.

Curli was the first functional amyloid to be described [5]. *Escherichia coli* uses the gene products from two divergently transcribed operons, *csgDEFG* and *csgBA*, to polymerize an amyloid fiber on the cell suface [6]. The fibers function as a component of the extracellular matrix required for the development of

biofilms [7-9]. The *csgBA* operon encodes the minor and major fiber subunits, CsgB and CsgA, respectively [10-12]. CsgB is required for CsgA polymerization *in vivo*, but *in vitro* CsgA can self assemble into amyloid fibers [11, 13]. *In silico* structural predictions suggest both CsgA and CsgB are β-sheet rich proteins composed of a domain that be divided into five repeats of imperfect homology [10-12]. Each repeat contains a β–sheet-loop-β-sheet-loop motif that feature conserved glutamine and asparagines residues. We call each of these repeats repeating units. The similarities between CsgA and CsgB led us to hypothesize that CsgB acts to convert CsgA into an amyloid via a template mediated mechanism. Therefore, CsgB may also have the ability to self assemble into an amyloid fiber *in vitro*.

CsgB can polymerize into an amyloid in vitro

Amyloid fibers are biochemically unique structures. The fibers are detergent insoluble, proteinase resistant, β-sheet rich polymers that bind the dyes Congo red and thioflavin-T (ThT) [1]. Amyloid fibers have a distinct morphology when viewed by electron micrsoscopy (EM). Because ThT fluoresces when bound to an amyloid fiber, the polymerization of amyloid fibers can be kinetically monitored by recording ThT fluorescence over time. Amyloid polymerization is nucleus dependent [14]. This means polymerization contains a distinct lag phase that represents the time necessary for monomeric protein to assemble into a nucleus. Rapid polymerization proceeds after the formation of the nucleus. The length of lag phase can be substantially decreased if preformed

amyloid fibers are added to the reaction. In this case the formation of the nucleus is not required because the preformed fibers act as a β-sheet rich folding template for the monomeric, unstructured protein.

When I joined the Chapman lab, I set out to elucidate the molecular mechanism of CsgB-mediated nucleation. My hypothesis was that CsgB presented an amyloid-like template to CsgA that stimulated CsgA polymerization and, thus curli formation on the cell surface. We have previously shown that fibers composed of self assembled CsgA have all the biochemical characteristics of amyloid [13]. CsgA polymerization *in vitro* has an approximate two-hour lag phase when incubated at concentrations between 5 and 50 μM [13]. To determine if CsgB also possessed the ability to self assemble into an amyloid, I purified a truncated version of CsgB ($CsgB_{trunc}$) that could be easily recovered from the extracellular milieu as a soluble unstructured protein. $CsgB_{trunc}$ adopted a β–sheet rich, SDS insoluble aggregate after a short incubation at room temperature. These aggregates looked identical to amyloid fibers when viewed by EM, and caused a red-shift when incubated in the presence of Congo red. Polymerization of $CsgB_{trunc}$ occurred after a two hour lag phase [15].

Using a modified procedure, I was able to purify wild type (WT) CsgB. CsgB was SDS insoluble after cells were induced to express the protein in the cytoplasm. Soluble CsgB could be recovered from the cytoplasm if cells were resuspended in 8 M guanidine hydrochloride. CsgB polymerized into SDS insoluble aggregates that fluoresced ThT, and the aggregates were also

morphologically similar to amyloid fibers when visualized by EM. These results suggest that CsgB was able to self assemble into an amyloid fiber *in vitro*.

WT CsgB polymerized with a lag phase of about 30 minutes suggesting the protein adopts an amyloid conformation faster than CsgA *in vitro*. It should be noted that three CsgB mutants had altered ThT polymerization kinetics. CsgB missing the third repeating unit appeared to polymerize faster that WT CsgB [Chapter 3]. A peptide composed of amino acids found in the third repeating unit did not fluoresce ThT over time. Moreover, both of the predicted β–sheets in the third repeating unit contain an aspartic acid residue. Aspartic acid residues in CsgA have been demonstrated to contribute to the lag phase associated with CsgA polymerization *in vitro* [unpublished data, Wang, X]. These results suggest the CsgB mutant missing the third repeating unit polymerizes faster due to the loss of these aspartic acid residues. Two other CsgB mutants polymerized with altered polymerization kinetics. A CsgB mutant missing the second repeating unit consistently induced less ThT fluorescence than WT CsgB, and the previously mentioned truncated $CsgB_{trunc}$ mutant had a longer lag phase when compared to WT polymerization. Because this mutant had a longer lag phase, these results suggest the fifth repeating unit plays a role in initiating CsgB-CsgB interactions.

CsgB templates CsgA polymerization

CsgA polymerization proceeds without a lag phase if preformed CsgA fibers are added to the reaction mix [13]. This recapitulates what we think happens *in vivo*, where the growing fiber tips act a folding template for soluble

CsgA secreted from the cell. If CsgB acts to template CsgA polymerization, preformed CsgB fibers will also be able to decrease the lag phase associated with CsgA polymerization. Indeed, when preformed CsgB fibers were added to freshly purified, soluble CsgA, polymerization proceeded without an apparent lag [Chapter 3]. The fibers produced by CsgB mutants missing the second or fifth repeating units, i.e. CsgB mutants with defective ThT kinetics, were able to seed CsgA polymerization [Chapter 3, 15]. Purified CsgB was also able to template the polymerization of CsgA secreted from *csgB* mutants [Chapter 3]. These results suggest a model where CsgB quickly adopts a β–sheet fold that templates CsgA polymerization.

CsgB mutants missing the fourth or the fifth repeating unit ($CsgB_{trunc}$) were unable to complement *csgB* cells for curli biogenesis despite the fact that both mutant proteins polymerized into amyloid fibers that seeded CsgA *in vitro* [Chapter 3,15]. These mutants were stably expressed, but were not anchored to the cell [Chapter 3]. These results highlight the importance of localizing CsgB at the membrane, and suggest this is a way of controlling amyloid biogenesis. By anchoring CsgB to the membrane the cell ensures polymerization occurs only when both proteins are in close proximity. Determining the molecular details of CsgB interaction with the membrane and how this interaction occurs without perturbing physiology may lead to new ways of inhibiting the damage done to membranes exposured to the disease associated amyloids. Comparing the *in vitro* results to the *in vivo* results also suggest that the parameters for *in vivo*

CsgB function are far more stringent than those required for *in vitro* CsgB polymerization.

CsgB on the surface of *csgA* mutants is soluble, but can polymerize CsgA secreted from *csgB* mutants grown in close proximity [11]. Both CsgA and CsgB are secreted as SDS-soluble, unstructured proteins [13, 15]. This suggests that the proteins first interact as soluble proteins. Experiments where varying concentrations of freshly purified, soluble CsgB are mixed with freshly purified, soluble CsgA should be performed to determine if soluble CsgB can decrease the CsgA lag phase *in vitro*.

CsgB is proficient at forming amyloids in vitro but does not form fibers in vivo

CsgB is incorporated into the curli fiber after nucleation [16]. All the data I have collected thus far demonstrates that CsgB is able to rapidly polymerize into an amyloid fiber *in vitro*. However, CsgB is soluble and does not polymerize in *csgA* mutants [11]. There are two possibilities why CsgB does not polymerize in *csgA* mutants *in vivo*. One explanation is that CsgB binding to the membrane sterically sequesters CsgB such that it physically cannot interact with other CsgB molecules. The other potential mechanism is that *csgB* expression is decreased in *csgA* mutants to the point that the resulting protein concentration is below what is necessary for polymerization. It has been difficult to determine if CsgB levels are decreased in *csgA* mutants. *csgA* mutants do not bind Congo red, however, an altered Congo red binding phenotype is observed when *csgA* mutants contain multiple copies of *csgB* [unpublished, 16]. CsgB stability is increased in these

mutants and morphologically distinct aggregates are also observed [unpublished data, 16]. These results suggest the cells have a way of regulating CsgB levels in order to keep it from polymerizing in the absence of CsgA.

Screening for *csgA* mutants with an altered Congo red binding phenotype is a way to identify factors that regulate CsgB stability. I generated random insertion mutants in the *csgA* background using a mariner-based transposon, and mutant cells were screened on Congo red-containing YESCA plates. Mutants that appeared to have increased Congo red binding were isolated and the mutation was confirmed by backcross. To determine if the Congo red binding phenotype was dependent on CsgB, P1 lysates prepared from the original mutant were transduced into a *csgBA* background. If the increased Congo red binding found in the original mutant is due to an increase in CsgB stability, the resulting *csgBA* transductants should not bind Congo red. In our preliminary screens we have found several CsgB-dependent insertion mutants. Two mutants were mapped to the *tol* and *rse* loci, genes involved in periplasmic maintenance and homeostasis [17-19]. Continuing this mutagenesis approach will uncover the strategy cells use to keep CsgB from polymerizing in *csgA* mutants, and may uncover the mechanism cells use to maintain optimum CsgA-CsgB ratios.

Nucleation in nature

Curli are required for the formation of biofilms [7-9]. Biofilms composed of multiple species of bacteria found in nature have been reported to contain amyloid-like structures [20]. Curli have been demonstrated to increase the

persistence of *E. coli* in the environment and *Salmonella enterica* serovar *Typhimurium* persistence in the host [21, 22]. Perhaps enteric bacteria increase persistence in the host by forming multi-species curli dependent communities formed when CsgB from one species nucleates CsgA secreted by another species. There is precedence that CsgB from *E. coli* can nucleate CsgA from another species. It has been reported that *Salmonella enterica* serovar *Typhimurium csgA* can complement *E. coli csgA* mutants for Congo red binding and fiber formation [23]. Moreover, *csgA* homologues found in the other enteric bacteria share a high degree of identity [unpublished data, Wang, X]. Studying the biofilms produced when various enteric bacteria are cocultured with our *E. coli* curli mutants will determine if curli are important for the formation of multi-species biofilms.

Functional amyloid inhibitors

An advantage of using curli as a model of amyloid polymerization is the ease with which it can be manipulated both genetically and biochemically. *In vitro* CsgA polymerization can be detected by the amyloid specific dye ThT and the polymerization kinetics can be reproduced with relative ease [13, 24]. I have discovered two inhibitors of *in vitro* CsgA polymerization using the ThT assay. The characterization of these inhibitors could lead to new avenues for therapies that target disease associated amyloid polymerization.

CsgE inhibits self-assembly of CsgA into amyloid fibers

One outstanding question in the biosynthesis of curli fibers is how cells prevent amyloid formation on the periplasmic side of the curli assembly apparatus. The secretion and the stability of CsgA and CsgB are dependent on CsgE and the outer membrane lipoprotein CsgG [5, 25]. CsgG is predicted to form a pore in the outer membrane, through which CsgA and CsgB are secreted [25]. Due to the decrease in stability of CsgA and CsgB in *csgE* mutants, I hypothesized that CsgE was acting to chaperone the curli subunits. If CsgE was acting as a curli specific chaperone, it may inhibit CsgA polymerization *in vitro*. I examined the effect of CsgE on *in vitro* polymerization of CsgA. CsgA is soluble and unstructured immediately following purification, but after several hours of incubation at room temperature the protein begins to self-assemble into β-sheet rich amyloid fiber aggregates [26]. *In vitro* polymerization of CsgA can be monitored over time by reactivity with the amyloid-specific dye, thioflavin T (ThT). Freshly purified CsgA was incubated with or without purified CsgE, as described in the appendix.

CsgA polymerization with or without CsgE was monitored using the ThT assay (Appendix). A reaction containing 25 μM CsgA exhibited exponential growth after 270 minutes of incubation at room temperature (Appendix). This lag is longer than what is usually observed, because we found that contaminating high molecular weight bands in CsgA preparations increase the lag phase. Nonetheless, a reaction containing 25μM CsgA and 22.5 μM of CsgE did not exhibit substantial ThT reactivity, even after 700 minutes of incubation (Appendix). Reactions containing CsgE alone showed no increase in ThT

fluorescence in this assay (data not shown). As a control, strains expressing an empty vector instead of a vector containing CsgE were subjected to the same CsgE purification protocol, and the fractions corresponding to the CsgE fractions (which contain similar contaminating bands by Coommassie stain as that of a CsgE purification) were added to 25 μM CsgA. This resulted in a similar ThT profile to that of CsgA alone, suggesting that inhibition of CsgA polymerization was CsgE specific (data not shown). We have since eliminated the high molecular weight contaminants in our CsgA preparations and found that CsgE still potently inhibits CsgA polymerization. These results suggest that, *in vitro*, CsgE prevents the self-assembly of CsgA into amyloid fibers.

Ring-fused 2-pyridone compounds prevent polymerization of the major curli subunit CsgA

A ring-fused 2-pyridone compound, called FN075, inhibited the *in vitro* polymerization of the disease associated polypetide Aβ [27]. FN075 and a closely related derivative, BibC6, also inhibited curli production *in vivo* and blocked curli-dependent pellicle formation by the uropathogenic *E. coli* UTI89 in broth [data submitted for publication, Hultgren lab].

I tested the hypothesis that FN075 and BibC6 were directly inhibiting CsgA polymerization using the ThT assay. CsgA was purified in a soluble, unstructured state, and allowed to incubate in the presence or absence of FN075 and BibC6. At a fivefold molar excess (125 μM), FN075 and BibC6 both completely inhibited ThT fluorescence of 25 μM CsgA over time (Appendix). FN075 proved to inhibit

ThT fluorescence at concentrations as low as 10 μM, representing a 2.5-fold excess of protein to compound (Appendix). Direct comparison of the two compounds at 25 μM indicated partial inhibition of CsgA polymerization by BibC6 and complete inhibition by FN075 at this concentration (data not shown). Thus, FN075 was more potent than BibC6 in this ThT assay. Increased levels of soluble CsgA were observed by immunoblot analysis when the protein was incubated in the presence of 125 μM of either compound (Appendix), demonstrating that the compounds inhibited CsgA polymerization and not ThT binding to the fibers. Furthermore, the relative fluorescent units of samples containing ThT and preformed CsgA fibers remained constant when incubated with the compounds, demonstrating that compounds were not inhibiting ThT binding to fibers or disassociating preformed fibers (data not shown). To determine if the observed inhibition of amyloid polymerization was specific to FN075 and BibC6, we also included a previously characterized ring-fused 2-pyridone that inhibits type 1 pilus biogenesis, BibC10. BibC10 did not inhibit curli assembly *in vivo*. As expected, CsgA was able to polymerize into an insoluble amyloid fiber in the presence of a five-fold molar excess of BibC10 (Appendix and data not shown).

These inhibitor studies highlight the efficacy of using CsgA polymerization and curli biogenesis as a platform to test novel compounds or proteins for the ability to inhibit amyloid biogenesis. The curli system has two advantages compared to using chemically synthesized disease associated peptides. First, CsgA protein purification is cheaper and more consistent than the synthesis and

preparation of the disease associated peptides such as Aβ and IAPP. Many studies use different protocols for preparing these peptides, but in our system CsgA can be purified as soluble protein using standard protein purification techniques. Second, curli biogenesis is an *in vivo* process that occurs in the presence of a dedicated nucleator. Any compound that inhibits amyloid polymerization *in vitro* will have to be tested in an animal model where seeded mechanisms of amyloid biogenesis have been difficult to reproduce. Initial *in vivo* studies for any novel compound can be tested cheaply by incubating the compound with curli-producing bacteria. The assembly of curli is a regulated, template mediated polymerization process. *E. coli* has evolved a mechanism of producing amyloid fibers without the accumulation of cytotoxic intermediates. Our continued study of curli biogenesis will enhance our perspective of amyloid folding pathways in general and could potentially lead to novel therapeutics targeting disease-associated amyloidosis.

References:

1. Chiti, F. and C.M. Dobson, *Protein misfolding, functional amyloid, and human disease.* Annu Rev Biochem, 2006. **75**: p. 333-66.

2. Fowler, D.M., et al., *Functional amyloid--from bacteria to humans.* Trends Biochem Sci, 2007. **32**(5): p. 217-24.

3. Hammer, N.D., et al., *Amyloids: friend or foe?* J Alzheimers Dis, 2008. **13**(4): p. 407-19.

4. Shorter, J. and S. Lindquist, *Prions as adaptive conduits of memory and inheritance.* Nat Rev Genet, 2005. **6**(6): p. 435-50.

5. Chapman, M.R., et al., *Role of Escherichia coli curli operons in directing amyloid fiber formation.* Science, 2002. **295**(5556): p. 851-5.

6. Hammar, M., et al., *Expression of two csg operons is required for production of fibronectin- and congo red-binding curli polymers in Escherichia coli K-12.* Mol Microbiol, 1995. **18**(4): p. 661-70.

7. Gerstel, U. and U. Romling, *The csgD promoter, a control unit for biofilm formation in Salmonella typhimurium.* Res Microbiol, 2003. **154**(10): p. 659-67.

8. Uhlich, G.A., P.H. Cooke, and E.B. Solomon, *Analyses of the red-dry-rough phenotype of an Escherichia coli O157:H7 strain and its role in biofilm formation and resistance to antibacterial agents.* Appl Environ Microbiol, 2006. **72**(4): p. 2564-72.

9. Vidal, O., et al., *Isolation of an Escherichia coli K-12 mutant strain able to form biofilms on inert surfaces: involvement of a new ompR allele that increases curli expression.* J Bacteriol, 1998. **180**(9): p. 2442-9.

10. Collinson, S.K., et al., *Structural predictions of AgfA, the insoluble fimbrial subunit of Salmonella thin aggregative fimbriae.* J Mol Biol, 1999. **290**(3): p. 741-56.

11. Hammar, M., Z. Bian, and S. Normark, *Nucleator-dependent intercellular assembly of adhesive curli organelles in Escherichia coli.* Proc Natl Acad Sci U S A, 1996. **93**(13): p. 6562-6.

12. White, A.P., et al., *Structure and characterization of AgfB from Salmonella enteritidis thin aggregative fimbriae.* J Mol Biol, 2001. **311**(4): p. 735-49.

13. Wang, X., et al., *In vitro polymerization of a functional Escherichia coli amyloid protein.* J Biol Chem, 2007. **282**(6): p. 3713-9.

14. Lashuel, H.A., et al., *Neurodegenerative disease: amyloid pores from pathogenic mutations.* Nature, 2002. **418**(6895): p. 291.

15. Hammer, N.D., J.C. Schmidt, and M.R. Chapman, *The curli nucleator protein, CsgB, contains an amyloidogenic domain that directs CsgA polymerization.* Proc Natl Acad Sci U S A, 2007. **104**(30): p. 12494-9.

16. Bian, Z. and S. Normark, *Nucleator function of CsgB for the assembly of adhesive surface organelles in Escherichia coli.* Embo J, 1997. **16**(19): p. 5827-36.

17. De Las Penas, A., L. Connolly, and C.A. Gross, *The sigmaE-mediated response to extracytoplasmic stress in Escherichia coli is transduced by RseA and RseB, two negative regulators of sigmaE.* Mol Microbiol, 1997. **24**(2): p. 373-85.

18. Malisauskas, M., et al., *Does the cytotoxic effect of transient amyloid oligomers from common equine lysozyme in vitro imply innate amyloid toxicity?* J Biol Chem, 2005. **280**(8): p. 6269-75.

19. Fognini-Lefebvre, N., J.C. Lazzaroni, and R. Portalier, *tolA, tolB and excC, three cistrons involved in the control of pleiotropic release of periplasmic proteins by Escherichia coli K12.* Mol Gen Genet, 1987. **209**(2): p. 391-5.

20. Larsen, P., et al., *Amyloid adhesins are abundant in natural biofilms.* Environ Microbiol, 2007. **9**(12): p. 3077-90.

21. Lawley, T.D., et al., *Genome-wide screen for Salmonella genes required for long-term systemic infection of the mouse.* PLoS Pathog, 2006. **2**(2): p. e11.

22. White, A.P., et al., *Thin aggregative fimbriae and cellulose enhance long-term survival and persistence of Salmonella.* J Bacteriol, 2006. **188**(9): p. 3219-27.

23. Romling, U., et al., *Curli fibers are highly conserved between Salmonella typhimurium and Escherichia coli with respect to operon structure and regulation.* J Bacteriol, 1998. **180**(3): p. 722-31.

24. Wang, X. and M.R. Chapman, *Sequence determinants of bacterial amyloid formation.* J Mol Biol, 2008. **380**(3): p. 570-80.

25. Robinson, L.S., et al., *Secretion of curli fibre subunits is mediated by the outer membrane-localized CsgG protein.* Mol Microbiol, 2006. **59**(3): p. 870-81.

26. Chapman, M.R., et al., *Role of Escherichia coli curli operons in directing amyloid fiber formation.* Science, 2002. **295**(5556): p. 851-5.

27. Aberg, V., et al., *Microwave-assisted decarboxylation of bicyclic 2-pyridone scaffolds and identification of Abeta-peptide aggregation inhibitors.* Org Biomol Chem, 2005. **3**(15): p. 2817-23.

Appendix: Investigating inhibitors of CsgA polymerization.

Amyloid fibers associated with neurodegenerative diseases are thought to polymerize *in vivo* via a nucleus dependent, template mediated mechanism. Curli fibers are an excellent model for *in vivo* study of amyloid fibers because curli polymerize via a nucleus dependent, template mediated mechanism. This makes developing assays that test inhibition of curli polymerization medically relevant. From an *in vitro* perspective, the ThT assay in particuar is a potent assay that can be used to screen small molecule libraries for inhibitors of amyloid biogenesis. I have used the ThT assay to demonstrate that both CsgE and ring-fused 2-pyridones inhibit CsgA polymerization (Fig. 1).

The ring-fused 2-pyridone inhibitor studies was recently accepted for publication in Nature Chemical Biology, and CsgE inhibition studies are being thoroughly investigated by Matthew Badtke. These results have been included in a manuscript currently.

Experimental Procedures

CsgA purification. C-terminal polyhistidine tagged CsgA was purified using a modified denaturing protocol. NEB 3016 *slyD* cells harboring a pET11d vector containing a *sec*-signal sequence minus CsgA (pNH11) were grown to OD_{600} 0.9, induced with 0.5 mM IPTG, and incubated for one hour at 37° C. Cells were collected by centifugation and stored at -80° C. Cells were lysed by addition of 8 M guanidine hydrochloride, 50 mM potassium phosphate solution pH 7.2. 50 mL

of lysis solution was used per pellet generated from a 500 ml culture. The lysate was incubated, stirring, at 4° C for 48hrs. The insoluble portion of the lysate was removed by centrifuging at 10,000 x g 4° C for 15 min and the resulting supernatant was incubated with NiNTA resin (Sigma Aldrich, Atlanta, GA) for 1 hour at room temperature with rocking. CsgA was purified using Nickel affinity beads in a Kontes column. The beads were washed with 50 mM potassium phosphate. CsgA was eluted from the column using a 0.5 M imidazole 50 mM potassium phosphate solution. Fractions were collected and analyzed for the presence of protein using the BCA assay (Thermo Scientific, Rockford, IL) and SDS PAGE.

CsgE purification. C-terminal polyhistidine tagged CsgE was purified from NEB 3016 cells (New England Biolabs, Ipswich, MA) harboring a pET11d vector containing a *sec*-signal sequence minus CsgE (pNH27). Cells were grown to OD_{600} 0.9, induced with 0.5 mM IPTG, and incubated for one hour at 37° C. The cells were harvested, resuspended in 50 mM potassium phosphate solution pH 7.2 solution that also contained, 1x PMSF, and 1 μg/ml DNAse. The cells were lysed with a French press. The insoluble portion of the lysate was removed by centrifuging at 10,000 x g 4° C for 15 min and the resulting supernatant was incubated with NiNTA resin (Sigma Aldrich, Atlanta, GA). The polyhistidine-tagged CsgE was affinity purified by collecting the nickel beads as the mixture passed through a Kontes column. The beads were washed with 50 mM KPi pH7.2 first, and then washed with 50 mM KPi containing 12.5 mM immidazole

pH7.2. CsgE was eluted from the column using 500 mM immidazole in 50 mM KPi pH 7.2. Fractions were collected and analyzed for the presence of protein by SDS PAGE. Protein concentration was determined by the BCA assay (Thermo Scientific, Rockford, IL). The CsgE mock purifications were performed as above, but the NE 3016 strain containing pET11d.

Thioflavin-T (ThT) Assay. Proteins were mixed with 20 μM thioflavin-T (ThT) in 96-well plates and incubated at room temperature. Every 10 minutes samples were excited at 438 nm and fluorescence emitted 495 nm with a 475 nm cutoff was measured using a Spectramax M2 plate reader (Molecular Devices, Sunnyvale, CA). Samples were shaken for 5 seconds before each read. Due to the differences in preparation–to-preparation protein yield, a representative ThT kinetic graph taken from a series of ThT assays is shown. ThT fluorescence was normalized using $(F_i - F_o)/(F_{max} - F_o)$ were F_o was the ThT background intensity (fluorescence arbitrary unit), F_i was the ThT intensity of samples, and F_{max} was the maximum ThT intensity of the reaction.

CsgA solubility, SDS/PAGE, Western Blotting. 25 μM CsgA was incubated in the presence of 125 μM FN075 or BibC6 for 4.5 or 14 hours. At the indicated time point, the samples were spun at 13, 200 rpms in a microcentrifuge (Eppendorf, Hamburg, Germany). The supernatant was collected and was probed for CsgA using previously described methods [25].

Figure legend

Figure 1. Inhibitors of CsgA Polymerization *in vitro*. (A) CsgE prevents *in vitro* polymerization of CsgA into amyloid fibers. Representative thioflavin-T kinetic plot of 25 μM CsgA incubated at room temperature alone (●) or in the presence of 22. 5 μM CsgE (●). Relative fluorescence units (RFUs) emitted at 495 nm were recorded every 30 min. after excitation at 438 nm. (B) Ring-fused 2-pyridone compounds inhibit *in vitro* polymerization of CsgA. The fluorescence of freshly purified CsgA mixed with 20 μM ThT, and respective ring-fused 2-pyridone compounds, was measured at 495 nm after excitation at 438 nm. Data points corresponding to 30-min intervals are displayed. (Inset) Reductions in ThT fluorescence corresponded to reduced CsgA polymerization. Soluble CsgA levels were confirmed by SDS-PAGE and western analysis using anti-CsgA antibodies. Polymerized CsgA is SDS insoluble and migration is impeded during electrophoresis.

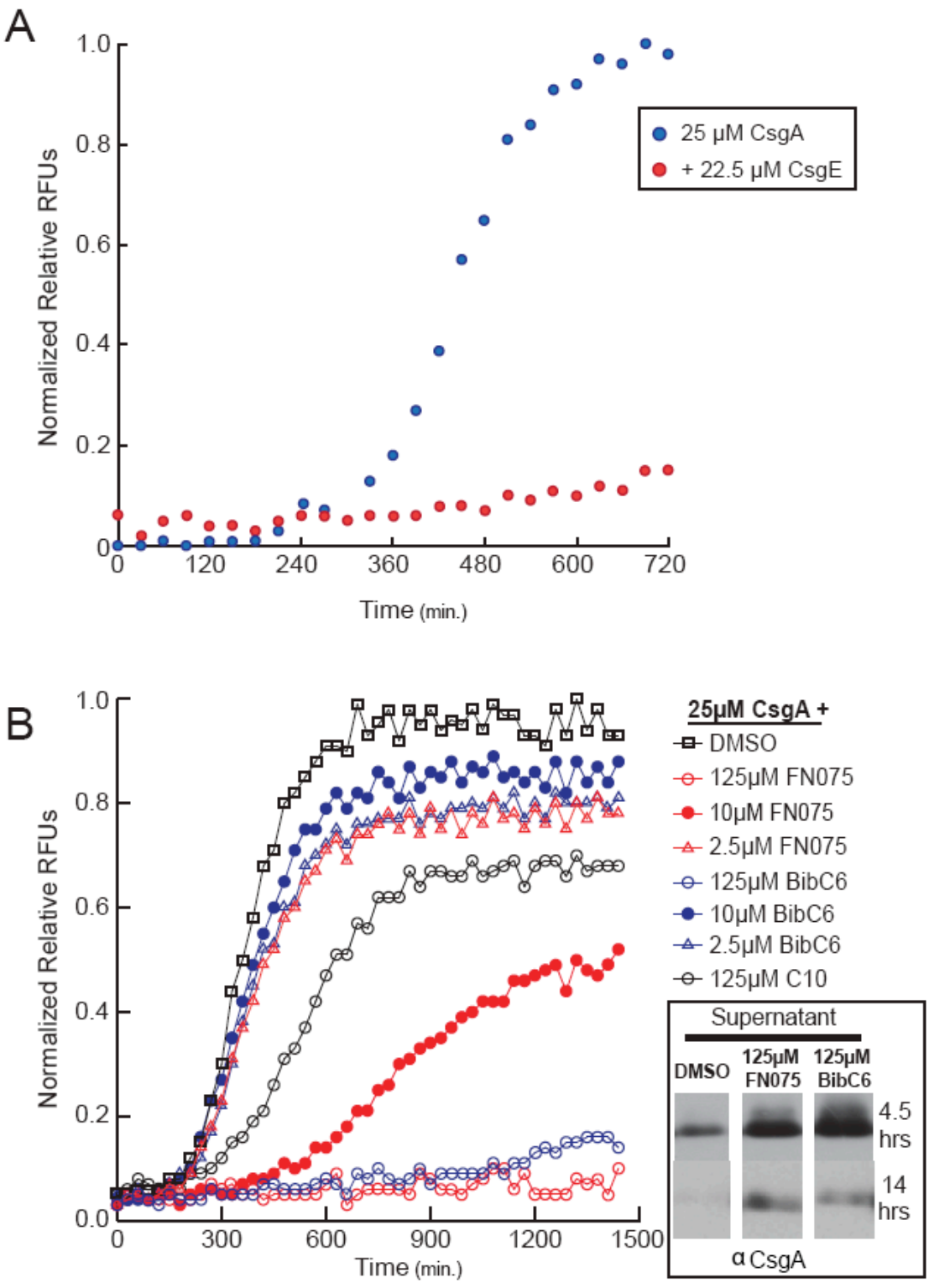

Figure A.1. Inhibitors of *in vitro* CsgA polymerization.